Brownian ratchet-inspired phenomena in Complex Systems: Quantum and Sociodynamical Parrondo's paradox

Submitted by
WeiJia, Joel LAI

Thesis Advisor
Asst. Prof. Kang Hao CHEONG

Science, Mathematics and Technology Cluster

A thesis submitted to the Singapore University of Technology and Design in fulfillment of the requirement for the degree of Doctor of Philosophy

2024

PhD Thesis Examination Committee

TEC Chair:	Prof. Lay Kee, Ricky Ang
Main Advisor:	Asst. Prof. Kang Hao Cheong
Internal TEC member 1:	Assoc. Prof. Kui Cai
Internal TEC member 2:	Assoc. Prof. Shengyuan Yang

Declaration

I, WeiJia, Joel LAI, declare that this thesis titled, "Brownian ratchet-inspired phenomena in Complex Systems: Quantum and Sociodynamical Parrondo's paradox" and the work presented in it are my own. I confirm that:

- The thesis work is original and has not been submitted to any other University or Institution for higher degree purposes.
- This work was done wholly while in candidature for a research degree at this University.
- Where I have consulted the published work of others, this is always clearly attributed.
- I have attached all publications and award list related to the thesis (e.g. journal, conference report and patent).
- The thesis does not contain patentable or confidential information.

Signature: _____

Date: _____

Abstract

Science, Mathematics and Technology Cluster

Doctor of Philosophy

Brownian ratchet-inspired phenomena in Complex Systems: Quantum and Sociodynamical Parrondo's paradox

by WeiJia, Joel LAI

Parrondo's paradox is the phenomenon whereby combining two individually losing choices results in a winning outcome. Parrondo's paradox is the convergent of concepts from convex linear combination, complexity theory, stochastic theory, Markov theory, discrete theory, nonlinear theory, dynamical systems, and fractals, all in a compact model. While much is still unexplored in Parrondo's paradox, this thesis provides a springboard for pathways into two fields: quantum and social physics.

This thesis first demonstrates a new form of quantum Parrondo's paradox - the quantum coin-toss protocol. In particular, the 2-sided fair quantum coin-toss protocol does not have a classical Parrondo's paradox counterpart. We will show that by stochastically or periodically switching between tossing two fair 2-sided quantum coins, we can achieve weak Parrondo's paradox. By increasing the dimension to the 4-sided fair quantum coin-toss protocol, we can improve the performance of Parrondo's paradox to achieve a strong Parrondo effect. Subsequently, by employing chaotic switching, we will show that it is possible to achieve strong Parrondo's paradox even for the 2-sided fair quantum coin-toss protocol. Developing on the dynamics of chaotic switching for 2-sided fair quantum coins, we then demonstrate a working example of semiclassical secret key exchange encryption using the classical chaotic switching protocol.

Next, we explore Parrondo's paradox in three aspects of sociodynamical Parrondo's paradox under a unified framework of preference aggregation. Firstly, we introduce the preference aggregation framework and provide insights into how preference aggregation Parrondo's paradox played in a network of interacting agents can lead to critical phenomena observed in statistical physics akin to a phase transition. Next, we consider agents in a network with preferences modelled as a mean-field synchronization. We show that synchronization and the population's average fitness have a sublinear relationship. Under a decision-making model, we also demonstrate that we can predict Dunbar's number for band sizes, a guide often followed for organizations to size their decision-making group. Lastly, we explored the outcome of single-prioritization voting between three losing options, where several theoretic phenomena, such as the volunteer's dilemma, emerge.

Publications

The following publications were used in the writing of this thesis (ordered by date of publication):

1. J. W. Lai, & K. H. Cheong (2023). Boosting Brownian-inspired games with network synchronization. Accepted for publication in *Chaos, Solitons & Fractals*.
2. J. W. Lai, & K. H. Cheong (2022). A comprehensive framework for preference aggregation Parrondo's paradox. *Chaos*.
3. J. W. Lai, & K. H. Cheong (2022). Risk-taking in social Parrondo's games can lead to Simpson's paradox. *Chaos, Solitons & Fractals*.
4. J. W. Lai, & K. H. Cheong (2021). Evaluation of single prioritization voting systems in controlled collective parrondo's games. *Nonlinear Dynamics*.
5. J. W. Lai, & K. H. Cheong (2021). Chaotic switching for quantum coin Parrondo's games with application to encryption. *Physical Review Research*.
6. J. W. Lai, J. R. A. Tan, H. Lu, Z. R. Yap, & K. H. Cheong (2020). Parrondo paradoxical walk using four-sided quantum coins. *Physical Review E*.
7. J. W. Lai, & K. H. Cheong (2020). Social dynamics and Parrondo's paradox: A narrative review. *Nonlinear Dynamics*.
8. J. W. Lai, & K. H. Cheong (2020). Parrondo effect in quantum coin toss simulations. *Physical Review E*.
9. J. W. Lai, & K. H. Cheong (2020). Parrondo's paradox from classical to quantum: A review. *Nonlinear Dynamics*.

The following publications were written during my candidature (ordered by category, and date of publication):

Parrondo's Paradox

10. T. Wen, J. W. Lai, & K. H. Cheong (2022). Switching between two losing stocks may enable paradoxical win: An empirical analysis. In press *Fractals*.
11. T. Wen, K. H. Cheong, J. W. Lai, & E. V. Koonin (2022). Extending the lifespan of multicellular organisms via periodic and stochastic intercellular competition. *Physical Review Letters*.
12. S. Jia, J. W. Lai, J. M. Koh & K. H. Cheong (2022). Periodic noise-induced framework for history-dependent Parrondo's switching. *Nonlinear Dynamics*.
13. K. H. Cheong, W. Tao, & J. W. Lai (2020). Relieving cost of epidemic by Parrondo's paradox: A COVID-19 case study. *Advanced Science*.
14. S. Jia, J. W. Lai, J. M. Koh, N. G. Xie, & K. H. Cheong (2020). Parrondo effect: Exploring the nature-inspired framework on periodic functions. *Physica A*.

15. J. W. Lai, J. Chang, L. K. Ang, & K. H. Cheong (2020). Multi-level information fusion to alleviate network congestion. *Information Fusion*.

Modelling and Analytics

16. B. H. Parikh, Z. Liu, P. Blakeley, Q. Lin, M. Singh, J. Y. Ong, K. H. Ho, J. W. Lai, H. Bogireddi, K. C. Tran, J. Y. C. Lim, K. Xue, A. Al-Mubaarak, B. Yang, S. Rajan, R. Kakkad, D. S. L. Wong, Q. S. W. Tan, Z. Zhang, A. D. Jeyasekharan, V. B. Veluchamy, W. Yu, K. H. Cheong ,T. A. Blenkinsop, H. Walter, G. Lingam, X. J. Loh, & X. Su (2022). A bio-functional polymer that prevents retinal scarring through modulation of NRF2 signalling pathway. *Nature Communications*.

17. N. G. Xie, M. Wang, Y. Dai, Y. Ye, J. W. Lai, L. Wang, & K. H. Cheong (2022). Decision-making psychology and method under the specific zero-knowledge context. *Scientific Reports*.

18. X. Zhao, I. Seah, K. Xue, W. Wong, Q. S. W. Tan, X. X. Ma, Q. Lin, J. Y. C. Lim, Z. Liu, B. H. Parikh, K. N. Mehta, J. W. Lai, B. Yang, K. C. Tran, V. A. Barathi, K. H. Cheong, W. Hunziker, X. Su, & X. J. Loh (2021). Anti-angiogenic nanomicelles for the topical delivery of aflibercept to treat retinal neovascular disease. *Advanced Materials*.

19. T. Liu, C. Li, C. Wang, J. W. Lai, & K. H. Cheong (2020). A simple FSDT-based isogeometric method for piezoelectric functionally graded plates. *Mathematics*.

20. J. W. Lai, & K. H. Cheong (2020). Superposition of COVID-19 Waves, Anticipating a Sustained Wave, and Lessons for the Future. *BioEssays*.

21. K. Mutthulakshmi, M. R. E. Wee, Y. C. K. Wong, J. W. Lai, J. M. Koh, U. R. Acharya, & K. H. Cheong (2020). Simulating forest fire spread and fire-fighting using cellular automata. *Chinese Journal of Physics*.

Artificial Intelligence, Education Research and Technology

22. X. Zhao, J. W. Lai, A. F. W. Ho, N. Liu, M. E. H. Ong, & K. H. Cheong (2022). Predicting hospital emergency department admissions with deep learning approaches. *Biocybernetics and Biomedical Engineering*.

23. J. W. Lai, & K. H. Cheong (2022). Educational opportunities and challenges in augmented reality: Featuring implementations in physics education. *IEEE Access*.

24. J. W. Lai, & K. H. Cheong (2022). Adoption of virtual and augmented reality for mathematics education: A scoping review. *IEEE Access*.

25. J. W. Lai, C. K. E. Ang, U. R. Acharya, & K. H. Cheong (2021). Schizophrenia: A survey of artificial intelligence techniques applied to detection and classification. *International Journal of Environmental Research and Public Health*.

26. K. H. Cheong, S. Poeschmann, J. W. Lai, J. M. Koh, U. R. Acharya, S. C. M. Yu, & K. J. W. Tang (2019). Practical automated video analytics for crowd monitoring and counting. *IEEE Access*.

Acknowledgements

I am thankful for the Almighty God for leading me in a journey of obedience during this season of life. It is through submission to His will that I am able to see His graces, strength, sustenance and above all, His faithfulness and love from the beginning of my academic life up to this doctoral level.

I would like to thank the following people, without whom I would not have been able to complete this research, and without whom I would not have made it through my doctoral degree:

The Complex Systems Science Group at the Singapore University of Technology and Design, especially to my supervisor Assistant Professor Dr Kang Hao Cheong, whose guidance have steered me through this research. Special mention and appreciation for all graduate students, research fellows, and research assistants (both past and present) whose support, both academically and socially, have supported me and had to put up with my moans for a couple of years of study!

I would like to extend gratitude to all my collaborators throughout my candidacy for teaching me valuable lessons vital in inspiring me to think outside the box. For challenging me to explore new skills beyond the projects of my thesis tackle cutting-edge research methods from multiple perspectives, and to form a comprehensive and objective critique.

Biggest thanks to my family for all the support you have shown me through this research. Though you all always don't say it, you guys always trust me to make the right life choices (I hope pursuing my doctoral study is the right choice). Your belief in me has kept my spirits and motivation high during this process. To my fiancée, Crystal, thank you for standing by me and for adding a greater purpose to life beyond academic work.

To God be the Glory!

Contents

List of Figures

List of Tables

List of Algorithms

Chapter 1

Introduction

Parrondo's paradox is inspired by the flashing Brownian ratchet. The flashing Brownian ratchet was first introduced by Ajdari and Prost [1], which eventually cumulated to the work published by Rousselet et al. [2]. A flashing Brownian ratchet is a stochastic process that alternates between two regimes, a one-dimensional Brownian motion, and a Brownian ratchet, producing directed motion. The Brownian ratchet is a one-dimensional diffusion process that drifts towards a minimum of a periodic asymmetric potential, giving rise to a net-directed motion (see FIGURE 1.1a).

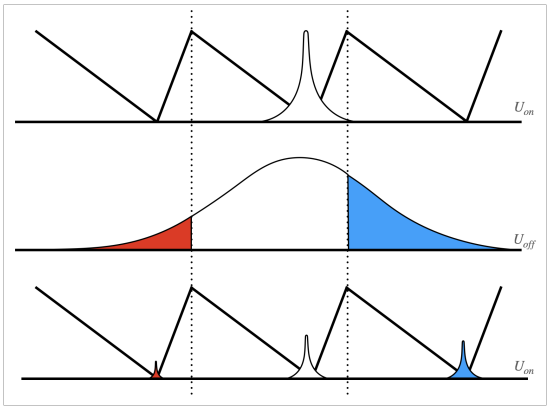

(A) The two regimes are denoted U_{on} and U_{off}, respectively.

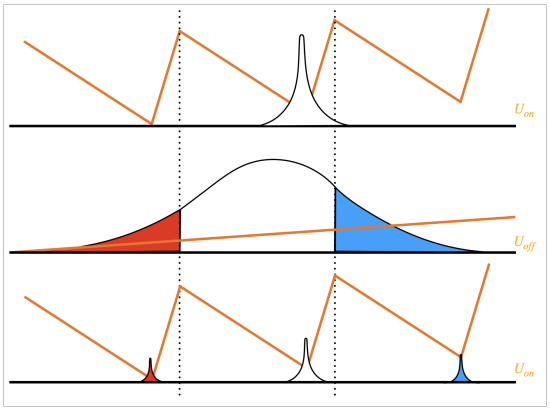

(B) The two regimes, now with a left-ward slope, are denoted U_{on} and U_{off}, respectively. The inspiration for Parrondo's paradox.

FIGURE 1.1: The probability densities of Brownian particles are denoted by the curves. When U_{on}, the Brownian particles are trapped in the asymmetric potential. When U_{off}, the Brownian particles are allowed to diffuse. Upon the reactivation of the potential U_{on}, due to the asymmetry of the potential, the ensemble of particles, on average, moved to the right. Figure redrawn from [3, 4].

In the initial years of its discovery, physicist and biologist alike were intrigued by the potential of its application and its occurrence in nature. For example, biologists have found that the flashing Brownian ratchet has connections to the so-called molecular motors [5] as well as the emergence of ecological population and biological evolutionary phenomena [6, 7]. It is with this underlying interest that resulted in the abstraction of Parrondo's paradox (see FIGURE 1.1b), where two losing games (as opposed to fair

potentials in the flashing Brownian ratchet), when alternated, result in a winning outcome [8, 9].

There are three seminal papers, each describing a type of Parrondo's paradox: the capital-dependent, history-dependent, and cooperative Parrondo's games. In each of these Parrondo's games, every player begins with an initial capital $c(t)$. Subsequently, at each time step t, the player plays one of the two losing games. If the player wins the losing game, the player's capital increases by 1, that is $c(t+1) = c(t) + 1$. Otherwise, the player's capital decreases by 1, $c(t+1) = c(t) - 1$.

1.1 Capital-dependent Parrondo's paradox

In the capital-dependent Parrondo's games, game A involves the toss of a single biased coin with winning probability $p_A = \frac{1}{2} - \epsilon$, where ϵ is the *bias parameter*. In game B, we toss coin B_1, with a winning probability of p_{B1}, if the capital is divisible by an integer M, otherwise, coin B_2 is used with winning probability p_{B2}. By choosing p_{B1} and p_{B2}, it is possible to achieve a scenario where games A and B individually, on average, give a net loss of capital, but playing a combination of games A and B randomly, denoted by [A+B], results in a gain in the capital. The decision tree for the capital-dependent Parrondo's paradox is shown in FIGURE 1.2. In particular, for $M = 3$, the choice of probabilities $p_{B1} = \frac{1}{10} - \epsilon$, $p_{B2} = \frac{3}{4} - \epsilon$, for $0 < \epsilon \leq 0.013$[1] satisfies the conditions for Parrondo's paradox to emerge.

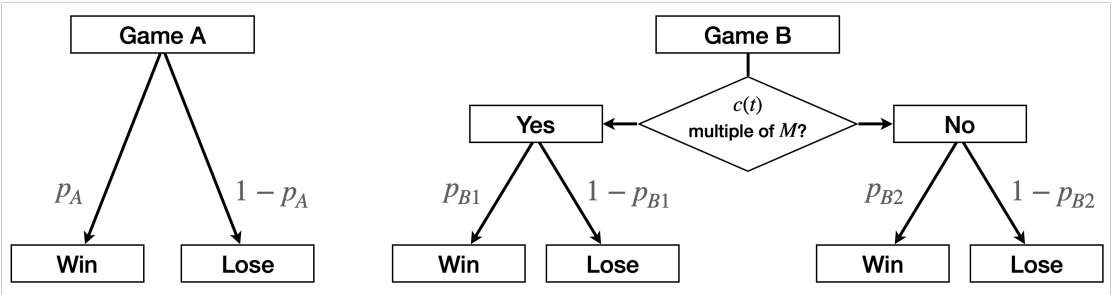

FIGURE 1.2: The capital-dependent Parrondo's paradox.

1.1.1 Proof via Markov chain

It is instructive to introduce the Markov chain representation of Parrondo's games. This representation is often used to analyze and classify equilibrium or detailed balance solutions in discrete state-based transitions. In the capital-dependent Parrondo's games, we have M states, each state corresponding to the remainder when dividing the capital by M, that is $c \equiv i \mod M$, where $i \in \{0, 1, \ldots, M-1\}$. For example, we illustrate the transition from one state to another for $M = 3$ in FIGURE 1.3. Firstly, we prove that game B is losing. The transition matrix shows the probability of moving from state i to state j. The transition matrix for game B is

[1]The upper limit of ϵ is rounded to 2 significant figures.

$$\mathbb{P}_B = \begin{pmatrix} 0 & \frac{1}{10} - \epsilon & \frac{9}{10} + \epsilon \\ \frac{1}{4} + \epsilon & 0 & \frac{3}{4} - \epsilon \\ \frac{3}{4} - \epsilon & \frac{1}{4} + \epsilon & 0 \end{pmatrix}. \tag{1.1}$$

According to Markov chain theory, the chain will converge to a steady state, which is also equivalent to finding the equilibrium distribution $\pi^\top \mathbb{P}_B = \pi^\top$, where $\pi^\top = (\pi_1, \pi_2, \pi_3)$, subjected to $\pi_1 + \pi_2 + \pi_3 = 1$. Alternatively, successive playing of game B is equivalently $\lim_{t\to\infty} \mathbb{P}_B^t$, for $\epsilon = 0.005$ gives us

$$\lim_{t\to\infty} \mathbb{P}_B^t \approx \begin{pmatrix} 0.383612 & 0.154281 & 0.462107 \\ 0.383612 & 0.154281 & 0.462107 \\ 0.383612 & 0.154281 & 0.462107 \end{pmatrix}. \tag{1.2}$$

Any row gives us the probability distribution of each state. Hence, the player will be in state 0 for approximately 38.4% of the time, and in states 1 and 2 for approximately 61.6% (0.154281+0.462107) of the time. Thus, the expected outcome of game B is

$$0.383612 p_{B1} + (0.154281 + 0.462107) p_{B2} \approx 0.4956522 < 0.5, \tag{1.3}$$

a losing game. For $\epsilon = 0.005$, it is clear that game A is a losing game. Thus, when we stochastically switch between games A and B with equal probability, this can be represented by the detailed equation

$$\mathbb{P}_S = \frac{1}{2}(\mathbb{P}_A + \mathbb{P}_B), \tag{1.4}$$

where $\mathbb{P}_A$ is the transition matrix for game A. The equilibrium distribution is $\pi^\top = (0.34507, 0.25411, 0.40082)$. The long-term probability of winning is

$$0.5[p_A + \pi_1 p_{B1} + (\pi_2 + \pi_3) p_{B2}] \approx 0.508 > 0.5, \tag{1.5}$$

indicating a higher probability of winning than losing, hence the resolution to the paradox.

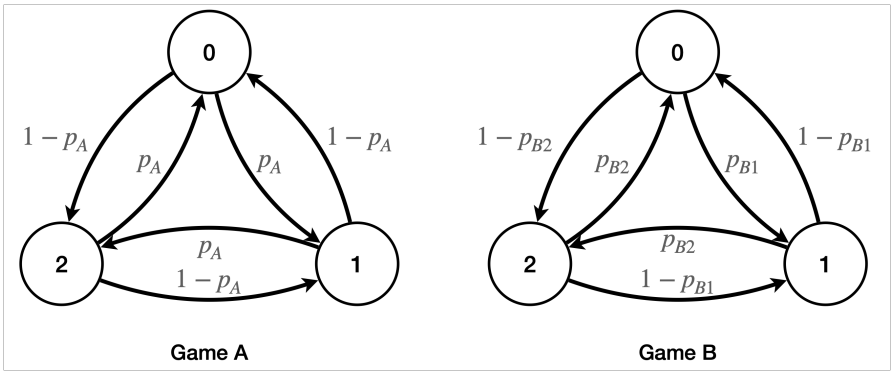

FIGURE 1.3: Markov chain representation of the capital-dependent Parrondo's games.

In the Markov chains in FIGURE 1.3, the clockwise transitions are "winning" while the

counter-clockwise transitions are “losing". It is easy to check that game A is a losing game if

$$1 - p_A > p_A \Rightarrow \frac{1 - p_A}{p_A} > 1. \tag{1.6}$$

For game B, it is losing if

$$(1 - p_{B1})(1 - p_{B2})^2 > p_{B1}p_{B2}^2 \Rightarrow \frac{(1 - p_{B1})(1 - p_{B2})^2}{p_{B1}p_{B2}^2} > 1. \tag{1.7}$$

For Parrondo's games, we can play a combination of games A and B, such that the combined game S can be written analogously as $S = \gamma A + (1 - \gamma)B$, where $0 \leq \gamma \leq 1$. If $\gamma = 1$, only game A is played; if $\gamma = 0$, only game B is played. Then at the stationary distribution, Parrondo's paradox occurs if

$$\frac{(1 - q_1)(1 - q_2)^2}{q_1 q_2^2} < 1, \tag{1.8}$$

where $q_1 = \gamma p_A + (1-\gamma)p_{B1}$ and $q_2 = \gamma p_A + (1-\gamma)p_{B2}$. In most literature, games A and B are played with the same probability for the capital-dependent Parrondo's games, so $\gamma = \frac{1}{2}$. Solving EQUATION (1.8), with the probabilities $p_A = \frac{1}{2} - \epsilon$, $p_{B1} = \frac{1}{10} - \epsilon$, and $p_{B2} = \frac{3}{4} - \epsilon$. We can numerically show that $\epsilon \leq 0.013109295$. For game A to be a losing game, we require the bias parameter, $\epsilon > 0$. Consequently, when rounded to the nearest two significant figures, we arrive at $0 < \epsilon \leq 0.013$.

The generalised formulation for capital-dependent Parrondo's paradox is documented in Harmer et al. [10], and Koh and Cheong [11]. For this thesis, we will assume that $M = 3$ when referring to the capital-dependent Parrondo's games unless otherwise specified.

1.1.2 Numerical simulations

Another way to present the solutions to the capital-dependent Parrondo's paradox is through numerical simulations. Computational methods are generally preferred as the algebraic and detailed balance methods can get complicated, with increasing complexity to the games or the number of players. In many cases formulated in this thesis, Parrondo's games cannot be represented in algebraic or Markov chain form. Thus, it is beneficial to report the results of Parrondo's paradox through empirical simulations. As an example, the pseudocode, **Algorithm 1.1** presents the process of a single player playing Parrondo's games once. Because of the stochastic nature of Parrondo's games, FIGURE 1.4 shows the empirical solutions, where $\langle c(t) \rangle$ is the average capital from 10^6 experiments, for $t_{max} = 100$. Without loss of generality, since we are only interested in a capital gain or loss, we can set the initial capital to be zero, i.e. $c(0) = 0$.

It is clear from FIGURE 1.4, that both games A and B are losing games, as the average capital decreases with successive games. However, when randomly combined, [A+B] is indeed a winning game. Other variations of the game, such as periodic switching using the sequence AABB until t_{max} is reached, also result in a winning outcome.

Algorithm 1.1 The capital-dependent Parrondo's paradox algorithm.

Generate random number $r \in [0, 1)$.
Choose a game to play from either A or B. Choose with equal probability if random.
if game is A **then** ▷ play game A
    $c \leftarrow c + 1$ **if** $r < 0.5 - \epsilon$, **else** $c \leftarrow c - 1$.
else ▷ play game B instead
    if $c \mod 3 = 0$ **then**
        $c \leftarrow c + 1$ **if** $r < 0.1 - \epsilon$, **else** $c \leftarrow c - 1$.
    else
        $c \leftarrow c + 1$ **if** $r < 0.75 - \epsilon$, **else** $c \leftarrow c - 1$.
    end if
end if

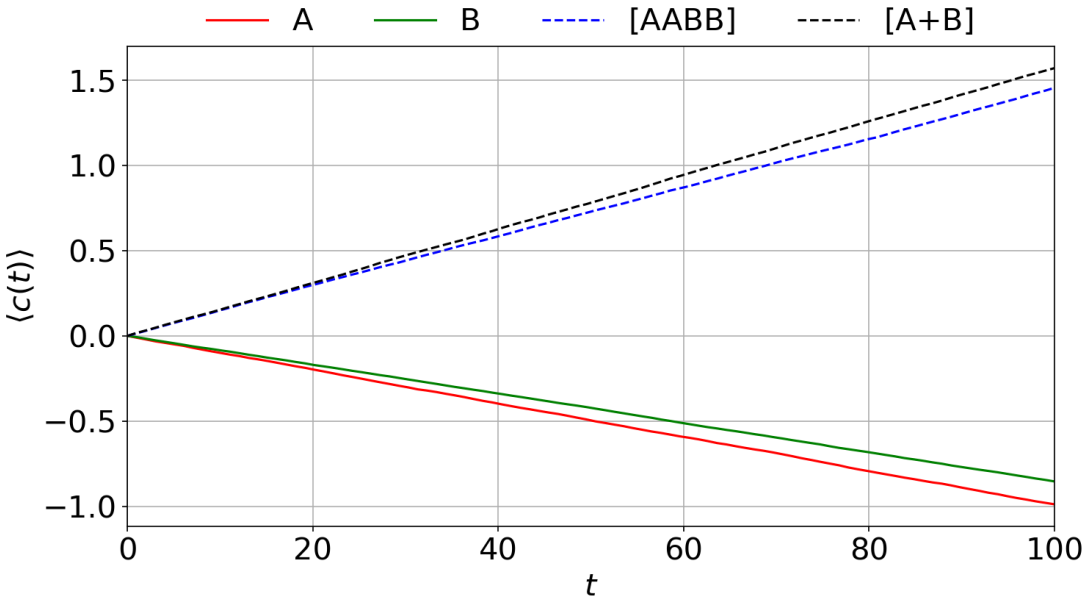

FIGURE 1.4: Average capital $\langle c(t) \rangle$ against time for the capital-dependent Parrondo's games. The capital is averaged over 10^6 simulations for $t_{max} = 100$ time steps for $\epsilon = 005$.

1.2 History-dependent Parrondo's paradox

The history-dependent version of Parrondo's games build on the concept of capital-dependent games by keeping game A. However, game B is now dependent on the outcome of the previous game — we call it game B′ so as not to confuse it with the earlier game B. In game B′, four coins are used, each is chosen depending on the *history* of the outcomes from previous games [12, 10]. At each discrete time step t, the player now chooses to play either game A or B′.

The rules for game B′ is defined according to the history of the past two time steps, where the probability of winning at time t is given by:

- p_1, if player "lose" at both $t-1$ and $t-2$,
- p_2, if player "lose" at $t-1$ but "win" at $t-2$,
- p_3, if player "win" at $t-1$ but "lose" at $t-2$, and
- p_4, if player "win" at both $t-1$ and $t-2$.

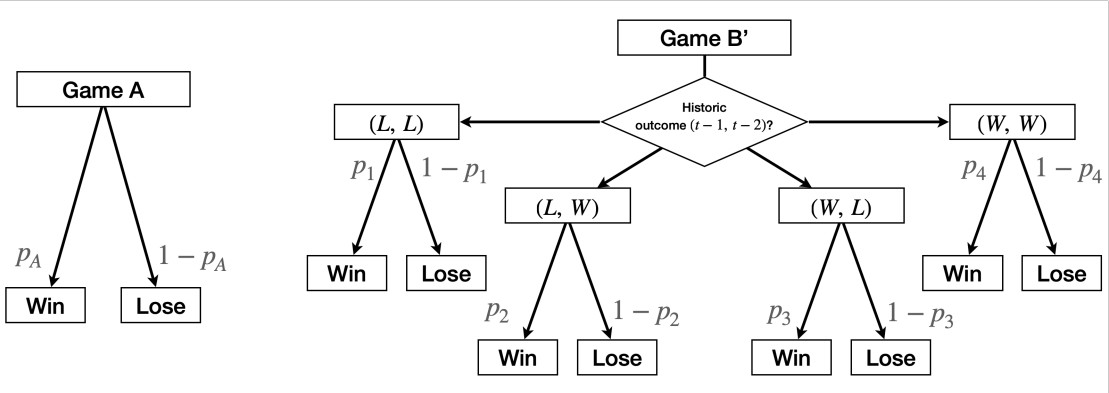

FIGURE 1.5: The history-dependent Parrondo's paradox.

The game's dynamics are described in FIGURE 1.5. Playing games A and B′ individually will lead to a net loss over time, but a winning outcome can be achieved under certain combinations of games A and B′. The claim is that if the choice of winning probabilities is $p_1 = \frac{9}{10} - \epsilon$, $p_2 = p_3 = \frac{1}{4} - \epsilon$, and $p_4 = \frac{7}{10} - \epsilon$, then game B′ is a losing game, while stochastic switching between games A and B′ with equal probabilities is a winning outcome for $\epsilon = 0.005$. A similar analysis to SECTION 1.1.1 can be performed to find the domain of ϵ for which Parrondo's effect is observed. Consequently, the Markov chain representation now contains four states, each corresponding to the historic states $(t-1,\ t-2)$, as shown in FIGURE 1.6.

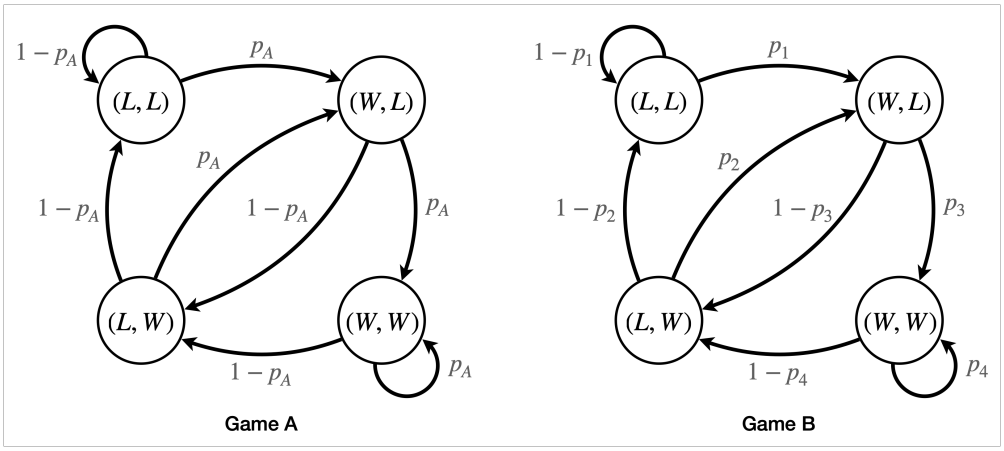

FIGURE 1.6: Markov chain representation of the history-dependent Parrondo's games.

The conditions for Parrondo's effect to be observed for a random switching are:

$$\begin{aligned} \frac{1-p}{p} &> 1, \\ \frac{(1-p_4)(1-p_3)}{p_1 p_2} &> 1, \quad \text{and} \\ \frac{(1-q_4)(1-q_3)}{q_1 q_1} &< 1, \end{aligned} \tag{1.9}$$

where $q_i = \gamma p_A + (1-\gamma)p_i$, for $i = 1, \ldots, 4$. In the case of random switching with equal probabilities, $\gamma = 0.5$. We can get the domain of the bias parameter to be $0 < \epsilon \leq 0.0059$ when rounded to the nearest two significant figures. Simulations can be performed for $\epsilon = 0.005$, and the empirical outcome is shown in FIGURE 1.7, with capital at $t = 100$ also recorded in TABLE 1.1. The latter is another way of showing Parrondo's paradox, as the change of capital, ∂c for games A and B is negative, while the capital for the random switching is positive.

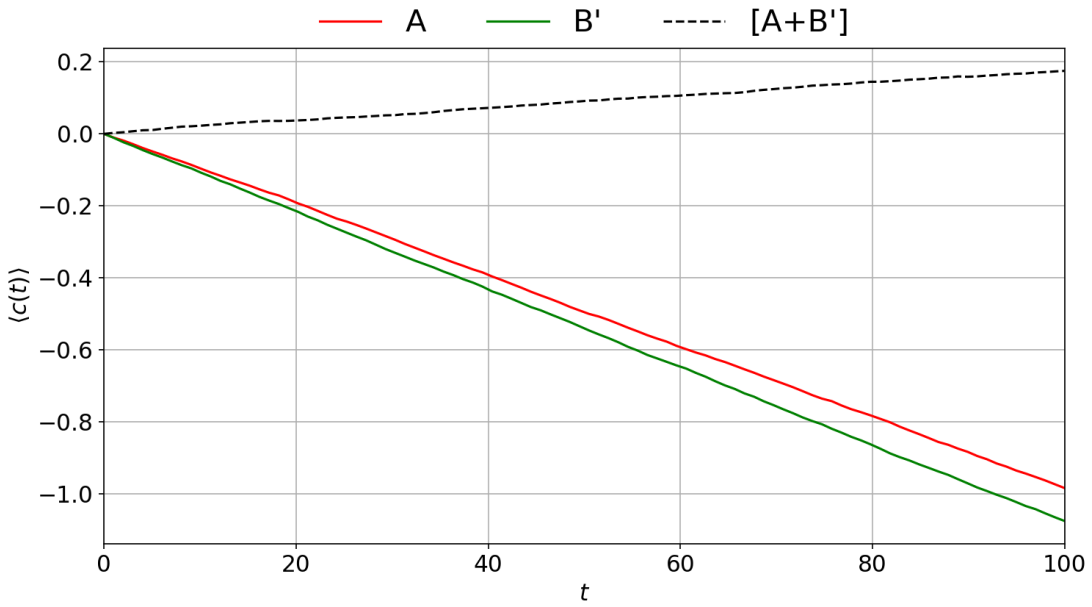

FIGURE 1.7: Average capital $\langle c(t) \rangle$ against time for the history-dependent Parrondo's games. The capital is averaged over 10^6 simulations for $t_{max} = 100$ time steps for $\epsilon = 005$.

TABLE 1.1: Rate of change of capital for games A and B, and average capital at $t = 100$.

	∂c ($\times 10^{-2}$)	$\langle c(100) \rangle$
Game A	-0.999	-1.01
Game B	-1.09	-1.07
[A+B']	0.196	0.190

1.3 Cooperative Parrondo's paradox

The third class of Parrondo's games is the cooperative Parrondo's paradox [13]. In this class of games, an ensemble of N players arranged in a ring topology, each with distinct capital $c_i(t)$, is considered. The rules for gaining or losing capital are the same as in the previous two classes. If a player wins, the capital of that player increases by one unit, $c_i(t) = c_i(t-1) + 1$. Conversely, a loss results in the loss of one unit of capital. Since there are N players, instead of considering each player's capital, it would be more meaningful to consider how the average capital evolves with time t. We define the average capital as

$$C(t) = \frac{1}{N}\sum_{i=1}^{N} c_i(t). \tag{1.10}$$

At each discrete time t, a player is randomly chosen from the ensemble of N players, say i. Player i then plays one of two losing games, in accordance with some rule. If i wins, i will be labelled "win", otherwise, i will be labelled "lose". This label remains unchanged until player i is selected to play again. In cooperative Parrondo's paradox, game A is unchanged from the one discussed in previous sections. The other losing game, we call it B", follows a social rule dependent on the labels of i's two neighbouring players, $i-1$ and $i+1$ (assuming periodic boundary conditions). The game's dynamics are described in FIGURE 1.8. The probability of winning at time t is given by:

- p_1, if player at $i-1$ is "lose" and player at $i+1$ is "lose",
- p_2, if player at $i-1$ is "lose" but player at $i+1$ is "win",
- p_3, if player at $i-1$ is "win" but player at $i+1$ is "lose", and
- p_4, if player at $i-1$ is "win" and player at $i+1$ is "win".

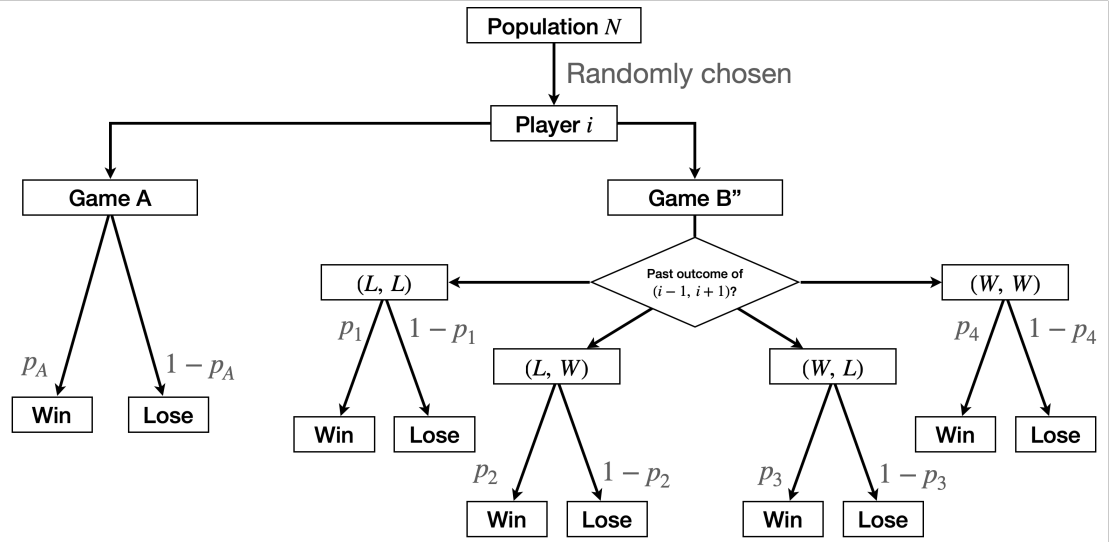

FIGURE 1.8: The cooperative Parrondo's paradox.

In such cases, master equations governing the dynamics of game B" cannot be solved explicitly. Thus, numerical simulations are helpful in proving that the choice of p_A for game A and p_i, $\forall i \in \{1, \ldots, 4\}$ for game B does indeed lead to Parrondo's paradox under stochastic switching. We show that for the population size of $N = 100$, with probabilities $p_A = 0.495$, $p_1 = 0.1$, $p_2 = p_3 = 0.16$, and $p_4 = 0.7$, Parrondo's paradox emerges (see FIGURE 1.9). We note that these probabilities are not exceptional examples. There are many other sets of probabilities that lead to this paradoxical result.

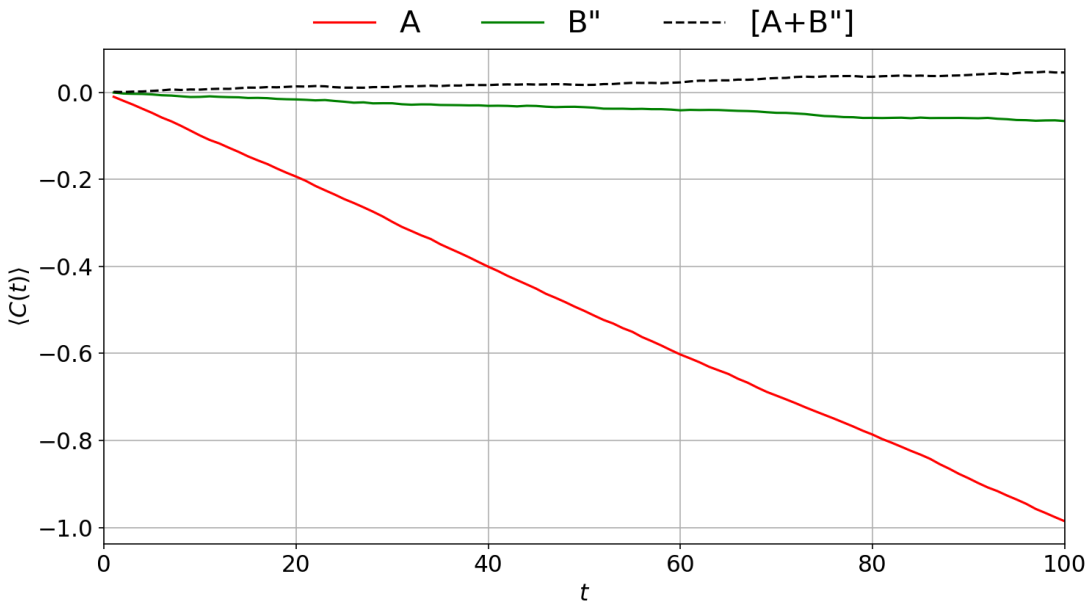

FIGURE 1.9: Average capital of the ensemble of players $\langle C(t) \rangle$ against time for the cooperative Parrondo's games. The capital is averaged over 10^6 simulations for a population size of $N = 100$, and $t_{max} = 100$ time steps.

1.4 Evidence of Parrondo's paradox

Having discussed the various forms of Parrondo's paradox, it is clear that for simple coin-toss games, it is possible to provide a resolution to the paradox. The study of apparent paradoxes, such as Simpson's and Braess's paradoxes, and that of Parrondo, is an exciting starting point for discovering or explaining real-world phenomena. Although the seminal capital-dependent Parrondo's paradox is constructed in the form of a toy model, it gets its inspiration from a physics phenomenon — the flashing Brownian ratchet. Thus, as a research community, the scope of Parrondo's paradox has broadened to be used as a sufficiently simplified model in search of an explanation for real-world phenomena. Consequently, simplified models can be made complex to simulate real-world observations and explain the emergence of complex phenomena to understand more complex systems.

Since it was first announced in 1996, Parrondo's paradox has been used to explain phenomena in various fields. In the following paragraphs, I will discuss a few of these

discoveries, which often take a more expansive definition depending on the area of discovery and application. But, in general, it can be described concisely in the form of an equation: Game A + Game B = Game C, where games A and B trend in the same way, but a combination of both games lead to an outcome that trends in the opposite way.

This paradoxical result can be found in dynamical systems, where the combination of chaotic and noise-induced systems results in ordered regularity [14]. Another surprising example that emerges from dynamical systems is a switched system that alternates between unstable modes but exhibits antiresonance for a wide range of switching frequencies [15]. In systems, and engineering optimization, an attempt to enhance efficiency in the design process of electron-optical systems, an optimization method based on the Levenberg–Marquardt algorithm, was adopted. The method proposed yields a superior convergence performance than the constituent genetic and Levenberg–Marquardt algorithms individually [16, 17].

Parrondo's paradox has also been applied, as a model, to explain phenomena in cell biology, ecological behaviour, and population dynamics. An example of the emergence of Parrondo's paradox in cell biology is cell growth research. Alternating between lysis and lysogeny is a winning strategy for a bacteriophage, even when each strategy individually is at a disadvantage compared with a competing bacteriophage. [18]. Specifically for tumorigenesis, given the environmental adversity in which malignant cells emerge and evolve, it is observed that oncogenic selection would favour Parrondo's dynamics. The alternation between various less optimal strategies would present a viable option to counteract the changing and deleterious environments that cells are exposed to [19]. Thus, for cancer therapy, the environment of a tumour can potentially be manipulated to suppress cancer progression [20]. For multicellular organisms, it is shown that the lifespan of organisms can be extended, and the onset of cancer can be delayed if cells alternate between competitive and cooperation [7]. In ecological behaviour, for instance, the alternation of ecological populations between nomadic and colonial behaviours is critical in allowing survival amidst resource scarcity [21, 22, 23, 24, 25].

Quantum Parrondo's paradox is another up-and-coming field that has emerged from the study of Parrondo's paradox. However, this area of research has been primarily contained in replicating classical Parrondo's games using quantum protocols. Various authors have successfully replicated the quantum equivalent of capital-dependent games by adapting various components of Parrondo's games. Miszczak et al. proposed a quantum implementation of a capital-dependent Parrondo's paradox [26, 27]. Flitney et al. extended the work on history-dependent Parrondo's paradox by presenting the results in two ways: operation on a qubit [28] and quantum walks [29]. Lastly, quantum walk implementation of the cooperative Parrondo's paradox was demonstrated by Bulger et al. through numerical simulations [30]. Further research in quantum Parrondo effects will be discussed in chapter 2.

Building on cooperative Parrondo's paradox, variants of the cooperative Parrondo's paradox, by attempting to change the social rules assigned to both games A and B" have been explored. This includes analysis of efficient voting [31, 32, 33] through collective

decision, expediting information spread [34], maximizing the matching problem [35], and redistributing wealth for effective resource management [36]. Further research in real-world sociodynamical systems and explaining sociodynamical phenomena will be discussed in chapter 4.

1.5 Objectives and scope of thesis

Based on the present literature in the broader field of Parrondo's paradox, the area of quantum Parrondo's paradox is identified to be a growing field with modern technological advances. There are two identified entry points to extend the field of quantum Parrondo's paradox. Firstly, current research focuses on finding an analogous quantum protocol to reproduce the quantum analogue of existing seminal Parrondo's games. The approach, however, is not to indefinitely determine more quantum analogues, as many of which collapse to the same classical outcome in the classical limit. Thus, one approach is to develop a working example of quantum Parrondo's paradox without having to start from classical systems as an analogue.

Secondly, in classical discrete Parrondo's paradox, stochasticity or randomness is necessary to allow the paradoxical result to emerge. Such stochasticity in classical Parrondo's games is almost always artificially introduced into the system to model natural phenomena. However, such randomness (noise or decoherence) is fundamentally built into the classical limit of quantum systems. The noise that results from the classical limit could come from approximations in observing quantum systems due to the lack of precision of instruments or decoherence where information is lost to the environment. Thus, a second approach to extending the field of quantum Parrondo's paradox is introducing naturally occurring quantum systems and measurement as a form of Parrondo's paradox. This includes introducing apparent randomness from quantum chaotic and chaotic dynamical systems as a form of switching further to develop the field of quantum Parrondo's games.

Having identified these two entry points, this thesis seeks to fill the critical gap by contributing to a deeper and more comprehensive understanding of chaotic switching between quantum systems and their application.

Another area of interest that is an emerging field is the extension of the cooperative Parrondo's paradox to real-world situations. Examining the current literature, the leading research focuses on cooperation and competition among agents, resource redistribution to boost collective social welfare, and effective information flow and decision-making, with the bulk of literature in the former two categories. However, the research in these categories often considers homogeneous agents and thus follows the same social rules. As in the case of the cooperative Parrondo's paradox, when randomly chosen, all players win or lose based on the state of their neighbours. In reality, players should respond differently. Thus, the possibility of multi-player, non-homogeneous social rules should be explored to simulate real-world phenomena. I have further assessed that research into information flow and decision-making can be further developed concerning Parrondo's paradox. Moreover, there is a need to consider complex systems that include how the effect of Parrondo's paradox can be affected by the network's topology.

The first aim of this research is to expand the contribution to the field of quantum Parrondo's paradox by considering quantum systems with no analogous classical system and to provide a working example of how it can be helpful in encryption. The second aim is to develop a comprehensive framework that applies to researchers to extend the field of Parrondo's paradox applied to sociodynamical systems and show its diverse use in real-world situations.

The objectives are outlined in the chapters forming the thesis. In Chapter 2, the quantum Parrondo effect emerging from quantum random walks by applying quantum algorithms for a 2-sided and 4-sided quantum coin toss is being studied. An attempt to explain the paradox, which has no classical counterpart, is then provided. Subsequently, in Chapter 3, classical chaotic switching is injected into the quantum coin toss protocol to show potential application to semi-classical encryption. Chapters 4-6 explores the various applications of Parrondo's paradox to model or solve problems in sociodynamical systems. Chapter 4 explores a new type of Parrondo's paradox framework that amalgamates sociodynamics and Parrondo's paradox, termed preference aggregation Parrondo's paradox. An extensive application of preference aggregation of Parrondo's paradox to real-life social phenomena, such as "ill-informed advising the ill-informed" and the emergence of Simpson's paradox in risk-taking Parrondo's games are explored. Chapter 5 shows that network synchronization based on real-world decision-making heuristics on Parrondo's games preference can boost capital. Chapter 6 analyzes how capital is affected in various controlled-collective single-prioritization voting schemes. Finally, in Chapter 7, the global outlook on Parrondo's paradox in these two domains—quantum Parrondo's paradox and Parrondo's paradox in sociodynamical systems are given.

Chapter 2

Quantum Parrondo's Paradox

The increasing development of quantum game theory and interest in quantum information and field-theoretic approaches to quantizing classical Parrondo's paradox has incentivised a further look into the field of quantum Parrondo's paradox [28]. In the immediate section, I will review the developments in translating the capital-dependent Parrondo's paradox into quantum Parrondo's games. In subsequent sections, I will lay out the framework for the quantum model that I introduced, and its uniqueness that adds to the knowledge in the field of quantum Parrondo's paradox. Followed by a concluding section to showcase the development in quantum Parrondo's paradox since my contribution to the field.

2.1 Quantum protocols and the capital-dependent Parrondo's paradox

To understand the evolution of quantum Parrondo's paradox from classical Parrondo's games, we first need to grasp the link between classical and quantum theories. This is schematically represented in FIGURE 2.1.

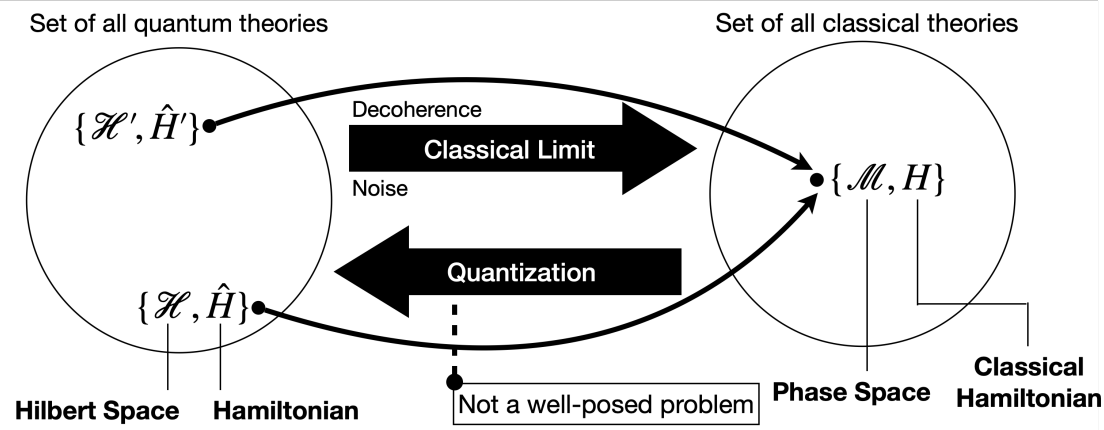

FIGURE 2.1: Schematic summary of the connection between Quantum theories and Classical theories. Image adapted from Advanced Quantum Theory, Lecture 1 by Tobias Osborne [37].

A quantum theory is defined by a tuple given by a Hilbert space $\mathcal{H}$ and Hamiltonian $\hat{H}$, where $\hat{H}$ is a self-adjoint time operator in $\mathcal{H}$, and generator of time evolution. Analogously, a classical theory is defined as a pair containing a phase space $\mathcal{M}$ and a classical Hamiltonian H. The "classical limit" is the process of obtaining an effective classical theory from an observation in quantum theory. The classical limit is the effective result of a combination of two factors, decoherence, and imperfection in measurements contributing to the noise. Conversely, "quantization" is the process of inverting a classical theory by mapping it to a quantum theory. However, quantization as a process is not a well-posed problem because there exist classical theories that are derived from multiple quantum theories in the classical limit.

Our universe is inherently quantum mechanical. However, we perceive the universe in its classical limit, largely described by classical theories through our observations of the universe. It is thus widely accepted that the developments in quantum mechanics have opened possibilities in many areas of applied physics and engineering that far supersede that of classical mechanics as we decipher the true nature of our universe. Therefore, a natural progression to Parrondo's paradox as a tool to explain a broader class of the natural world is to advance our knowledge in quantum Parrondo's games. Intuitively, the first step is to model classical games using quantum protocols in commutative algebra to recreate classical results. This is the first thrust in developing quantum Parrondo's paradox, by starting from known classical results and reconstructing its quantum counterpart. We discuss these developments in this section.

The quantum equivalent of the capital-dependent, or the intuitively-named position-dependent Parrondo's games (for the quantum equivalent), has been successfully simulated in various works. Meyer and Blumer devised a "coin"-flipping quantum model by mapping the capital to the discrete one-dimensional position of a particle in Brownian motion [38]. Meyer extended this work to include noise [39].

When measured, the quantum particle is in the state $|x, \alpha\rangle$. The first component is the position of the quantum particle $x \in \mathbb{Z}$, and the second is the momentum of the particle $\alpha \in \{\pm 1\}$. In the work of Meyer and Blumer, an initial zero-momentum state is chosen, given by

$$\frac{1}{\sqrt{2}} \left(|0, +1\rangle + |0, -1\rangle \right). \tag{2.1}$$

The 2-sided quantum coin is represented by a two-level system, such as a spin-$\frac{1}{2}$ particle in the superposition states $|+1\rangle$ and $|-1\rangle$. An unbiased coin is represented by the unitary matrix

$$\hat{C} = \begin{pmatrix} \cos\theta & i\sin\theta \\ i\sin\theta & \cos\theta \end{pmatrix}. \tag{2.2}$$

Thus, a particle in the Hilbert space must satisfy

$$\psi = \sum \psi_{x,\alpha} |x, \alpha\rangle, \text{and} \sum |\psi_{x,\alpha}|^2 = 1, \tag{2.3}$$

where $\psi_{x,\alpha} \in \mathbb{C}$ is the probability amplitude of the state $|x, \alpha\rangle$, and $|\psi_{x,\alpha}|^2$ is the probability that, if measured in this basis, the particle is observed to be in the state $|x, \alpha\rangle$. Noting that a position-dependent phase $e^{-iV(x)}$, with potential $V(x)$, will not change the

unitary property of the evolution, the quantum Parrondo's problem is reduced to picking parameters θ and $V(x)$ to achieve the paradoxical effect. Meyer and Blumer managed to show Parrondo effect by choosing $\theta = \frac{\pi}{4}$, and potential functions $V_A(x) = \frac{2\pi}{5000}x$ and $V_B(x) = \frac{\pi}{3}[1 - \frac{1}{2}(x \mod 3)] + V_A(x)$, with corresponding unitary evolution matrix $\hat{C}_A$ and $\hat{C}_B$, respectively. This effect is realised by applying the 5-play sequence $\hat{C}_B\hat{C}_A\hat{C}_A\hat{C}_A\hat{C}_A$ periodically for 100 plays. However, with an increasing number of plays (Meyer and Blumer showed up to 5000 plays), Meyer and Blumer noted that Parrondo effect disappears in favour of oscillatory behaviours.

The position-dependent phase is the term that resulted in the oscillatory behaviour that resulted in the disappearance of Parrondo effect. In keeping with the aim of recreating the seminal capital-dependent Parrondo's paradox using quantum states, Meyer and Blumer introduced the position-dependent phases to the evolution unitary matrix. As a result, the oscillatory behaviour emerges at a longer time scale. Thus, this motivated my work to simplify the model used by Meyer and Blumer to obtain a minimum working protocol of quantum Parrondo's games, while ensuring that Parrondo effect is present at longer time scales.

2.2 Quantum coin-toss random walk Parrondo's paradox

Consider a classical discrete walk along $x \in \mathbb{Z}$, determined purely by the result of a fair coin toss. A fair coin toss has two possible faces as outcomes, heads and tails, with an equal probability of landing on either face. In the case when the coin-toss lands on heads, the classical walker is boosted in the positive direction, that is $x + 1$; otherwise, the walker is boosted in the negative direction, $x - 1$. The probability distribution of a classical discrete walk determined by a fair coin toss can be visualized using a tableau. The symmetric entries of TABLE 2.1 imply that the mean position of the discrete classical walk is zero, that is $\langle x_m \rangle_{\mathrm{C}} = 0$, which remains true for $m \to \infty$, where m is the number of coin tosses, and steps taken. Here, the subscript C denotes the expected position in the *classical* regime.

TABLE 2.1: Probabilities for each position in a classical walk determined by a coin toss for $m \in [0, 4]$ steps. Empty entries have a probability of zero.

	-4	-3	-2	-1	0	1	2	3	4
$m = 0$					1				
$m = 1$				$\frac{1}{2}$		$\frac{1}{2}$			
$m = 2$			$\frac{1}{4}$		$\frac{1}{2}$		$\frac{1}{4}$		
$m = 3$		$\frac{1}{8}$		$\frac{3}{8}$		$\frac{3}{8}$		$\frac{1}{8}$	
$m = 4$	$\frac{1}{16}$		$\frac{1}{4}$		$\frac{3}{8}$		$\frac{1}{4}$		$\frac{1}{16}$

Inspired by the classical random walk, and the operation of two quantum coins on a single walker [40], we devise a new form of quantum Parrondo's paradox. Suppose we have a quantum process with basis state $|x, \alpha\rangle$. The Hilbert space of this state is $\mathcal{H} = \mathcal{H}_c \otimes \mathcal{H}_x$, where in the case of a 2-sided quantum coin, $\mathcal{H}_c = \mathrm{span}\{|\uparrow\rangle, |\downarrow\rangle\}$ indicates heads and tails, respectively, and in a 1-dimensional quantum walk, $\mathcal{H}_x = \mathrm{span}\{|x\rangle : x \in \mathbb{Z}\}$ indicating the position along the x-axis. A transformation analogous

to a discrete walk involves two operations. At each step, we (1) flip the quantum coin (the coin operator $\hat{C}$) and (2) boost the walker corresponding to the result of the first transformation by discrete steps s_x (the translation operator $\hat{S}$).

A general 2-sided quantum coin is an arbitrary superposition of two states,

$$|c\rangle = a_\uparrow|\uparrow\rangle_c + a_\downarrow|\downarrow\rangle_c, \quad |a_\uparrow|^2 + |a_\downarrow|^2 = 1, \tag{2.4}$$

with the basis (corresponding to heads and tails),

$$|\uparrow\rangle_c = \begin{bmatrix}1\\0\end{bmatrix}, \quad |\downarrow\rangle_c = \begin{bmatrix}0\\1\end{bmatrix}. \tag{2.5}$$

The transformation given by the coin operator $\hat{C}$ takes the form of a 2×2 general unitary operator,

$$\hat{C}(\rho, \alpha, \beta) = \begin{pmatrix} \sqrt{\rho} & \sqrt{1-\rho}e^{i\alpha} \\ \sqrt{1-\rho}e^{i\beta} & -\sqrt{\rho}e^{i\alpha\beta} \end{pmatrix}, \tag{2.6}$$

where $0 \leq \rho \leq 1$, $0 \leq \alpha, \beta \leq \pi$. The position of the quantum walker is represented as a superposition of Sp possible states,

$$|x\rangle = \sum_k a_k|k\rangle_p, \quad \sum_k |a_k|^2 = 1. \tag{2.7}$$

The shift operator $\hat{S}$ takes the form:

$$\hat{S} = |\uparrow\rangle_c\langle\uparrow| \otimes \sum_k |k + s_\uparrow\rangle_p\langle k| + |\downarrow\rangle_c\langle\downarrow| \otimes \sum_k |k + s_\downarrow\rangle_p\langle k|, \tag{2.8}$$

where $s_j, j \in \{\uparrow, \downarrow\}$ is the number of steps taken by the walker in a random walk. Thus, the entire transformation is unitary and combines the coin operator and translation operator, given by

$$\hat{U} = \hat{S}(\hat{C} \otimes \hat{I}_p), \tag{2.9}$$

where $\hat{I}_p$ is the identity operator of size $p \times p$. The initial state of the quantum walker is $|\psi\rangle_0$, and m steps are taken by applying the unitary operator m times, the state is thus represented by

$$|\psi\rangle_m = \hat{U}^m|\psi\rangle_0. \tag{2.10}$$

2.2.1 Example of calculation

Consider the following:

1. An initial state
$$|\psi\rangle_0 = |\alpha\rangle_c \otimes |x\rangle_p \tag{2.11}$$
the initial position x, with momentum α, which can also be written simply as $|x, \alpha\rangle$.

2. A coin operator

$$\hat{C} = \begin{pmatrix} a & b \\ c & d \end{pmatrix}, \tag{2.12}$$

satisfying $|a|^2 + |b|^2 = |c|^2 + |d|^2 = 1$, where $a, b, c, d \in \mathbb{C}$. The coin operator has the following effect on a state $|x, \alpha\rangle$:

$$\hat{C}|x, \uparrow\rangle = a|x, \uparrow\rangle + b|x, \downarrow\rangle, \tag{2.13}$$

$$\hat{C}|x, \downarrow\rangle = c|x, \uparrow\rangle + d|x, \downarrow\rangle. \tag{2.14}$$

3. A shift operator

$$\hat{S} = |\uparrow\rangle_c\langle\uparrow| \otimes \sum_k |k + s_\uparrow\rangle_p\langle k| + |\downarrow\rangle_c\langle\downarrow| \otimes \sum_k |k + s_\downarrow\rangle_p\langle k|, \tag{2.15}$$

The shift operator has the following effect on a general state $|x, \alpha\rangle$:

$$\hat{S}|x, \uparrow\rangle = |x + s_\uparrow, \uparrow\rangle, \tag{2.16}$$

$$\hat{S}|x, \downarrow\rangle = |x + s_\downarrow, \downarrow\rangle, \tag{2.17}$$

in short, the quantum walker shifts $s_\uparrow$ "steps" if "heads", and $s_\downarrow$ "step" if "tails". To parallel the classical random walk, we set $s_\uparrow = 1$, and $s_\downarrow = -1$; this is also called a symmetric boost.

Consider an initial state $|0, \uparrow\rangle$, with quantum coin

$$\hat{C} = \frac{1}{\sqrt{2}} \begin{pmatrix} 1 & 1 \\ 1 & -1 \end{pmatrix}, \tag{2.18}$$

and shift operator $s_\uparrow = 1$, and $s_\downarrow = -1$. We compute up to 4 steps, with the probability distribution found in TABLE 2.2. We obtain the probabilities by taking $\sum_k \langle x|\psi\rangle_m, \forall x$, $m = 1, \ldots, 4$.

Step 0: $|0, \uparrow\rangle$ (2.19)

Step 1: $\frac{1}{\sqrt{2}}|1, \uparrow\rangle + \frac{1}{\sqrt{2}}|-1, \downarrow\rangle$

Step 2: $\frac{1}{2}|2, \uparrow\rangle + \frac{1}{2}|0, \downarrow\rangle + \frac{1}{2}|0, \uparrow\rangle - \frac{1}{2}|-2, \downarrow\rangle$

Step 3: $\frac{1}{2\sqrt{2}}|3, \uparrow\rangle + \frac{1}{2\sqrt{2}}|1, \downarrow\rangle + \frac{1}{\sqrt{2}}|1, \uparrow\rangle - \frac{1}{2\sqrt{2}}|-1, \uparrow\rangle + \frac{1}{2\sqrt{2}}|-3, \downarrow\rangle$

Step 4: $\frac{1}{4}|4, \uparrow\rangle + \frac{1}{4}|2, \downarrow\rangle + \frac{3}{4}|2, \uparrow\rangle + \frac{1}{4}|0, \downarrow\rangle - \frac{1}{4}|0, \uparrow\rangle - \frac{1}{4}|-2, \downarrow\rangle + \frac{1}{4}|-2, \uparrow\rangle - \frac{1}{4}|-4, \downarrow\rangle$

Despite using a fair quantum coin, with a symmetric boost ($s_\uparrow = -s_\downarrow$), we note that the final state has a higher probability of being found in the $+x$-position, and not zero.

TABLE 2.2: Probabilities for each position in a quantum random walk. Empty entries have a probability of zero.

	-4	-3	-2	-1	0	1	2	3	4
$m=0$					1				
$m=1$				$\frac{1}{2}$		$\frac{1}{2}$			
$m=2$			$\frac{1}{4}$		$\frac{1}{2}$		$\frac{1}{4}$		
$m=3$		$\frac{1}{8}$		$\frac{1}{8}$		$\frac{5}{8}$		$\frac{1}{8}$	
$m=4$	$\frac{1}{16}$		$\frac{1}{8}$		$\frac{1}{8}$		$\frac{5}{8}$		$\frac{1}{16}$

2.3 Quantum Parrondo's methodology and results

This section considers the paradoxical outcome of tossing two fair quantum coins. For the purpose of simplicity, we consider the following fair quantum coins

$$\hat{C}_A = \frac{1}{\sqrt{2}}\begin{pmatrix} 1 & 1 \\ 1 & -1 \end{pmatrix}, \quad \hat{C}_B = \frac{1}{\sqrt{2}}\begin{pmatrix} -1 & -i \\ i & 1 \end{pmatrix}. \tag{2.20}$$

The shift operator is given by EQUATION (2.15), with $s_\uparrow = 1$ and $s_\downarrow = -1$. Lastly, the initial state is $|0, \uparrow\rangle$. We perform three experiments and present $\langle x_m \rangle_Q$ as a function of m, the number of quantum coin tosses:

(i) Successive tossing of a single fair quantum coin for both $\hat{C}_A$ and $\hat{C}_B$.

(ii) Random tossing of quantum coins $\hat{C}_A$ and $\hat{C}_B$ with equal probability.

(iii) Sequential periodic tossing of quantum coins $\hat{C}_A$ and $\hat{C}_B$.

The pseudocode to fully implement the quantum coin-toss Parrondo's paradox algorithm is presented in **Algorithm 2.1**.

Algorithm 2.1 The quantum coin-toss Parrondo's paradox algorithm.

1: Define up and down states as:
```
up = array([1,0]), down = array([0,1])
```
2: Define basis states for generic $\hat{C}$ (where `Cij` are the entries of $\hat{C}$):
```
C00 = outer(up,up), C01 = outer(up,down),
C10 = outer(down,up), C11 = outer(down,down)
```
3: Construct $\hat{C}_A$ and $\hat{C}_B$ from the basis states (termed `C_A and C_B`, respectively).
4: Construct $\hat{S}$ (where `P` is the number of possible positions `2m+1`):
```
S_hat = kron(roll(eye(P),1,axis=0),C00)
 + kron(roll(eye(P),-1,axis=0),C11)
```
5: Define initial state probability density array of $|x\rangle$:
```
posn0 = zeros(P), posn0[m] = 1
```
6: Define unitary operator $\hat{U}_A$ and $\hat{U}_B$ (termed `U_A and U_B`, respectively).
`U_i = S_hat.dot(kron(eye(P), C_i))`, here `i` $\in \{A, B\}$.
7: **while** $m < m_{max}$ **do** Evolution of state $|x\rangle$ through various strategies:
```
psi_m = matrix_power(U_i, 1).dot(psi0), psi0 = psi_m
```
8: **end while**

2.3.1 Results

We now consider the outcomes of tossing (i) $\hat{C}_A$ and $\hat{C}_B$ individually, (ii) $\hat{C}_A$ and $\hat{C}_B$ with random switching (denoted as $[\hat{C}'_A + \hat{C}'_B]$), and (iii) $\hat{C}_A$ and $\hat{C}_B$ with periodic switching. The average position $\langle x_m \rangle_Q$, against the number of steps m is plotted in FIGURE 2.2. The random switching protocol is averaged over 1000 simulations, and the periodic switching protocol, $[\hat{C}_A\hat{C}_B\hat{C}_B\hat{C}_A\hat{C}_B]$, is presented.

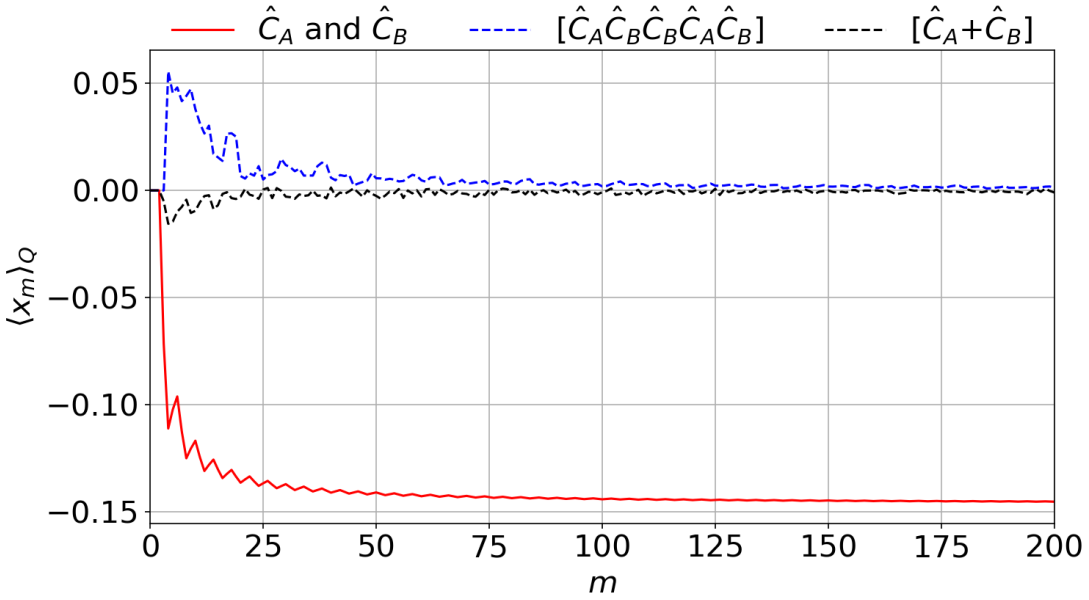

FIGURE 2.2: Expected position when tossing two 2-sided fair quantum coins $\hat{C}_A$ and $\hat{C}_B$ individually ($\langle x_{200} \rangle_Q \approx -0.14527$), randomly with equal probabilities ($\langle x_{200} \rangle_Q \approx -0.00097$), averaged over 1000 simulations, and in a periodic sequence $[\hat{C}_A\hat{C}_B\hat{C}_B\hat{C}_A\hat{C}_B]$ ($\langle x_{200} \rangle_Q \approx 0.00130$).

The tossing of $\hat{C}_A$ and $\hat{C}_B$ individually both result in the same outcome. The random switching $[\hat{C}'_A + \hat{C}'_B]$ with equal probabilities results in an almost-zero average position, while we show a single periodic switching $[\hat{C}_A\hat{C}_B\hat{C}_B\hat{C}_A\hat{C}_B]$ which leads to a net positive average position despite switching between two supposedly losing outcomes. However, an empirical observation suggests that both the random and periodic switching tends towards $\langle x_m \rangle \approx 0$ Hence, while we cannot conclude that we have strong Parrondo's paradox, we can conclude that the 2-sided fair quantum coin toss protocol leads to weak Parrondo's paradox [41][1].

2.4 Discussion

Two paradoxical outcomes need to be addressed:

(i) How does tossing a 2-sided fair quantum coin lead to a biased outcome?

[1]Weak Parrondo's paradox is a class of Parrondo's games where the combination of two losing games lead to a better-performing outcome.

(ii) How does switching between two 2-sided fair quantum coins, with inherently biased outcomes, lead to a fair outcome?

2.4.1 Biased outcome from tossing fair quantum coins

The first paradox is a known result and can be explained from the analytical derivation at each step. The paradox emerges because of the underlying principles of superposition and the collapse of a wave function. For any given state, it can be described by the position basis $|x\rangle_p$, $x \in \mathbb{Z}$, and the coin basis $|\alpha\rangle_c$, $\alpha \in \{\uparrow, \downarrow\}$. If at every step we measure the probability of the quantum walker being in each state, we recover the classical random walk with a probability distribution given in TABLE 2.1. Take for example Step 2 of EQUATION (2.19): the wave function is a superposition of four possible states, however, with only three possible outcomes, $(-2,\ 0,\ 2)$. Measurement at this stage collapses the wave function into one of three possible states with the following probabilities: $P(x = -2) = \frac{1}{4}$, $P(x = 0) = \frac{1}{2}$, and $P(x = 2) = \frac{1}{4}$; thus we recover row $m = 2$ of TABLE 2.1. By making a measurement, the wave function collapses, and the quantum mechanical information of the coin state is lost.

Consequently, by not making a measurement at every step, allowing the state to evolve with successive quantum coin tosses, a bias emerges based on the interaction of the quantum coin and shift operator on the initial state that the quantum walker is prepared in. Figure 2.3 shows the outcome from using the 2-sided quantum coin given by EQUATION (2.18), and shift operator given by EQUATION (2.15) (with $s_\uparrow = 1$ and $s_\downarrow = -1$) on various initial states, each with initial position 0.

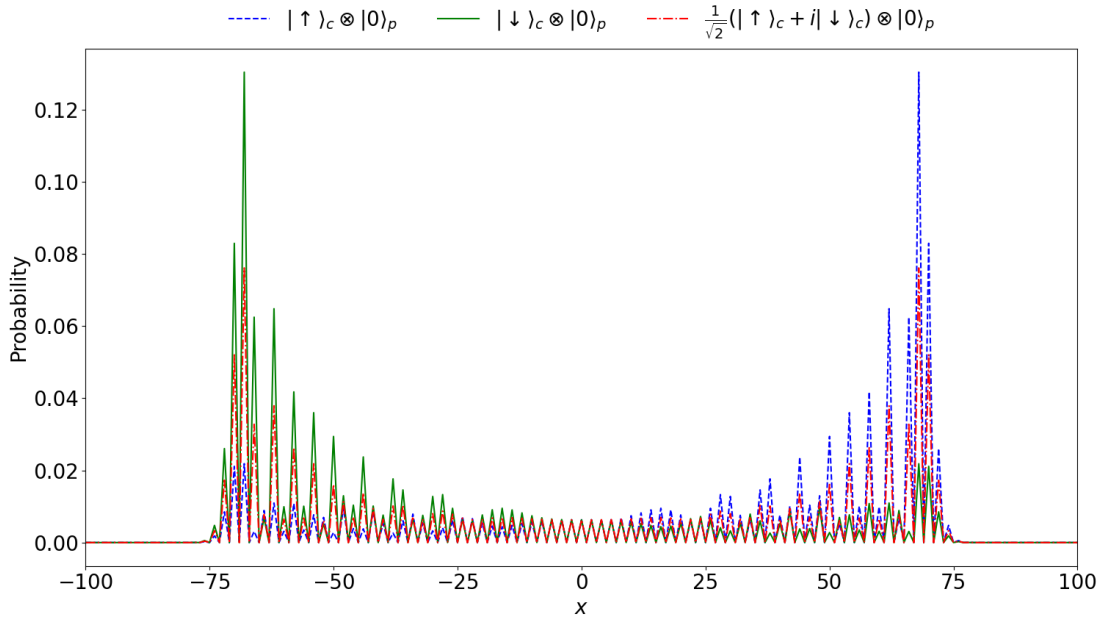

FIGURE 2.3: The probability distribution of the quantum coin toss protocol on various initial states can return net positive (blue, dashed), negative (green, solid), and fair (red, dotted-dashed) outcomes.

Figure 2.3 reveal that an initial state $|\uparrow\rangle_c \otimes |0\rangle_p$ yields a positive average position, while an initial state $|\downarrow\rangle_c \otimes |0\rangle_p$ yields a negative average position. Finally, a state with no initial boost $\frac{1}{\sqrt{2}}(|\uparrow\rangle_c + i|\downarrow\rangle_c) \otimes |0\rangle_p$ returns a fair outcome. Thus to design the 2-sided quantum coin-toss Parrondo's paradox, the initial state was specially chosen to have a negative average position for both quantum coins, despite the coins being inherently fair.

2.4.2 Weak Parrondo's paradox from the random tossing of quantum coins

FIGURE 2.2 suggests that the random and periodic switching between two fair quantum coins results in an average walking position of approximately zero. Let us now examine and attempt to explain why this is the case for random switching.

In general, $[\hat{C}_A, \hat{C}_B] \neq 0$, here the square bracket is the quantum commutator, and the order of coin-toss can be distinguished. However, it is noted that when periodic switching is employed, both the periodic switching $[\hat{C}_A\hat{C}_B]$ and $[\hat{C}_B\hat{C}_A]$ produce the same outcome (if acting on the same initial state), as does $[\hat{C}_A\hat{C}_A\hat{C}_B]$ and $[\hat{C}_B\hat{C}_B\hat{C}_A]$. In fact, these are not unique examples. If we have a sequence of tosses, we can change the sequence by swapping coin A for coin B, and vice-versa, i.e $\hat{C}_i \leftrightarrow \hat{C}_j$, and the sequence outcome will be the same. This is because all fair quantum coins are a linear combination of the outer products of states $|\uparrow\rangle$ and $|\downarrow\rangle$, as we have defined these two states to be the standard basis of dimension 2, thus both quantum coin operators are diagonalizable. Consequently, we can show that both quantum coin operators are similar, i.e we are able to express $\hat{C}_B = P^{-1}\hat{C}_A P$. Indeed this is true as, for the diagonal matrix J corresponding to the eigenvalues $\lambda = \pm 1$, we have

$$Q^{-1}\hat{C}_B Q = J = R^{-1}\hat{C}_A R \Rightarrow \hat{C}_B = (QR^{-1})\hat{C}_A(RQ^{-1}) \equiv P^{-1}\hat{C}_A P \tag{2.21}$$

Since both quantum coin operators are *similar matrices*, they represent the same operator under different bases [42]. This implies that the quantum superposition of states under the quantum coin operator $\hat{C}_i$ is a linear combination of the coordinates of $\hat{C}_j$. Thus, at each step m, when a quantum coin $\hat{C}_i$ is chosen, the information prior to the toss of that coin is preserved and represented on a different basis. This explains why despite $[\hat{C}_A, \hat{C}_B] \neq 0$, we obtain the same result when any sequence of fair quantum coins produces the same outcome even under $\hat{C}_i \leftrightarrow \hat{C}_j$. Furthermore, a combination of switching between the two coins is analogous to defining a new quantum coin $\hat{C}_R$, where $\hat{C}_R = \hat{C}_A + \hat{C}_B$,

$$\hat{C}_R = \begin{pmatrix} 0 & \frac{1}{\sqrt{2}}(1-i) \\ \frac{1}{\sqrt{2}}(1+i) & 0 \end{pmatrix}. \tag{2.22}$$

Following the rules stated in **Example 2.2.1**, we observe that given an initial state $|\psi\rangle_0 = |0,\uparrow\rangle$, under the quantum coin $\hat{C}_R$ and standard shift operator, we get the following:

$$\text{Step 0: } |\psi\rangle_0 = |0,\uparrow\rangle \tag{2.23}$$

$$\text{Step 1: } a|-1,\downarrow\rangle,\ a = \frac{1}{\sqrt{2}}(1-i)$$

$$\text{Step 2: } ba|0,\uparrow\rangle = ba|\psi\rangle_0,\ b = \frac{1}{\sqrt{2}}(1+i)$$

We always return to the state $|\psi\rangle_0$ with every even number of steps. At the odd number of steps, the average position diminishes with increasing m, hence it also has a limit of 0. This explains why the random switching between the two quantum coins gives a fair outcome. Hence the resolution to the paradox. Further work has to be done to example the properties of biased quantum coins to shed light on the effect of biased coins on the quantum coin-toss Parrondo's paradox. However, sticking to the ideas of fair quantum coins, is it possible to achieve strong Parrondo's paradox? One way is to change the step sizes $s_{\uparrow/\downarrow}$. For example, consider the initial state $|\psi\rangle_0 = |\downarrow\rangle_c \otimes |0\rangle_p$, the coin operators are the same as before, and the shift operator

$$\hat{S} = |\uparrow\rangle_c\langle\uparrow| \otimes \sum_k |k+2\rangle_p\langle k| + |\downarrow\rangle_c\langle\downarrow| \otimes \sum_k |k-1\rangle_p\langle k|, \tag{2.24}$$

here we boost the quantum walker 2 steps in the positive direction for the coin state $|\uparrow\rangle_c$, and 1 step in the negative direction for the coin state $|\downarrow\rangle_c$. The results are shown in FIGURE 2.4, again Parrondo's paradox can be achieved under random switching. This time, we get a strong Parrondo effect due to the boost in the positive direction. The ratcheting effect, also exhibited in the classical version of the capital-dependent Parrondo's paradox, is seen from the boost in the positive direction for coin state $|\uparrow\rangle_c$ by 2 steps, as opposed to a single boost in the negative direction for the state $|\downarrow\rangle_c$. We note, in hindsight, that this ratcheting effect is necessary for the emergence of Parrondo effect to be observed for random switching.

The other (more interesting) way is to consider other types of quantum coins. We attempt to get Parrondo's paradox from a shift operator with a fair boost.

2.5 4-sided quantum coin-toss Parrondo's paradox

There remains a critical gap when it comes to the generalization of Parrondo's paradox to the 2^n-sided quantum coin problem. We have shown that random switching is a weak form of the 2-sided fair quantum coin-toss framework. This begs the question, is it possible to construct a strong form of Parrondo's paradox with fair coins and shift? We show that by using the 4-sided quantum coin-toss protocol[2], it is possible.

[2]The 4-sided quantum coin can also be called the d4 quantum die. It is analogous to the 4-sided tetrahedral die. However, in this thesis, we will use the term "4-sided quantum coin" to highlight that it is, in theory, no different from the 2-sided quantum coin, but in a higher dimension.

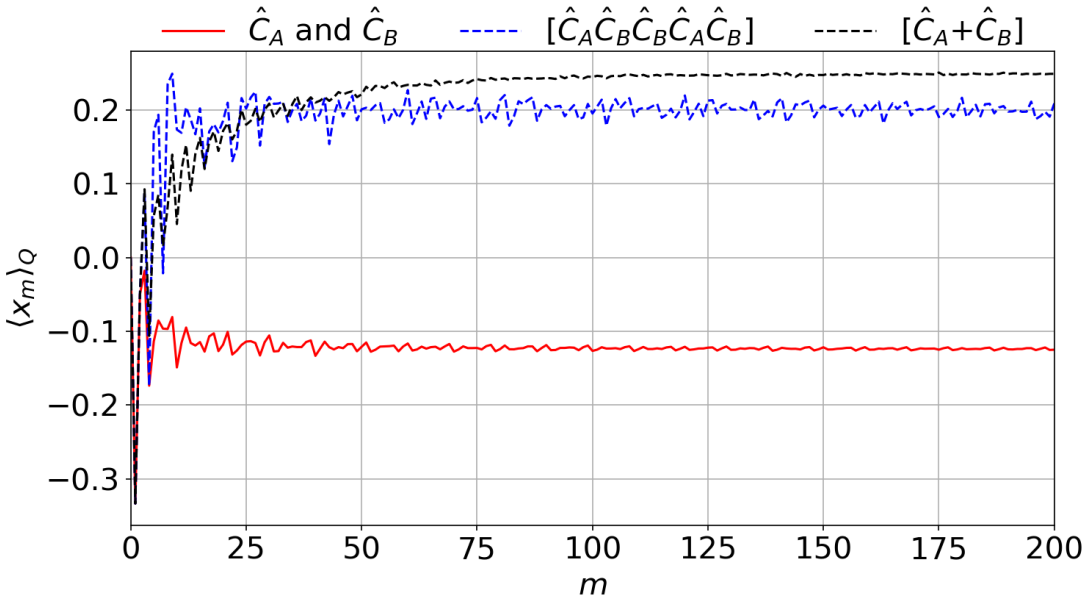

FIGURE 2.4: Expected position when tossing two 2-sided fair quantum coins $\hat{C}_A$ and $\hat{C}_B$ individually ($\langle x_{200}\rangle_Q \approx -0.12485$), randomly with equal probabilities ($\langle x_{200}\rangle_Q \approx 0.24900$), , averaged over 1000 simulations, and in a periodic sequence $[\hat{C}_A\hat{C}_B\hat{C}_B\hat{C}_A\hat{C}_B]$ ($\langle x_{200}\rangle_Q \approx 0.20885$).

A general four-sided quantum coin is an arbitrary superposition of four states,

$$|c\rangle = \sum_{n=0}^{3} a_n |n\rangle_c, \quad \text{where} \sum_n |a_n|^2 = 1, \tag{2.25}$$

with the basis,

$$|0\rangle_c = \begin{bmatrix} 1 \\ 0 \\ 0 \\ 0 \end{bmatrix}, \quad |1\rangle_c = \begin{bmatrix} 0 \\ 1 \\ 0 \\ 0 \end{bmatrix}, \quad |2\rangle_c = \begin{bmatrix} 0 \\ 0 \\ 1 \\ 0 \end{bmatrix}, \quad |3\rangle_c = \begin{bmatrix} 0 \\ 0 \\ 0 \\ 1 \end{bmatrix}. \tag{2.26}$$

The transformation given by the coin operator $\hat{C}'$ (the primed version is used to distinguish this from the 2-sided case) takes the form of a 4×4 unitary operator. The position of the quantum walker is represented as a superposition of p possible states The position of the quantum walker is represented as a superposition of p possible states,

$$|x\rangle = \sum_k \alpha_k |k\rangle_p, \quad \sum_k |\alpha_k|^2 = 1. \tag{2.27}$$

The shift operator $\hat{S}'$ takes the form:

$$\hat{S} = \sum_{n=0}^{3} \left(|n\rangle_c\langle n| \otimes \sum_k |k + s_n\rangle_p\langle k| \right), \tag{2.28}$$

where s_n is the number of steps taken by the walker in a random walk in any of the four possible boosts corresponding to the side of the quantum coin. Thus, the entire transformation is unitary and combines the coin operator and translation operator, given by

$$\hat{U}' = \hat{S}'(\hat{C}' \otimes \hat{I}_p), \tag{2.29}$$

where $\hat{I}_p$ is the identity operator of size $p \times p$. The initial state of the quantum walker is $|\psi\rangle_0$, and m steps are taken by applying the unitary operator m times, the state is thus represented by

$$|\psi\rangle_m = \hat{U}'^m|\psi\rangle_0. \tag{2.30}$$

Unlike the 2-sided quantum coin-toss version, the choice of coin operators is important in achieving the emergence of Parrondo's paradox. The coin operator takes the following Hadamard-like forms:

$$\begin{aligned} \hat{C}'_A &= \frac{1}{2}\begin{pmatrix} 1 & 1 & 1 & 1 \\ 1 & -1 & 1 & -1 \\ 1 & 1 & -1 & -1 \\ 1 & -1 & -1 & 1 \end{pmatrix}, \\ \hat{C}'_B &= \frac{1}{2}\begin{pmatrix} 1 & 1 & 1 & 1 \\ 1 & iAe^{i\beta} & -1 & -iAe^{i\beta} \\ 1 & -1 & 1 & -1 \\ 1 & -iAe^{i\beta} & -1 & iAe^{i\beta} \end{pmatrix}, \text{ with } \beta \in [0, \pi). \end{aligned} \tag{2.31}$$

In the case where $\beta \neq \{0, \pi\}$, then $\hat{C}'_B$ must be normalized with an appropriate constant A, otherwise $A = 1$. For the purposes of revealing that it is possible to obtain strong Parrondo effect, we set $\beta = 0$. The shift operator is:

$$\begin{aligned} \hat{S}' = |0\rangle_c\langle 0| \otimes \sum_k |k-1\rangle_p\langle k| + |1\rangle_c\langle 1| \otimes \sum_k |k+1\rangle_p\langle k| \\ + |2\rangle_c\langle 2| \otimes \sum_k |k-1\rangle_p\langle k| + |3\rangle_c\langle 3| \otimes \sum_k |k+1\rangle_p\langle k| \end{aligned} \tag{2.32}$$

Here, we see that the quantum walker is boosted 1 step in the negative direction for quantum states $|0\rangle_c$, and $|2\rangle_c$, while being boosted in the positive direction, by 1 step, for quantum states $|1\rangle_c$ and $|3\rangle_c$. In theory, there is an equal magnitude of boosts in the positive and negative direction, this is a fair shift operator. Thus, what we have now are two fair coin and shift operators. We use the initial state

$$|\psi\rangle_0 = |2\rangle_c \otimes |0\rangle_p. \tag{2.33}$$

2.5.1 Results and observations

Similar to the 2-sided quantum coin experiments, we now consider experiments for the 4-sided quantum coin-toss protocol. The simulation results for

(i) successive tossing of a single fair quantum coin for both $\hat{C}'_A$ and $\hat{C}'_B$,

(ii) random tossing of quantum coins $\hat{C}'_A$ and $\hat{C}'_B$ with equal probability, and

(iii) sequential periodic tossing of quantum coins $\hat{C}'_A$ and $\hat{C}'_B$,

are compiled in FIGURE 2.5, where the random switching protocol is averaged over 1000 simulations, and the best performing periodic protocol, $[\hat{C}'_A\hat{C}'_B\hat{C}'_B\hat{C}'_A]$, is presented. The remaining outcomes (for $m = 100$ steps) from other periodic protocols are found in TABLE 2.3.

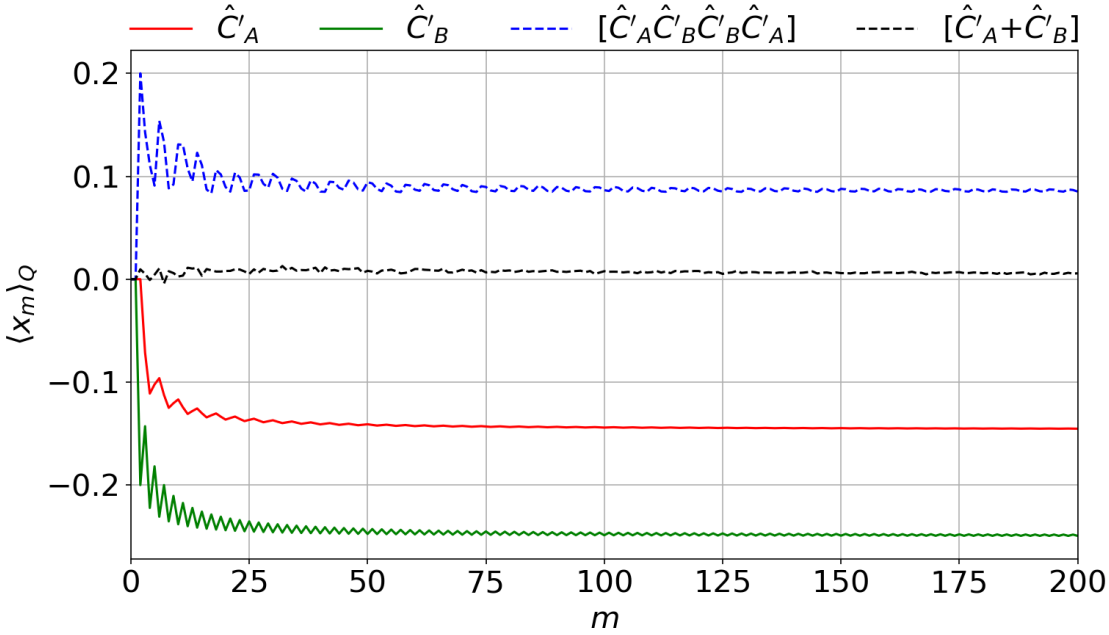

FIGURE 2.5: Expected position when tossing two 4-sided fair quantum coins $\hat{C}'_A$ and $\hat{C}'_B$ individually, randomly with equal probabilities, averaged over 1000 simulations, and in a periodic sequence $[\hat{C}'_A\hat{C}'_B\hat{C}'_B\hat{C}'_A]$.

FIGURE 2.5 and TABLE 2.3 show that under random switching and some periodic switching, it is now possible for two negative-position quantum walks derived from 4-sided quantum coin tosses to combine to give a positive-position quantum walk for fair quantum coin and shift operators. This was observed to be impossible for the tossing twir 2-sided quantum coins. Numerical simulations suggest that the average positions for all strategies asymptotically approach a constant. This leads me to conjecture that for any simple initial state $|\psi\rangle_0 = |i\rangle_c \otimes |0\rangle_p$, for $i = 0, \ldots, 3$, there exists a pair of fair 4-sided fair quantum coins $\hat{C}'$ and shift operator $\hat{S}'$, such that it will always lead to Parrondo's paradox under periodic switching. However, the task of finding a possible combination of operators and an initial state to achieve this is not efficient. Future

TABLE 2.3: A positive average position denotes a net "winning" outcome Notice that the average positions for $\hat{C}'_A$ and $\hat{C}'_B$ are individually negative but a random switching, and periodic switching produce positive outcomes.

Protocol	$\langle x_{100}\rangle_Q$	Protocol	$\langle x_{100}\rangle_Q$	Protocol	$\langle x_{100}\rangle_Q$
$\hat{C}'_A$ only	-0.14415	$[\hat{C}'_A\hat{C}'_B\hat{C}'_A]$	0.03987	$[\hat{C}'_A\hat{C}'_B\hat{C}'_B\hat{C}'_A]$	0.08650
$\hat{C}'_B$ only	-0.24876	$[\hat{C}'_B\hat{C}'_A\hat{C}'_A]$	-0.02021	$[\hat{C}'_B\hat{C}'_A\hat{C}'_A\hat{C}'_B]$	-0.06400
Random	0.00768	$[\hat{C}'_A\hat{C}'_B\hat{C}'_B\hat{C}'_B]$	0.00651	$[\hat{C}'_B\hat{C}'_A\hat{C}'_B\hat{C}'_A]$	0.00137
$[\hat{C}'_A\hat{C}'_B]$	-0.05437	$[\hat{C}'_B\hat{C}'_A\hat{C}'_B\hat{C}'_B]$	-0.05437	$[\hat{C}'_B\hat{C}'_B\hat{C}'_A\hat{C}'_A]$	-0.09677
$[\hat{C}'_B\hat{C}'_A]$	0.00137	$[\hat{C}'_B\hat{C}'_B\hat{C}'_A\hat{C}'_B]$	-0.05858	$[\hat{C}'_A\hat{C}'_A\hat{C}'_A\hat{C}'_B]$	0.02600
$[\hat{C}'_A\hat{C}'_B\hat{C}'_B]$	-0.02550	$[\hat{C}'_B\hat{C}'_B\hat{C}'_B\hat{C}'_A]$	-0.00131	$[\hat{C}'_A\hat{C}'_A\hat{C}'_B\hat{C}'_A]$	0.00903
$[\hat{C}'_B\hat{C}'_A\hat{C}'_B]$	-0.01624	$[\hat{C}'_A\hat{C}'_A\hat{C}'_B\hat{C}'_B]$	-0.09324	$[\hat{C}'_A\hat{C}'_B\hat{C}'_A\hat{C}'_A]$	0.01390
$[\hat{C}'_B\hat{C}'_B\hat{C}'_A]$	-0.03268	$[\hat{C}'_A\hat{C}'_B\hat{C}'_A\hat{C}'_B]$	0.00436	$[\hat{C}'_B\hat{C}'_A\hat{C}'_A\hat{C}'_A]$	0.02636
$[\hat{C}'_A\hat{C}'_A\hat{C}'_B]$	-0.01941				

work can examine and explore efficient methods to find such combinations that lead to Parrondo's paradox.

Additionally, FIGURE 2.5 suggests that the average position of all strategies has a sublinear relationship with the number of steps taken, the deterministic strategies with a negative correlation. In contrast, the random switching strategy has a positive correlation. In this sense, the 4-sided quantum coin-toss protocol with random switching is a quantum Parrondo's paradox. Our results also agree with the physical limits imposed by the Dirac equation, which is relativistic. The 4-sided quantum coin-toss Parrondo's paradox is a discretization of the Dirac equation for a single particle. The sublinear growth (and decay) of all the strategies ensure that the average position $\langle x_m\rangle_Q$ will not continue to grow quadratically beyond the light cone, thus not displaying relativistic behaviour. As such, I postulate that there is a limiting average position for all these strategies. However, there are no affirmative analytical means of proving this result, which motivates future work.

Furthermore, we have seen the introduction of a new form of Parrondo's paradox that does not have a classical equivalent. Note that the ratcheting boost provided by the shift operator alone is insufficient in leading to the emergence of Parrondo effect since pure strategies are also subjected to the same shift operator. Hence in the 4-sided quantum coin-toss Parrondo's paradox, the combined dynamics of the initial state $|\psi\rangle_0$, fair quantum coins $\hat{C}'$, and fair shift operator $\hat{S}'$ results in the emergence of strong Parrondo effect; a phenomenon not seen in its 2-sided counterpart.

2.6 Summary

The focus of this chapter is to introduce the 2- and 4-sided quantum coin-toss protocol, the former exhibiting weak Parrondo effect, while the latter displaying strong Parrondo's paradox. While it is computationally more straightforward to achieve weak Parrondo's paradox for the 2-sided quantum coin-toss, of interest in the community is strong Parrondo's paradox, which led to the first development of the 4-sided quantum

coin-toss, which is computationally more expensive to find a set of coins and shift operators that works. Since the development of the coin-toss protocol for use to show Parrondo's paradox, several extensions have been related to my work. For example, the work by Pires and Queirós [43] show that strong Parrondo's paradox can emerge from 2-sided quantum coin-toss quantum walks without requiring the use of 4-sided quantum coins (or higher-dimensional coins). They showed this by employing time-dependent coin operators without breaking the translation symmetry of the shift operator. Recently, Walczak and Bauer [44] further showed a form of Parrondo's paradox involving three quantum coins. They also experimented on quantum random walks for entangled states. While these developments have contributed to the theoretical extension of knowledge in the field of quantum coin-toss Parrondo's paradox, there is a need for practical application of these theories. Thus, in the next chapter, we explore an application of the quantum coin-toss protocol for an engineering problem.

Chapter 3

Semiclassical Chaotic Quantum Parrondo's Paradox

Semiclassical theory can be multiply defined. It can refer to a theory in which some parts of the system are described quantum mechanically while the other parts are treated classically. The other way in which semiclassical theory can be defined is by studying the classical limit of a quantum system where approximations are applied to gain clarity of the dynamics of the system. In this chapter, we adopt the first definition by using classical chaotic maps as a means of performing switching between two 2-sided fair quantum coins.

Previous work showed the benefits of adopting chaotic switching for various optimization problems, in particular, whether the introduction of chaos can help order to arise from disorder [45]. This has far-reaching applications, including self-organization of coupled systems with chaotic dissymmetry, chaos control, chaos-driven optimization strategies, and biological pattern formation in fruit fly embryos [46]. Other previous studies include adopting chaotic switching in classical Parrondo's games [47, 48]. The developments in classical Parrondo's games with chaotic switching with potential application to chaos control, and the developments in the use of controllable quantum systems to investigate certain fundamental aspects of nature [49, 50, 51] have motivated our study of applying chaotic switching to quantum Parrondo's games in search for applications of the two-sided quantum coin toss games.

3.1 Chaotic maps

Chaos is aperiodic long-term behaviour in a deterministic system that exhibits sensitive dependence on initial conditions. Chaotic and random sequences can be differentiated by their phase diagrams. Consecutive points of a chaotic sequence on a phase diagram are highly correlated (hence deterministic) but not in the case of a purely random sequence. A chaotic sequence is defined as, $X = (x_i)_{i=0}^{n}$, is generated by a map through an iterative composition of the function $f_n(\cdot)$, where the n-th term is

$$x_n = f_n(f_{n-1}(\dots f_2(f_1(x_0))\dots)). \tag{3.1}$$

For the purposes of instruction[1], we demonstrate the application of the following chaotic maps on the 2-sided quantum coin toss protocol:

1. Logistic map
$$x_{n+1} = ax_n(1 - x_n) \tag{3.2}$$

2. Sinusoidal map
$$x_{n+1} = ax_n^2 \sin(\pi x_n) \tag{3.3}$$

3. Tent map
$$x_{n+1} = \begin{cases} ax_n & \text{if } x_n \leq 0.5 \\ a(1 - x_n) & \text{otherwise} \end{cases} \tag{3.4}$$

The functions in these chaotic maps have a few things in common, namely, they depend only on the previous iteration value, and there is a parameter a, which we will term the *control parameter*. The value of the control parameter leads to a chaotic phenomenon termed *bifurcation*.

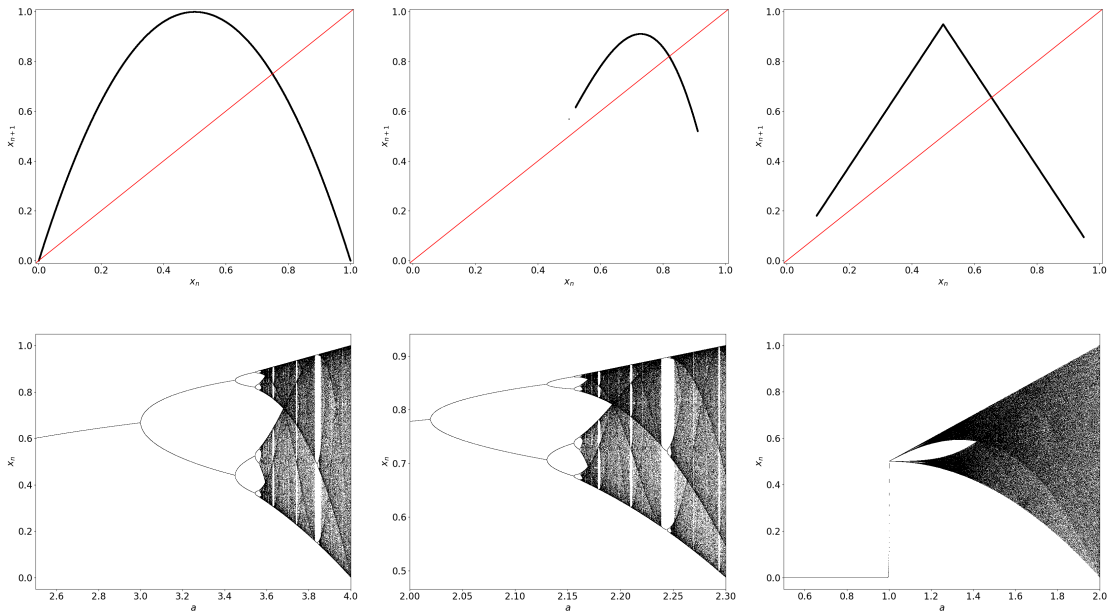

(A) Logistic map. (B) Sinusoidal map. (C) Tent map.

FIGURE 3.1: Phase portraits and bifurcation diagrams of the three chaotic maps. The control parameters chosen to generate the phase diagrams are $a = 4$, $a = 2.28$, and $a = 1.9$, with initial conditions $x_0 = 0.1$, $x_0 = 0.5$, and $x_0 = 0.8$, respectively. The diagrams are generated by plotting the next 1000 values of x_n after 10^5 iterations.

[1]There is a broad research field in dynamical and nonlinear systems to study the abstract equivalency of various chaotic maps [52]. Specifically, some fundamental aspects of chaotic dynamics are preserved under topological conjugacy. Consequently, showing that chaotic maps are topologically conjugate allows us to collect different maps of equivalent classes and therefore facilitates the understanding of more complicated dynamical systems in terms of simpler ones, thus further expanding the applications of chaotic switching in quantum Parrondo's games.

The phase portraits in FIGURE 3.1 show a strong correlation between each successive iteration. This is unlike the random map, where, in theory, there is no relationship between successive iterations. This begs the question: if random switching of two 2-sided quantum coin tosses on a quantum walker leads to weak Parrondo's paradox, can chaotic switching result in strong Parrondo's paradox?

3.2 The switching strategy and Parrondo's paradox results

In this section, we will first see the advantages of using chaotic switching over random switching. Similar to previous setups, we first choose:

1. an initial state

$$|\psi\rangle_0 = \frac{1}{2}[|\uparrow\rangle_c \otimes |2\rangle_p] - \frac{1}{2}[|\uparrow\rangle_c \otimes |0\rangle_p] + \frac{1}{2}[|\downarrow\rangle_c \otimes |0\rangle_p] + \frac{1}{2}[|\downarrow\rangle_c \otimes |-2\rangle_p], \quad (3.5)$$

   the choice of this initial state is chosen in retrospect;

2. two 2-sided coin operators

$$\hat{C}_A = \frac{1}{\sqrt{2}}\begin{pmatrix} 1 & 1 \\ 1 & -1 \end{pmatrix} \text{ and } \hat{C}_B = \frac{1}{\sqrt{2}}\begin{pmatrix} -1 & -i \\ i & 1 \end{pmatrix}; \quad (3.6)$$

   and

3. a shift operator

$$\hat{S} = |\uparrow\rangle_c\langle\uparrow| \otimes \sum_k |k+1\rangle_p\langle k| + |\downarrow\rangle_c\langle\downarrow| \otimes \sum_k |k-1\rangle_p\langle k|. \quad (3.7)$$

3.2.1 Adopting chaotic switching strategy

Consider three parameters, the control parameter a, the initial value x_0, and the switching threshold γ. Each of these three parameters is important in determining the switching strategy. Firstly, let us fix the condition for switching. The condition for switching for this chapter will be set as such: if $x_n < \gamma$, quantum coin A will be used; otherwise, quantum coin B will be used. Thus, for example, if we use the logistic map and set $a = 2.8$ and $\gamma = 0.6$, then, regardless of initial condition x_0, the chaotic sequence generated by these parameters will eventually converge towards the transient coin-toss sequence $[\ldots \hat{C}_B\hat{C}_B\hat{C}_B\hat{C}_B \ldots]$, as the bifurcation diagram in FIGURE 3.1, shows that the stable point for $a = 2.8$ is greater than γ. A different choice of a, say $a = 3.4$ will generate a different transient coin-toss sequence $[\ldots \hat{C}_A\hat{C}_B\hat{C}_A\hat{C}_B \ldots]$ regardless of initial condition. However, at the onset of chaos, it is imperative to note that a transient coin-toss sequence no longer exists, as the chaotic sequence is now sensitive to initial conditions.

As an example, take $a = 4.0$ and $\gamma = 0.5$. Two initial conditions $x_0 = 0.10, 0.11$ produce the chaotic sequences of the first ten iterations, $(A, A, B, A, B, B, B, A, A, B)$ and $(A, A, B, A, B, B, A, A, B, A)$, respectively. These are two distinctly different coin-toss sequences sensitive to the initial conditions. Having seen previously that the order

of applying quantum coin-toss affects the outcome, we can exploit this property of chaotic sequences in our quantum coin-toss protocol, especially for determining the switching sequence.

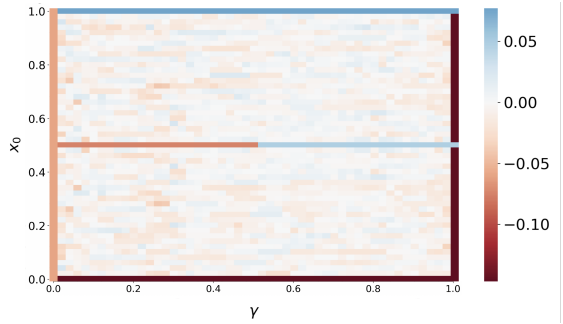

(A) Logistic map $a = 4.0$.

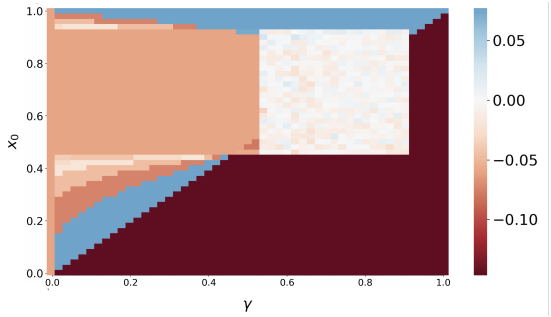

(B) Sinusoidal map $a = 2.28$.

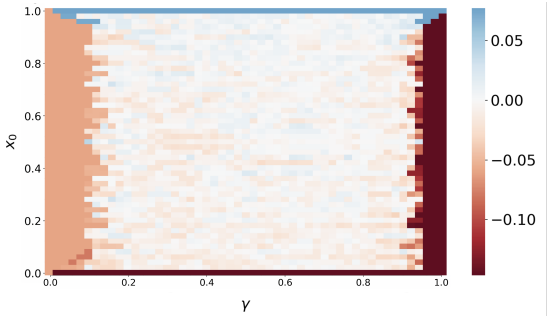

(C) Tent map $a = 1.9$.

FIGURE 3.2: Mean position of the chaotic walker for each of the chaotic maps at $m = 100$ by varying $x_0,\ \gamma \in [0, 1]$.

Using the deterministic sequences generated by the chaotic maps, we seek to find the values of x_0 and γ and their respective mean position when tossing two 2-sided quantum coins. To illustrate the method, we use the setup given by EQUATIONS (3.5)-(3.7) and the following values of a: $a = 4$ for the logistic map, $a = 2.28$ for the sinusoidal map, and $a = 1.9$ for the tent map. The mean position of the random walker after $m = 100$ steps for various values of x_0 and γ is plotted in a heat map in FIGURE 3.2. As it turns out, we can achieve strong Parrondo's paradox using chaotic sequences, the results are shown in FIGURE 3.3 and TABLE 3.1.

TABLE 3.1: Compilation of the mean positions of the quantum walker and parameter values for performing chaotic switching sequence.

Game/Map	a	x_0	γ	$\langle x_{100} \rangle_Q$
$\hat{C}_A$				-0.14668
$\hat{C}_B$				-0.06046
$[\hat{C}_A + \hat{C}_B]$				-0.002664
Logistic	4.00	0.58	0.30	0.02606
Sinusoidal	2.28	0.72	0.60	0.02182
Tent	1.90	0.28	0.16	0.03006

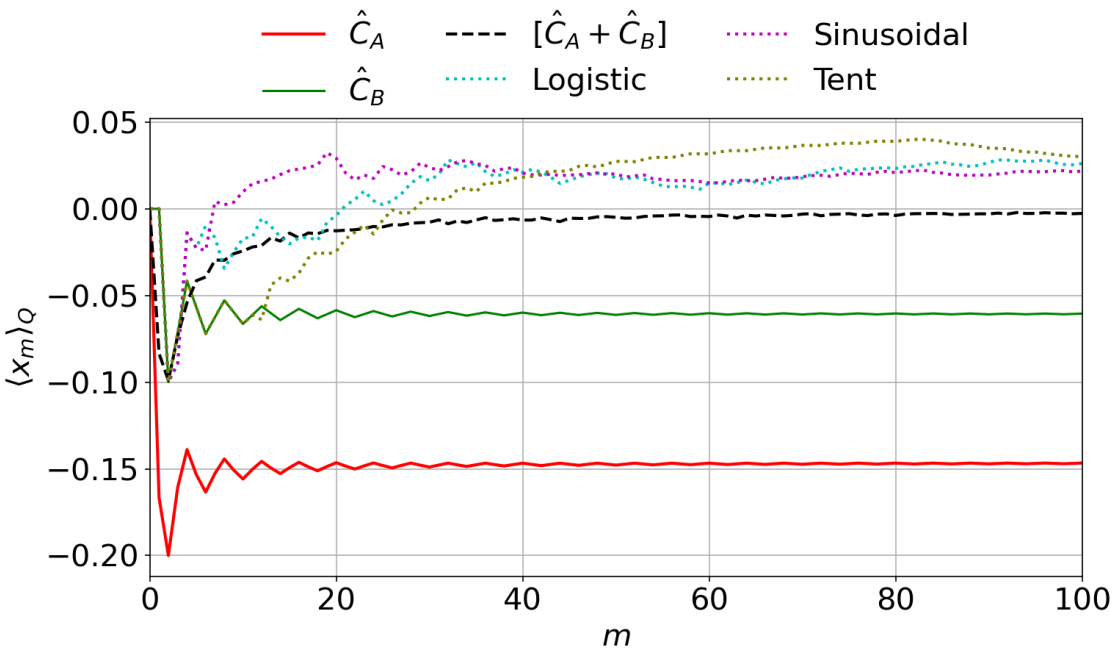

FIGURE 3.3: The mean position of the quantum walker from tossing quantum coins $\hat{C}_A$ and $\hat{C}_B$ individually, randomly averaged over 10^4 experiments, and for each chaotic map with parameters x_0 and γ stated in TABLE 3.1.

The experiment conducted may have used a different initial state $|\psi\rangle_0$, regardless, the outcome of randomly switching between the quantum coins still reflects weak Parrondo's paradox. The adoption of chaotic switching allows for the emergence of strong Parrondo's paradox.

3.3 Potential application for encryption

We put aside Parrondo's paradox in this section and consider a potential application of the innovative framework designed in Chapters 2 and 3. We first argue for the advantages of chaotic switching instead of random or periodic switching. Random switching is not deterministic; thus, in the event where one receives the final state $|\psi\rangle_f$ and seeks to determine the sequence of coin-tosses to arrive at $|\psi\rangle_f$ from $|\psi\rangle_0$, this will be an impossible task as there is no inverse map for the random switching. The chaotic map, on the other hand, is surjective. Thus, knowing the control parameter a, initial condition x_0, and in the case of chaotic switching, the switching threshold γ would reveal the sequence of coin tosses. Comparatively, periodic switching, while deterministic, is severely constrained. Unlike the three parameters of a chaotic sequence, the degree of freedom of the periodic sequence is limited to a single parameter - the length of the period. Thus, chaotic switching is advantageous over random switching because it is deterministic, while advantageous over periodic switching because it has a larger degree of freedom.

Having understood the advantages of using chaotic switching, we now discuss the elements of encryption. Modern encryption comprises several elements:

1. Plain text. The unencrypted message that anyone can read. The original message is $|\Psi\rangle_0 = \sum_j |\psi\rangle^{(j)}$.
2. Cipher text. The result of encryption. Cipher text can be decrypted to obtain the plaintext. In the case of this framework, the cipher text is $|\Psi\rangle_f$.
3. Keys. Keys are elements in the encryption and decryption process that instruct the algorithm to transform plaintext to cipher text and vice versa. In our setup, there is a pre-agreed chaotic map with control parameter a and switching threshold γ. The pre-agreed chaotic map and switching threshold γ are publicly shared information. The control parameter $a \in [3.6, 4.0]$ is a shared secret generated by the original Diffie-Hellman algorithm. The private keys are x_A and x_B, the initial conditions for Alice and Bob, respectively.

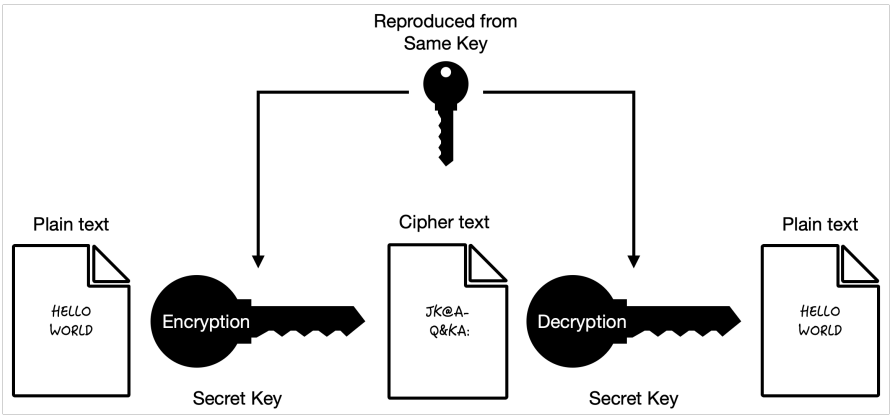

FIGURE 3.4: The secret key is reproduced from the same source to ensure that the information is properly copied. The secret key is used in both encrypting the plain text and decrypting the cipher text.

For the purpose of this chapter, we explore symmetric encryption as it will have an application in the encryption algorithm introduced later. Symmetric key encryption is a set of algorithms that form the simplest kind of encryption. It involves only one secret key to cipher and decipher the information. The general working principle is shown in FIGURE 3.4. It uses a secret key, a number, a word, a string of random letters, or a set of instructions. The key gives instructions to change the plain text of a message in a particular way to obtain the cipher text. The sender and the recipient should know the secret key used to encrypt and decrypt all the messages. However, how do the sender and recipient reliably agree on the secret key? It requires a smart way to perform key exchange, where the sender and receiver have all the instructions needed to generate the secret key, but a public channel only receives partial information, where obtaining the secret key could be computationally impossible.

3.3.1 Secret key exchange quantum coin-toss encryption algorithm

The Diffie–Hellman key exchange protocol [53, 54] is a method used for securely exchanging keys over a public channel. It is one of the first public-key protocols conceived by Ralph Merkle (the protocol is often named Diffie-Hellman-Merkle for this

reason) and named after Whitfield Diffie and Martin Hellman. The method introduced in 1976 is one of the earliest practical examples of public key exchange implemented within the field of cryptography. It has been used since to secure online services with high public traffic. However, with advances in computing power and technology, research published in 2015 suggests that the parameters in use for many Diffie-Hellman applications are not strong enough to prevent compromise [55]. Thus, a possible practical approach to enhance the version of the Diffie-Hellman key exchange that uses chaotic switching between tossing two 2-sided quantum coins is suggested here: the secret key exchange quantum coin-toss encryption algorithm.

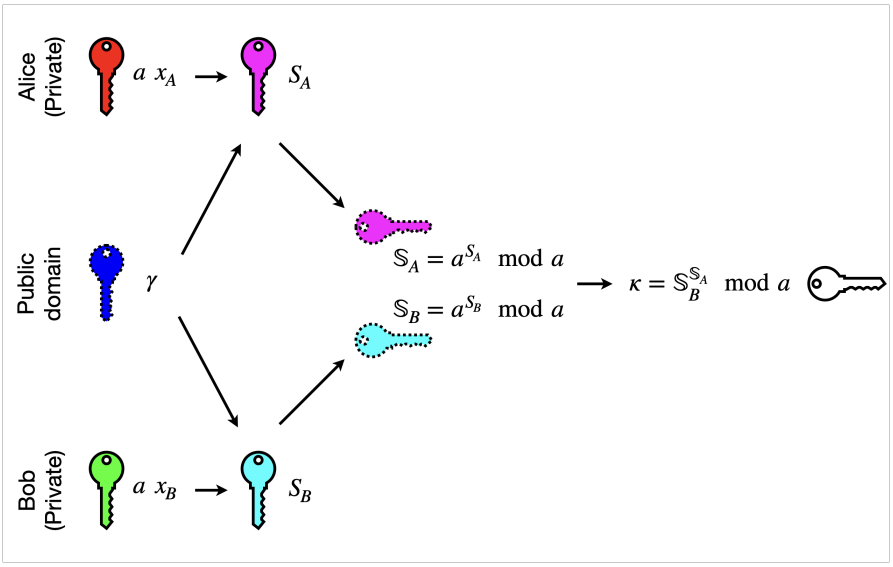

FIGURE 3.5: The secret key is produced from public information and privately generated parameters. Alice and Bob do not share keys in solid outlines; these include the privately chosen initial condition, chaotic sequence, and secret key. The remaining keys, in dashed outlines, are publicly known information. An attacker with these keys is unable to obtain the secret key $\mathcal{K}$.

Step 1: Secret chaotic sequence exchange. The first step of the encryption algorithm is to generate a pair of symmetric secret keys. In our illustration, Alice is the sender, and Bob is the receiver. All information they send between them is stored in the public channel where any attacker can access it. The protocol is summarised in FIG. 3.5. To accomplish the secret chaotic sequence exchange:

(I) Generating the initial conditions. Alice and Bob both privately generate an initial condition x_A for Alice and x_B for Bob, where $x_\alpha \in (0,1), \alpha \in \{A,B\}$. The control parameter $a = \frac{1}{s}(4.0 - 3.6) + 3.6$, where s is a secret key generated by the Diffie-Hellman algorithm with private x_A and x_B. To generate the secret key s, Alice and Bob need to first agree on a prime number p and primitive root g. Alice sends to Bob $\chi_A = g^{x_A} \mod p$; correspondingly, Bob sends to Alice $\chi_B = g^{x_B} \mod p$. Thus, Alice is able to obtain s by using the formula $\chi_B^{x_A} \mod p$. Concurrently, Bob obtains the same s with $\chi_A^{x_B} \mod p$. This formula for a ensures that $a \in [3.6, 4.0]$;

thus, we are in a chaotic regime. In the public domain, there is a publicly known chaotic map and switching threshold γ.

(II) Sharing generated sequences. Alice and Bob then use the secret key to generate a chaotic sequence S_α, where their respective x_α is the initial condition. The length of the generated sequences should be sufficiently long, say n iterations, and of the same length. We label this sequence S_α. Following which, Alice will share with Bob the sequence $\mathbb{S}_A$, with sequence elements $(\mathbb{S}_A)_i = a^{(S_A)_i} \mod a$, for $i = 0, \ldots, n$. Similarly, Bob shares with Alice his sequence $\mathbb{S}_B$. Note that S_A and S_B are still within each person's private channel.

(III) Obtain private key $\mathcal{K}$. In Alice's possession now is her private sequence S_A, publicly shared sequence $\mathbb{S}_A$, and the sequence shared by Bob $\mathbb{S}_B$. To generate the private key $\mathcal{K}$, Alice performs an element-wise operation where $(\mathcal{K})_i = (\mathbb{S}_B)_i^{(\mathbb{S}_A)_i} \mod a$. Bob does the same operation, thus guaranteed to obtain the same secret sequence.

(IV) Convert to chaotic alphabet sequence $\mathbb{K}$. The final step is to compare the sequence elements with the public switching threshold γ, $\min(\mathcal{K}) \leq \gamma \leq \max(\mathcal{K})$. If $x_n < \gamma$, then $\kappa_n = A$, for κ_n being the nth element of the sequence $\mathbb{K}$; otherwise, $\kappa_n = B$. This will produce a secret instruction on the order of the quantum coin tosses.

Step 2: Encryption using chaotic switching between two 2-sided quantum coins (see FIG. 3.6). The original text can first be converted into plain text using a public register. Every symbol in the original text is mapped to a unique basis state $|\psi\rangle^{(j)}$. Thus, the plain text, $|\Psi\rangle_0$ put together by collecting all the initial basis states in order. The plain text is then encrypted using the chaotic switching protocol using two publicly chosen quantum coins $\hat{C}_A$ and $\hat{C}_B$, and applying Equations (2.29) to (2.30). This cipher text can be sent to Bob through a public channel.

Step 3: Decrypting using inverse switching. Bob, knowing all the elements of the secret key exchange quantum coin-toss encryption process, can, in theory, perform the inverse operations to obtain the plain text and match the plain text to the public register to obtain the original message. However, while the encryption process is straightforward, the length of the chaotic sequence can significantly increase the computational resources required to decrypt the cipher text. This is, regardless, a possible task. However, an outsider attempting to decipher the message using purely information from the public channel will face a mountainous task.

This completes the secret key exchange quantum coin-toss encryption algorithm.

3.4 Summary

Thus far, we have seen three methods of switching: random, chaotic, and periodic. In the context of theoretical quantum Parrondo's paradox research, this work bridges the

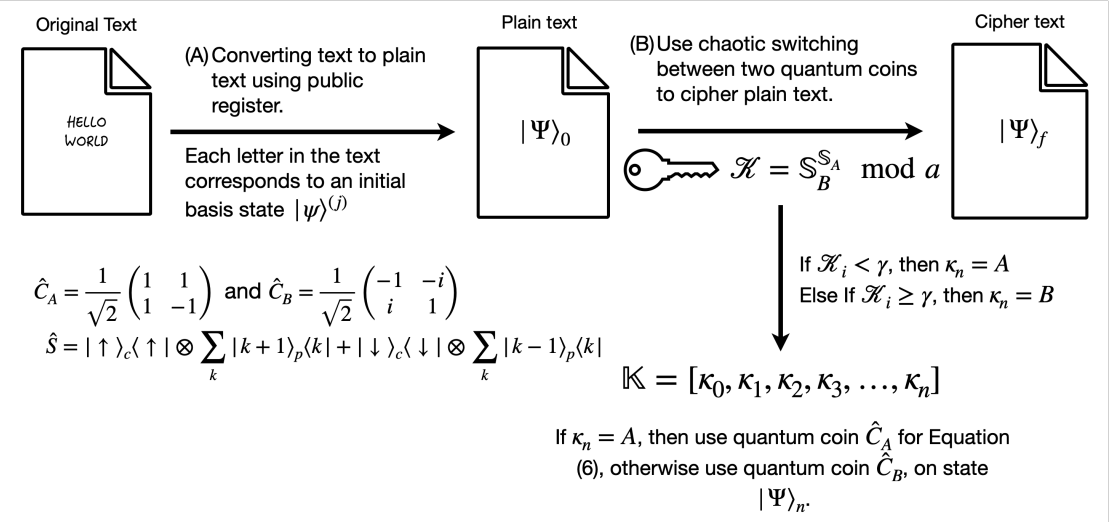

FIGURE 3.6: The secret alphabet sequence is produced from public information and privately generated parameters. The chaotic alphabet sequence $\mathbb{K}$ is then used to cipher the plain text by successively tossing two 2-sided quantum coins. The plain text $|\Psi\rangle_0$ is encrypted to give the cipher text $|\Psi\rangle_f$.

gap to find the best possible mean position in a 2-sided quantum coin-toss Parrondo's game. The introduction of chaotic switching, when combined with Parrondo's paradox, extends the application of Parrondo's paradox to one with real-world engineering applications. Following the publication of these works, there have been advances in aperiodic switching, resulting in Parrondo's paradox [44]. The proliferation of research in this area will only continue if there is known application and potential technological advances through the implementation of quantum coin toss Parrondo's paradox.

It is instructive to note that while chaos in quantum systems is not defined in the same way as it is in classical chaotic and dynamical systems, there are quantum systems whose fundamental physical properties exhibit properties of chaos [56]. Furthermore, there is no concept of entanglement within classical systems, while research has shown that chaos and entanglement are very clearly and strongly related [51, 57]. Thus, using a purely quantum system to derive quantum Parrondo's paradox is potentially the next step in closing the gap in quantum Parrondo's paradox research. It can prove to be a better description of fundamental nature than that proposed in classical Parrondo's paradox.

As we close the chapters on quantum Parrondo's paradox, there is evidence that advances in the field of quantum coin Parrondo's paradox are plentiful. One such application is through the secret key exchange quantum coin-toss algorithm used in the field of cryptography. Numerical simulations have shown that the secret key exchange quantum coin-toss encryption algorithm works. Thus, the first obvious step to advancing the secret key exchange quantum coin-toss encryption algorithm is to prove its theoretical correctness. The final chapter will lay out a possible road map for such advances, both for theoretical research and application of quantum Parrondo's paradox.

Chapter 4

Preference Aggregation Parrondo's Paradox

We move from quantum Parrondo's to another area gaining interest. Social physics is the intersection of social phenomena with computer science, mathematics, and statistical physics. As such, there is potential interest emerging from the field of Parrondo's paradox in the context of social interactions. Social changes can be investigated through means of agent-based modelling involving multiple interacting individuals. Social physics aims to examine how individuals, with differing characteristics, rules of behaviour, and sources of information affect group dynamics. Interactions between individuals can shape group dynamics, and group dynamics can result in the evolution of individual behaviour.

With improving computational power and resource, coupled with advances in computational experimentation in social physics to investigate complex systems, there is a demand to explain phenomena in social settings, usually those including uncertainty, stochastic processes and nonlinear dynamics [58]. The dynamics of such systems are usually quite complex as it involves high dimensionality and connectivity between the agents. Analysis of interactions in a group often reveals counter-intuitive results. We have previously seen a semblance of sociodynamical Parrondo's paradox in the form of the cooperative Parrondo's paradox [13]. However, that is a single example of many potential occurrences of Parrondo's paradox in this domain.

In the immediate section, We will review the developments in sociodynamical Parrondo's paradox with emphasis on our results in three areas: a general framework for organising sociodynamical Parrondo's games, a realistic synchronization and decision-making heuristic of a network of agents leading to the emergence of Parrondo's paradox, and the effect of community voting on the outcomes of playing Parrondo's games.

4.1 Sociodynamical Parrondo's paradox

Sociodynamical Parrondo's paradox involves a large, and potentially infinite, number of interacting agents with different social rules to govern behaviour or information flow. Agent behaviours and interaction of information flow are often simplified through various stochastic mathematical modelling to remain analytically tractable.

Indeed, more complex modes of modelling behaviours and information can be considered. In such cases, computational simulations are often preferred to make empirical deductions on the outcomes. This section will review related work involving Parrondo's paradox on behaviour in social dynamics.

4.1.1 The fitness index

As various network topologies and population sizes will be used for comparison across multiple works, it would be instructive to introduce a means to compare results across different networks by calculating the average fitness index of the population

$$\bar{d}(t) = \frac{\sum_{i=1}^{N} w_i(t)/N}{T}, \tag{4.1}$$

where $w_i(t) = c_i(t) - c_i(0)$, $w_i(t)$ and $c_i(t)$ are the winnings (i.e. change in the capital) and capital at time t of agent i, respectively. $c_i(0)$ is the original capital of agent i, and T is the total time of the game with population size N. Without loss of generality, we can set $c_i(0) = 0, \forall i$ as we are only interested in the net change of fitness when investigating Parrondo's effect. Thus, the average fitness index of the population can be simplified to give

$$\bar{d}(t) = \frac{\sum_{i=1}^{N} c_i(t)/N}{T}. \tag{4.2}$$

4.1.2 Cooperation and competition

One of the key aspects of examining social dynamics is to understand how interactions, through cooperation and competition among agents, within a group lead to changes in the group. In most cases of cooperation and competition, examining how it benefits the group would suffice. Several ways to model cooperation or competition are discussed in earlier works by Wang et al. and Ye et al. [59, 60, 61].

Wang et al. [59] investigated agent-based cooperation and competition (collectively termed coopetition) behaviours in a network of agents. The dynamics of Parrondo's games consist of a zero-sum game played between agents (fair game A) and a negative-sum game between an agent and the environment (losing game B). This falls under the realm of weak Parrondo's paradox. Consider a population of N agents connected according to some network topology, at each time step, a principal agent i is randomly chosen to play game A, with a probability of p, or game B, with a probability of $1 - p$.

- If game A is chosen, a partner j is chosen from the set of nodes connected to i. Game A changes the distribution of benefits in the population without affecting the net benefit of the population. According to Wang et al., they considered four versions of zero-sum game patterns:

  1. Competition: the winning probabilities of the i and j are both 0.5. When i wins, j pays one unit to i; otherwise, j receives one unit from i.

  2. Cooperation: i pays one unit to the partner j for free.

3. Harmony: when capital $c_i(t) \geq c_j(t)$, i pays one unit to j; otherwise, j receives one unit from i.
4. Self-cultivation: when capital $c_i(t) \geq c_i(0)$, the original capital of principal i, i will act according to the cooperation pattern; otherwise i will compete using the competition pattern.

- Game B is modelled exactly according to the seminal capital-dependent game B.

Wang et al. [59] examined the fitness of the population in two network topologies – the Barabási–Albert (BA) scale-free network and a fully connected network. Agents can only interact with other agents if they are pair-wise connected by an edge. In the BA network, the nodes are connected based on a degree distribution that follows a power distribution [62]. While in a fully connected network, all nodes are pair-wise connected. The dynamics of such a sociodynamical Parrondo's game is summarised in FIGURE 4.1.

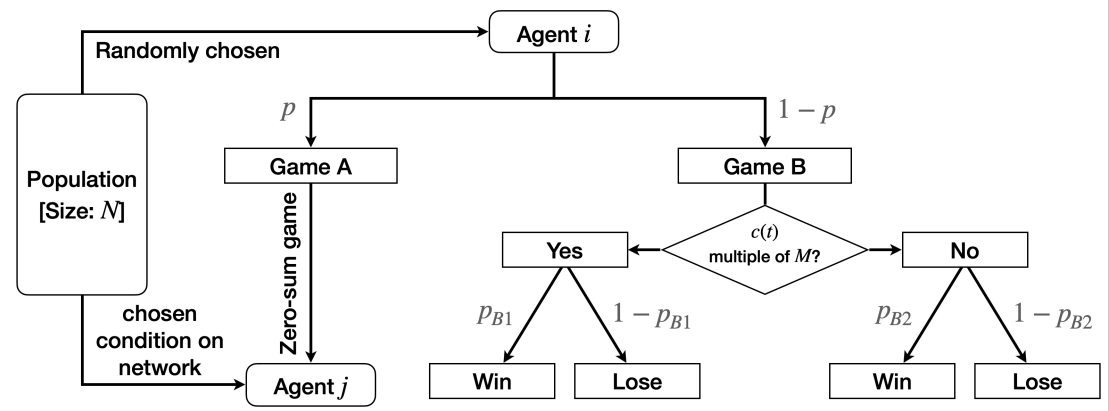

FIGURE 4.1: Population Parrondo's games model on a network, modified from the capital-dependent Parrondo's games.

A similar version is investigated by Ye et al. [60, 61] considering coopetition in history-dependent Parrondo's games on networks. Game B was substituted with game B′ of the seminal history-dependent game to reflect the favourable and adverse impact of the environment on agents.

4.1.3 Resource redistribution and social welfare

The study of resource distribution is another important aspect of social dynamics. It provides an explanation and a moral assessment of both individual and collective decisions. In the context of sociology, resource distribution has been invoked in discussions pertaining to distributive justice. The aim of investigating Parrondo's paradox in such a scenario is to observe how modelling social groups through individually losing options can lead to increased resources or welfare of groups. The seminal cooperative [13] Parrondo's paradox was extended to feature wealth redistribution which will be explored in this section [36, 63]. Toral's extension of the cooperative Parrondo's paradox simply permutates various losing games of the capital-, history-dependent, and cooperative Parrondo's paradox on a network of agents in a ring network topology.

Zappalà et al. [63] developed a selfish-altruistic agent model by considering the potential of agents in the network to have different strategies. In the model, the population N is partitioned into selfish agents and altruistic agents, where their strategy is as such:

- Selfish agents: always choose game B of the capital-dependent Parrondo's paradox.
- Altruistic agents: choose game A′ with probability p. For game A′, the altruistic agent i gives away one unit of capital to a randomly selected agent j; otherwise, choose game B of the capital-dependent Parrondo's paradox with probability $1 - p$.

Game A′ is a losing game for altruistic agent i, but it is a zero-sum game across the network as the unit of capital is kept within the network of agents. In a modified version of the game, Zappalà et al. [63] altered the behaviour of the altruistic agents. Instead of always giving away one unit of capital, such agents are selective as to who they give a unit of their capital. Selective altruistic agents give a unit of capital if the recipient is also an altruistic agent. The dynamics of both versions of the selfish-altruistic agent models are illustrated in FIGURE 4.2.

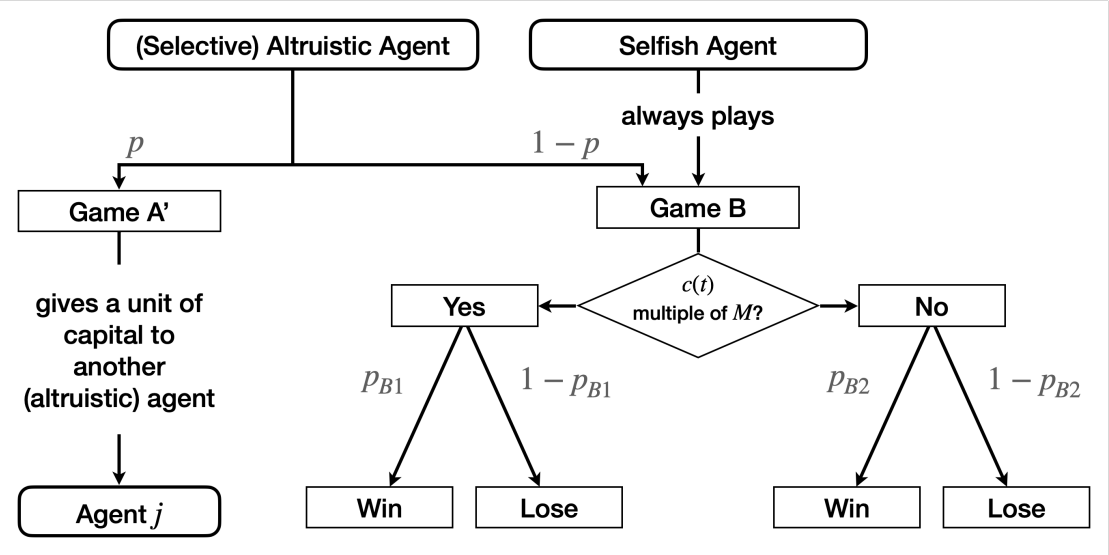

FIGURE 4.2: Selective altruism-selfishness model played by a population N agents. Selfish agents only play game B where their interaction is purely with the external environment. Altruistic and selective altruistic agents consider two games A′ and B. In the case when A′ is played, they give away a unit of capital to another agent or selective altruistic agent, respectively.

It is observed that selfish agents tend to get richer, while altruistic agents get poorer. Zappalà et al. concluded that altruistic behaviour is discouraged as they are "taken advantage" of. Instead, by adopting "selective altruism", these agents respond only to altruistic behaviour according to reputation, or past information. This ensures that selective altruistic agents are not "taken advantage" of by their selfish counterparts. With a mechanism of "reputation" built into the model, altruistic agents are made aware of which agents are "trustworthy" so that they can overcome the adverse effects of naive

altruism. Zappalà et al further showed that in a network topology of fully connected nodes, for $p = 0.5$, selectively altruistic agents are in a better position as they, on average, have higher fitness than their selfish counterparts.

The use of Parrondo's games in modelling social dynamics can be beneficial in understanding social phenomena such as cooperation and competition and wealth redistribution and welfare. However, as we observe in these studies, the agents in the network have homogeneous behaviours, in the language of game theory, the agents employ pure strategies. This means that agents are "forced" to follow the same social rules provided by Parrondo's games and the switching rules . Such homogeneous behaviours do not account for potential adaptive behaviours without means of responding to the outcome of previously played games. For example, in the case of the altruism-selfish model, selfish agents do not evolve to become altruistic despite the strategy being unfavourable. This is not a reflection of real-world social dynamics. Furthermore, a deeper investigation into the direction of social Parrondo's paradox reveals that each work is independently designed within research groups with little to no coordinating framework to guide subsequent research to steer the field in a coordinated effort. To close these gaps, we design a versatile framework that allows agents in the network to adapt according to the outcome of playing Parrondo's games. The framework is also broadly defined to ensure that previously published work on social dynamics Parrondo's paradox can be translated to fit the framework. This framework also attempts to coordinate efforts in the social dynamics field Parrondo's paradox by setting a guiding reference for developing more complicated models. It will inspire future research related to Parrondo's games in the network setting, we call this the preference aggregation Parrondo's paradox framework [64].

4.2 Preference Aggregation Parrondo's paradox

The preference aggregation Parrondo's paradox comprise three broad steps:

Initialisation: Let $\mathcal{N} = \{1, 2, \ldots, N\}$ represent a set of individuals in a group deciding on a set of strategies. Each individual $i \in \mathcal{N}$ is a node in the network and is connected to a subset of individuals $\mathcal{M}_i \subseteq \mathcal{N} \backslash \{i\}$ by either directed edges for a directed network or edges for an undirected network. Furthermore, we can assign to each individual $i \in \mathcal{N}$ any number of parameters such as a preference, $p^{(i)}(t)$, the capital, $c^{(i)}(t)$, or even parameters such as the confidence towards one's preference. In the case of directed networks, we say that if individuals $i, j \in \mathcal{N}$ are connected, the edge $j \to i$ represents j influencing i. Thus, we can further enhance the network by labelling the directed edges with an influence index, $\psi_{ji}(t)$, that varies with time. There is potential for this framework to be developed to include simple to complex modelling of social relationships.

Iteration: After determining the network topology and features, the preference aggregate framework introduces social rules for how the nodes and edges interact. The preference aggregate framework comprises three distinct steps for each iteration:

1. Aggregate rule. A preference profile determines the preferences of every individual in the network $(p^{(1)}, p^{(2)}, \ldots, p^{(n)})$, where $p^{(i)} = \{-1, 1\}$, $\forall i$. At discrete time

t, each individual has a preference of which Parrondo's games to play, denoted by $p^{(i)}(t)$, by convention, we set $p^{(i)} = 1$ to represent a preference for game A (or generally, the first losing option) and $p^{(i)} = -1$, a preference for game B. If an individual abstains or decides not to act on any preference, the preference profile can be extended to include this. The aggregate rule is described by a mathematical function that takes the preference profile of a subset of individuals in a social network and assigns an option, i.e., $f : \mathbb{R}^m \to \mathbb{R}$, where $m \leq n$. The function f outputs an option. The aggregate rule is likened to a social rule that governs the interaction of agents in the network.

2. Decision rule. The option obtained from the aggregate rule is then passed to the decision rule. The decision rule is a choice function that either accepts or rejects the option by assigning a decision. The choice function returns a binary output, i.e., $g : \mathbb{R} \to \{-1, 1\}$. Thus, if $g = 1$, the decision is accepted and game A is played (or generally, the first losing option), otherwise, the decision is to play game B (or generally, the second losing option). Generally, this decision can be applied to an individual, any subset, or the whole network. When applied to a group, we call this a collective decision.

3. Feedback loop. The feedback is a set of rules applied to a subset of the network and modifies the network in preparation for the next iteration.

Outcome: Finally, in most cases, we are interested in the average fitness of the population, $\bar{d}(t)$. Other factors can also be considered as required. To simulate results from the preference aggregation framework, we employ the use of the `NetworkX 2.5` package with the Python programming language. For consistency and comparison, we set the bias of Parrondo's games to be $\epsilon = 0.01$, unless explicitly mentioned. As mentioned earlier, we are interested in the average fitness of the population, thus, we set the initial capitals $c^{(i)}(0) = 0$.

4.2.1 Example of application of framework

We want to show that previously discussed literature on social dynamics Parrondo's paradox can be fully described by this framework. Consider Wang et al. [59] as described in the earlier section. The network used in their work is the BA network and a fully connected undirected network. The preference aggregation framework accepts any directed or undirected network, with weighted or unweighted edges. Thus, our framework is general enough to encompass the network topology used by Wang et al. Game A involves a zero-sum game between a randomly selected agent i and a randomly selected partner j, where j is connected to i. Game B is the usual capital-dependent Parrondo's game B. i decides to play game A with probability p and game B with probability $1 - p$. The aggregate rule $f : \mathbb{R}^2 \to \mathbb{R}$ is

$$f = \begin{cases} 1 & \text{if } r < p \\ -1 & \text{otherwise} \end{cases}, \tag{4.3}$$

where $r \sim U(0, 1)$ is a real number drawn randomly from a uniform distribution of interval $[0, 1)$. Notice here that since the dynamics of the competition pattern is simple,

the aggregate rule did not take into account the preference profile of either agent. The decision rule is $g : \mathbb{R} \to \mathbb{R}$, specifically,

$$g = \begin{cases} 1 & \text{if } f = 1 \\ -1 & \text{if } f = -1 \end{cases}. \tag{4.4}$$

There is no feedback loop as all agents do not change behaviour. The same framework can be applied to other works, demonstrating the usefulness of the preference aggregation framework.

4.3 Parrondo's paradox and real-world phenomena

It will be instructive to go beyond the simple examples considered in previous literature to consider more complex sociodynamical phenomena. In this section, we look at three different applications of preference aggregation Parrondo's paradox and the versatility of using such a framework. First, we show the algorithmic pseudocode (ALGORITHM 4.1) that can be applied to the preference aggregation framework.

Algorithm 4.1 The preference aggregation Parrondo's paradox algorithm.

1: **Initialization:** Generate a network for which Parrondo's games will be played.
2: **Initialization:** Initiate parameters on nodes and edges.
3: Obtain option by passing preference profile to aggregate rule, f.
4: Pass outcome of the aggregate rule to decision rule, g
5: **if** decision is A **then**
6: Play game A according to social setup and update via the feedback loop.
7: **else**
8: Play game A according to social setup and update via the feedback loop.
9: **end if**
10: Calculate average fitness of population $\bar{d}(t)$.

4.3.1 Ill-informed advising the ill-informed

Consider the capital-dependent Parrondo's game. Recall that it is designed to be played by an individual. In the case of random switching between games A and B, the individual has full knowledge but has no control over which game to play. However, if the rules of the capital-dependent game are changed to allow the individual to choose the game to execute at each discrete time t, then the agent can always make an informed choice by choosing the game that has the lowest risk of losing at each time step. However, consider the case with multiple agents, each with individual capitals, and at each discrete time, only one of the randomly selected agents can choose which game to play without having any knowledge of one's present capital. This scenario is not unimaginable in the context of financial markets where investments are made without a full picture of future outcomes. Thus, this would prompt the chosen individual to seek the advice of other agents in the network with whom one is connected to. This is a form of preference aggregation.

Thus, the first application of aggregate choice is what we would call "ill-informed advising the ill-informed". An *ill-informed* individual is defined as an agent who has no knowledge of one's capital nor the outcome of the coin-toss Parrondo's games. As such, the ill-informed individual always selects a game by consulting its network connections. The ill-informed agent aggregates the preference of other ill-informed (who by construct have no knowledge of their capital or the game that benefits them). After playing that game, the agent remains clueless about the outcome and continues being an ill-informed advisor to one's neighbours.

To simulate this, we consider an undirected BA network generated with the following properties: Network nodal size $N = 500$ with an average degree $\langle k \rangle = 3.984$, this is achieved with`NetworkX` function `barabasi_albert_graph(500,2)`. These parameters also fit the network properties for domain-level interactions on Internet social networks.

The aggregate rule for a randomly chosen agent i is given by

$$f(p^{(i)}, p^{(j)}) = \frac{1}{|\mathcal{M}_i| + 1} \left[\alpha p^{(i)} + (1 - \alpha) \sum_{\forall j \in \mathcal{M}_i} p^{(j)} \right], \tag{4.5}$$

where α is a parameter likened to the weight that i assigns to the preference profile of all neighbouring agents. In the extremes, when $\alpha = 1$, then agent i only considers one's own preference; at the other extreme, if $\alpha = 0$, then i only considers the collective preference of one's connections. The aggregate rule f outputs an option in the range $[-1, 1]$.

The decision rule here is a naive decision-making process where

$$g = \begin{cases} 1 & \text{if } f \geq 0 \\ -1 & \text{if } f < 0 \end{cases}, \tag{4.6}$$

where $g = 1$, denotes i's decision to play game A; otherwise, if $g = -1$, i plays game B. Finally, the feedback loop, the capital $c^{(i)}(t + 1)$ is updated accordingly, and $p^{(i)}(t + 1)$ will be randomized with equal probability for preference 1 or -1. Let us vary α to investigate how the average fitness of the population $\bar{d}(t)$.

From the results from FIGURE 4.3, we observe that the average fitness of the population, $\bar{d}_\alpha(t = 100)$, for the network of ill-informed individuals is at best equivalent to the outcome from all agents adopting a random strategy. This is achieved in the limit $\alpha \to 1$. We provide a sociological explanation for this: As $\alpha \to 1$, the aggregate rule tends toward a selfish decision-making process with greater emphasis placed on one's individual preference. This is equivalent to the scenario described in the random choice game, thus the results for "ill-informed advising ill-informed" is at best equivalent to the random choice. In the limit of $\alpha \to 1$, the agents in the network no longer interact with each other. This is analogous to a network of isolated agents all playing a random. Thus, we see that Parrondo's paradox is achievable for a network of ill-informed individuals providing feedback to other ill-informed individuals by shifting the weight towards one's own preference. The aggregate rule in this example is analogous to the

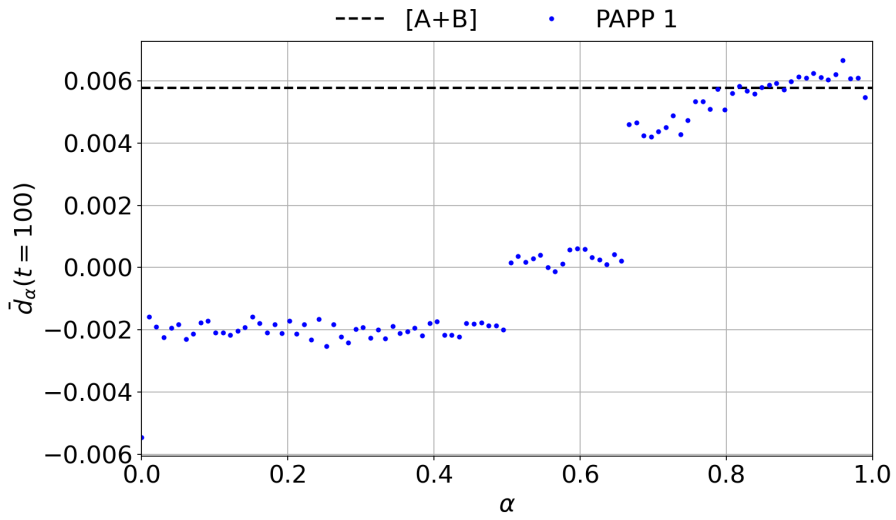

(A) Average fitness of the population ($N = 500$) at $t = 100$ as a function of the weight α for a BA network. The average fitness of the population plotted is averaged over 10^5 simulations each. The black dashed line represents the gain from the random switching strategy.

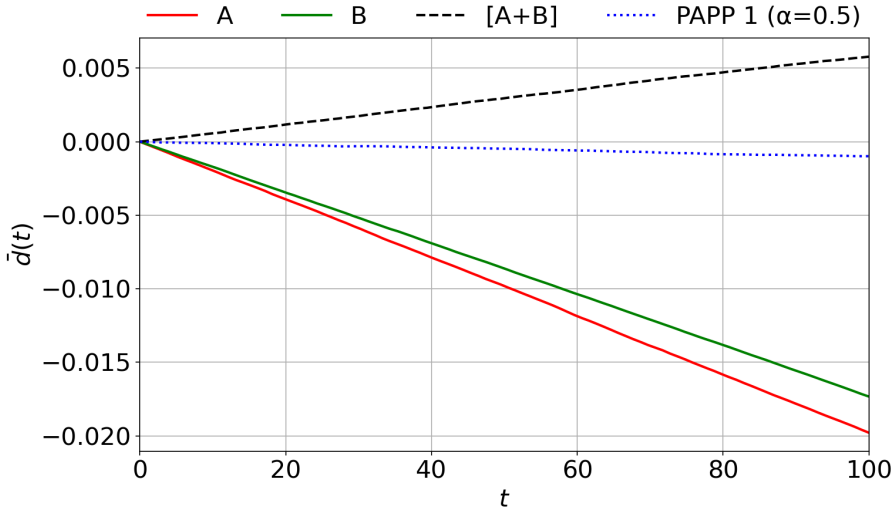

(B) Average fitness of the population ($N = 500$) against time for a BA network. Note that both games A and B are losing (decreasing with time), and so is the outcome for "ill-informed advising the ill-informed" for the aggregate rule with $\alpha = 0.5$.

FIGURE 4.3: Empirical results from applying the preference aggregation framework for the case "ill-informed advising the ill-informed", (A) by varying α for $t = 100$, and (B) by varying t for $\alpha = 0.5$.

lack of information provided to individuals in a network. The agents in the network are ill-informed about the significance of their choice to their individual welfare (i.e. average fitness). Our result is akin to a social shutting out chatter (influence) from other ill-informed individuals, where one is better off making a choice at random.

4.3.2 Weighted influence and confidence

Let us now demonstrate the advanced use of the preference aggregation framework for directed networks. In this example, we demonstrate a possible means of accounting for multiple real-world scenarios in complex networks by considering a directed, weighted network. In this example, individuals make decisions based on one's own confidence in their own preferences. Unlike the previous example, in this example, individuals give weight to other individuals' influence. A neighbouring node given more weight will influence the principal node more than a neighbouring node given less weight. This is true in many social settings, for example, a close friend's preference might influence someone more than a mere acquaintance. The aggregate rule for agent i, at discrete time t, is

$$f(p^{(i)}, p^{(j)}) = \begin{cases} p^{(i)} & \text{if } i \text{ has no predecessors and } \mu^{(i)} \geq \eta \\ \text{rand}\{-1, 1\} & \text{if } i \text{ has no predecessors and } \mu^{(i)} < \eta \\ \frac{1}{|\mathcal{M}_i|+1}\left[\mu^{(i)}p^{(i)} + \sum_{\forall j \in \mathcal{M}_i} \beta^{(j)} p^{(j)}\right] & \text{if } i \text{ has predecessors} \end{cases}, \tag{4.7}$$

where $\mu^{(i)}$ is the confidence index, representing the self-confidence that i has over one's own preference, satisfying $\mu^{(i)}(t) \in [0, 1], \forall i$. rand$\{\cdot\}$ denotes a random choice between the options with equal probability. $\beta(j)$ is the weighted preference that i assigns to all predecessors j, satisfying

$$\beta^{(j)} = \frac{\psi_{ji}}{\sum_{j'=1}^{|\mathcal{M}_i|} \psi_{j'i}} - \frac{\mu^{(i)}}{|\mathcal{M}_i|}. \tag{4.8}$$

Here, $\psi_{ji}(t)$ is the influence index, representing the influence that j has over i, satisfying $\psi_{ji}(t) \in [0, 1]$. The first two cases for EQUATION (4.7) cover the scenario where an individual has no predecessors. If the confidence of i is high (here we define high as $\eta = 0.75$), then i's option will be the same as its preference; otherwise, i will randomly choose an option.

The decision rule is modified to take into consideration i's influence over one's successors. If i does not have any successors, then i will play the game according to the decision rule given by EQUATION (4.6). If agent i has successors k and i has influence over them, i.e. $\psi_{ik}(t) > \gamma$, then the successors k will play the same game as i at that particular time step; otherwise, successors k will not play any games this round. Similarly, the game played will be according to EQUATION (4.6). Consequently, if $\gamma = 0$, then all of i's successors will play the same game as i for that round. If $\gamma = 1$, then only agent i plays the game decided by the decision rule for that round.

Lastly, for the feedback loop, the confidence of individual i improves if i gains capital in that round and decreases otherwise, given by

$$\mu^{(i)}(t+1) = \begin{cases} \tanh\left(\frac{5\mu^{(i)}(t)}{2}\right) & \text{if } i \text{ gained capital} \\ 0.1\mu^{(i)}(t) & \text{otherwise} \end{cases}. \tag{4.9}$$

Here, we model a greater penalty on the confidence index when capital is lost. This

is supported by studies that show that losses often result in a drastic decrease in self-confidence, while a gain in capital eventually saturates one's confidence [65, 66]. Finally, we examine how various values of γ affect the average fitness of the population by considering two cases (i) Random: $p^{(i)}$ at the next iteration is set to be random, and (ii) Historic: $p^{(i)}$ at the next iteration is set to be the last game that resulted in a capital gain for i.

A directed scale-free network `scale_free_graph(500)` is generated, with default network growth parameters. The other parameters $\mu(t)$, $p(t)$ and ψ_{ji} are assigned random values uniformly from their respective domains. The results are shown in FIGURE 4.4.

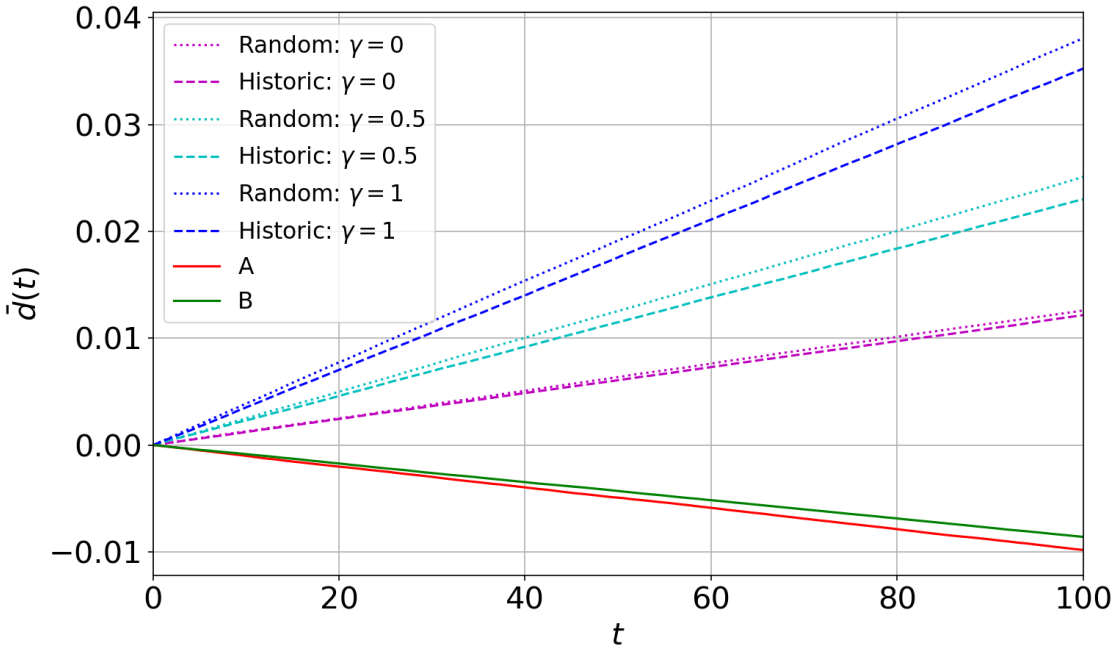

FIGURE 4.4: The average fitness of the population $\bar{d}(t)$ is plotted against time t for a scale-free directed network with population $N = 500$.

TABLE 4.1: Summary table of the average fitness of the population at $t = 100$, and the proportion of game A played during the simulation of each case. The results are obtained by taking the average of 10^6 simulations.

	$\gamma = 0$		$\gamma = 0.5$		$\gamma = 1$	
	Random	Historic	Random	Historic	Random	Historic
$\bar{d}(t = 100)$	0.01260	0.01216	0.02511	0.02300	0.03808	0.03524
Prop. of game A	50.00%	49.99%	50.00%	49.83%	50.02%	49.74%

We observe, from FIGURE 4.4, that the case for $\gamma = 0$, where all of i's successors are subjected to play the same game as i, outperforms the case for $\gamma = 0$, where only i plays the game at time step t. Consequently, in the case of playing losing games, in order to benefit the population, we see that imposing the decision on all successors ($\gamma = 0$) is detrimental to the fitness of the population compared to $\gamma = 1$, where the average

fitness is almost twice the value. In fact, we can say more, that is, the average fitness of the population $\bar{d}(t = 100)$ decreases linearly with γ. We further observe from TABLE 4.1 that for all three cases ($\gamma = 0, 0.5, 1$), despite playing an approximately equal proportion of game A, a change in the decision rule subjected to the same aggregate rule and feedback loop allows one form of preference aggregation to outperform another.

4.3.3 Risk-taking framework leading to Simpson's paradox

In our final example, we consider the case where the population is partitioned, each with a varying feedback loop [67]. The partition is determined by a risk parameter, $\beta \in [0, 1]$, assigned to each individual. An overlapping region is built into the model to allow individuals with the same β to possess different risk-taking behaviour. $\beta \in [0, 10/24]$ are assigned to *cautious* agents, $\beta \in [7/24, 17/24]$ to *risk-takers*, and $\beta \in [14/24, 1]$ are assigned to *reckless* individuals. This is a simple risk parameter model adopted for illustrative purposes to demonstrate the versatility of the preference aggregation framework.

The aggregate rule for a randomly chosen agent i is given by

$$f(p^{(i)}, p^{(j)}) = \frac{1}{|\mathcal{M}_i| + 1}\left[p^{(i)} + \sum_{\forall j \in \mathcal{M}_i} p^{(j)}\right]. \tag{4.10}$$

The aggregate rule outputs an option which is decided upon by the decision rule given by several possible cases:

(i) If $p^{(i)}\left(\sum_{j\in\mathcal{M}_i} p^{(j)}\right) < 0$ and $r < \exp(-1/2\beta^{(i)})$, where $r \in [0, 1]$ is a random number also known as the acceptance number, then i decides using the decision rule

$$g = \begin{cases} 1 & \text{if } f \geq 0 \\ -1 & \text{if } f < 0 \end{cases}. \tag{4.11}$$

This means that if individual i has a preference opposite to the sum of the preferences of its connections and is within an acceptable threshold, then i will decide to play the game according to the outcome of the aggregate rule. This is analogous to real-world decision making where individuals decide on an option when it is within a threshold of acceptance [68, 69].

(ii) However, if $p^{(i)}\left(\sum_{j\in\mathcal{M}_i} p^{(j)}\right) > 0$, then i simply chooses to play one's preference. That is

$$g = \begin{cases} 1 & \text{if } p^{(i)} = 1 \\ -1 & \text{if } p^{(i)} = -1 \end{cases}. \tag{4.12}$$

(iii) Otherwise, if the conditions in (i) and (ii) are not met, because the sum of preferences of i's connections is not within the acceptable threshold, then the following decision rule is used

$$g = \text{rand}\{-1, 1\}, \tag{4.13}$$

where rand$\{\cdot\}$ denotes a random choice between the options with equal probability. In such cases, i rejects the preference aggregation and plays a random game.

The aggregation and decision rules are kept similar for the three risk-taking behaviours to ensure that the only factor that affects the average fitness is purely its feedback, which itself is modelled according to the various characteristics of risk-taking behaviours.

We now model the feedback which varies according to β. Individuals in the network with $\beta \in [0, 10/24]$ are determined to be *cautious* agents. Cautious agents adopt the principle of "once bitten, twice shy", which describes the action of avoiding bad situations, the feedback is

$$p^{(i)}(t+1) = \begin{cases} -p^{(i)}(t) & \text{if } \Delta c^{(i)} < 0 \text{ and } p^{(i)}(t) = g \\ p^{(i)}(t) & \text{if } \Delta c^{(i)} < 0 \text{ and } p^{(i)}(t) = -g \\ \text{rand}\{-1, 1\} & \text{otherwise} \end{cases}. \tag{4.14}$$

$\Delta c^{(i)} = c^{(i)}(t+1) - c^{(i)}(t)$, denotes the change in the capital at time step t. The cautious individual only reacts when capital is lost, by either switching or reinforcing one's preference. In other words, if i loses capital by playing the game that one prefers, i is "bitten" and thus deviates from that game at the next iteration. Otherwise, if i loses capital from playing the game according to the aggregate rule, but is not aligned to i's preference, then i's preference will not deviate. For the other cases, i gains capital, and will continue to randomise its preference.

Individuals with $\beta \in [7/24, 17/24]$ are set as *risk-takers*. The overlap of β is purposely designed to model the possibility that individuals with similar thresholds can adopt fuzzy risk-taking behaviours. Risk-takers have the feedback:

$$p^{(i)}(t+1) = \begin{cases} p^{(i)}(t) & \text{if } \Delta c^{(i)} < 0 \text{ and } p^{(i)}(t) = g \\ p^{(i)}(t) & \text{if } \Delta c^{(i)} > 0 \text{ and } p^{(i)}(t) = -g \\ \text{rand}\{-1, 1\} & \text{otherwise} \end{cases}. \tag{4.15}$$

If the risk-taker i loses capital by playing the preferred game, i will take the risk by staying put with the same preference. Furthermore, if i gains capital despite not playing one's preferred game, i will continue to take the risk by not switching preference.

Lastly, individuals with risk parameter $\beta \in [14/24, 1]$ are *reckless* agents. Reckless agents adopt an irrational strategy while at the same time giving greater weight to their own preference when considering one's preference for the next iteration of games. Thus, the feedback is

$$p^{(i)}(t+1) = \begin{cases} p^{(i)}(t) & \text{if } \Delta c^{(i)} < 0 \text{ and } p^{(i)}(t) = g \\ p^{(i)}(t) & \text{if } \Delta c^{(i)} > 0 \text{ and } p^{(i)}(t) = -g \\ -p^{(i)}(t) & \text{if } \Delta c^{(i)} < 0 \text{ and } p^{(i)}(t) = -g \\ -p^{(i)}(t) & \text{if } \Delta c^{(i)} > 0 \text{ and } p^{(i)}(t) = g \\ \text{rand}\{-1, 1\} & \text{otherwise} \end{cases}. \tag{4.16}$$

The first two scenarios are similar to the risk-takers. However, the reckless goes further by considering other choices that are not favourable. Specifically, if i loses capital by playing the game opposite to its preference, i will be reckless and switch preference to the game preference that resulted in the loss. Furthermore, if i gains capital by playing the game preferred, i will deviate from the game that resulted in the gain.

TABLE 4.2: Network properties of ego-Facebook dataset [70, 71].

Properties	ego-Facebook network
Nodes	4039
Edges	88234
Average clustering coefficient	0.6055
Average degree	43.6910
Number of triangles	$1,612,010$
Diameter	8

To simulate this, we consider an undirected real-world social media network [70, 71] with network properties summarised in TABLE 4.2. For each network, we set the initial capitals of each node to $c^{(i)}(0) = 0$. Again, this can be done in general because we are only interested in the evolution of the population's average fitness with time t. The other parameters in this preference aggregation model, $\beta^{(i)}$ and $p^{(i)}(t)$, are assigned random values drawn uniformly from their respective domains. We investigate the average fitness of the population $\bar{d}(t)$ as a function of discrete time t to show Parrondo's paradox. In order to observe the relationship between β and the individual capitals of all agents $c^{(i)}$, we also plotted the individual capitals $c^{(i)}(t = 100)$ as a function of β. A total of 10^6 simulations were performed and averaged over. Simpson's paradox emerges under such a set-up.

TABLE 4.3: Empirical results and the emergence of Simpson's paradox from applying the preference aggregation framework on a partitioned network. Notice that the correlation m of the network is positive, while that of individual risk-taking behaviour type is negative, a signature of Simpson's paradox. The table is to be read together with FIGURE 4.5.

	Network	Cautious	Risk-taker	Reckless
$\bar{d}(t = 100)$	0.40144	0.07968	0.13366	0.18811
$m \times 10^{-4}$	8.3252	-4.2086	-5.7517	-4.6975

4.4 Summary

The focus of this chapter is to introduce the preference aggregation Parrondo's paradox. We demonstrated the robustness of the preference aggregation framework by explaining results through social phenomena, playing Parrondo's games on a dynamic feedback loop on a bi-directional network, and demonstrating the emergence of Simpson's paradox when partitioning a social network. These are interesting results for which deeper analysis can be performed in future work. For example, in the case of "ill-informed advising the ill-informed", we observe three distinct phase transitions at

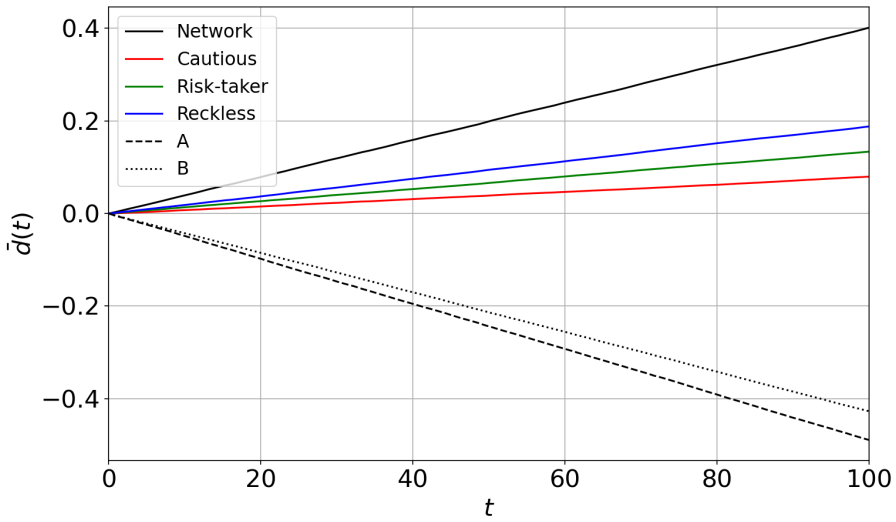

(A) Average fitness of the population $\bar{d}(t)$, and respective partitions of the network, against $t = 100$ for a social media network. For all cases, Parrondo effect is observed. The label *Network* denotes the average fitness of the entire population.

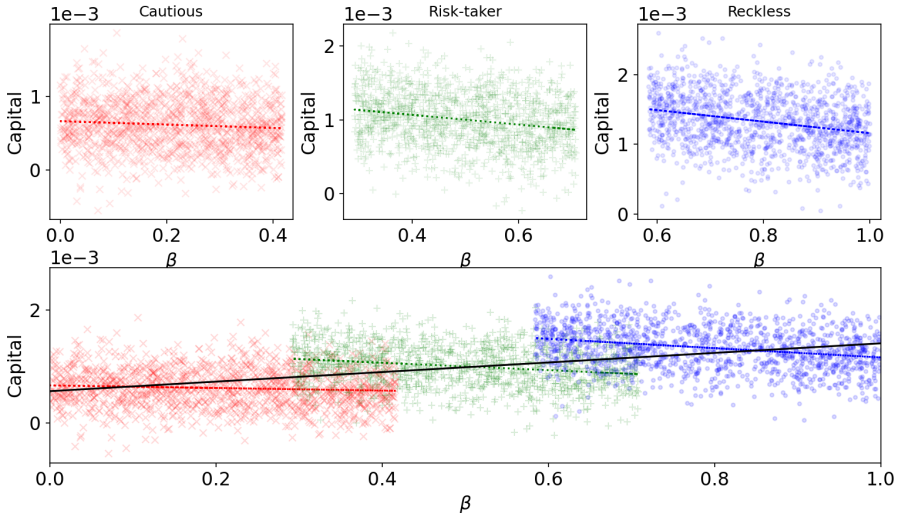

(B) The emergence of Simpson's paradox is seen when plotting individual capitals $c^{(i)}(t = 100)$ against β for a social media network. The value of β characterizes the risk-taking response to the outcome of playing Parrondo's games.

FIGURE 4.5: Empirical results and the emergence of Simpson's paradox from applying the preference aggregation framework on a partitioned network. These plots are to be read together with TABLE 4.3.

the inter-phase of $\alpha = 0$, $\alpha = 1/2$, and $\alpha = 1/3$. Phase transitions indicate critical changes at the micro-level (agent level) that result in a macro-level (network) change. The explanation for such changes is still an open problem worth investigating. While we have shown examples of different types of networks, this is the tip of the iceberg. We could potentially include other types of networks, including dynamic and multilevel networks, or synthesize the various social rules to fit real-world responses through data collection. As this interdisciplinary research area still has untapped potential. But we leave it for now to investigate another social phenomenon – network synchronization

and its effect on decision-making for Parrondo's games.

Chapter 5

Network Synchronization Parrondo's Games with Decision Heuristic

In most social cases, individuals make decisions based on their limited interaction with their immediate community instead of gathering information from the entire group. In this chapter, we investigate the behaviour that emerges from a mean-field synchronization of opinions and an application of a decision-making heuristic between two disadvantageous choices in a social network that benefits the group. First, we introduce some inter-node dynamics that emerge from network science.

5.1 Definitions

5.1.1 Community modularity

The concept of communities is an area of research in network science that mimics real-life understanding of communities. Various algorithms exist for revealing and investigating the community structure in networks. A qualitative definition of network communities is based on a real-world interpretation of social identification of the community structure. Modularity is a computational means of measuring community partition. The modularity $Q \in [0, 1]$ is defined as

$$Q = \frac{1}{2m} \sum_{ij} \left(A_{ij} - \gamma \frac{k_i k_j}{2m} \right) \delta(c_i, c_j), \tag{5.1}$$

where m is the number of edges, A is the adjacency matrix of network, k_i is the degree of node i, and γ is the resolution parameter which allows Q to be maximized. $\delta(c_i, c_j)$ is 1 if i and j are in the same community; otherwise, it is 0. This can be reduced to

$$Q = \sum_{c=1}^{n_c} \left[\frac{L_c}{m} - \gamma \left(\frac{k_c}{2m} \right) \right], \tag{5.2}$$

where the sum iterates over communities c, n_c is the number of communities, L_c is the number of intra-community edges for community c, k_c is the sum of degrees of nodes in community c.

A certain community partition of the network will maximize the modularity. A modularity with a value closer to 1 indicates that the community partition identified is a better representation of community partition. A well-defined community algorithm is the Clauset-Newman-Moore greedy modularity maximization which seeks to find the community partition with the largest modularity [72]. The Clauset-Newman-Moore greedy modularity maximization can be achieved by invoking the `NetworkX` function `greedy_modularity_communities(G)`.

5.1.2 Mean-field synchronization: Kuramoto model

Synchronization is the coordination of events such that individual parts of a system operate in approximate unison. Synchronization can be found in multiple natural systems including neural signalling, heartbeat, and fire-fly flashing light waves. Dynamical systems, including social network systems, are known to exhibit synchronization. Thus, to model the synchronization of agents in a network, we adopt a mean-field synchronization phenomenon, characterized by the Kuramoto model [73]. The Kuramoto model consists of an ensemble of coupled oscillators with intrinsic randomly distributed natural frequencies and the interaction between oscillators depends sinusoidally on the phase difference between pairs of oscillators.

Let $\mathcal{N} = \{1, 2, \ldots, N\}$ represent a set of individuals in a group deciding on a set of strategies. Each individual $i \in \mathcal{N}$ is a node in the network and is connected to a subset of individuals $\mathcal{M}_i \subseteq \mathcal{N} \backslash \{i\}$ by edges. Consequently, network synchronization is a system of differential equations governed by the equation, for node i,

$$\dot{z}_i = \omega_i + \frac{K}{|\mathcal{M}^{(i)}|} \sum_{j=1}^{|\mathcal{M}^{(i)}|} a_{ij} \, \sin(z_j - z_i), \tag{5.3}$$

where $z_i(t)$ is the position at discrete time t, ω_i is the natural frequency, a_{ij} are the entries of the adjacency matrix of the network, and K is a global coupling of synchronization placed on the entire network.

The Kuramoto model has been studied for its theoretical dynamical behaviour such as its stability in nonlinear coupling systems [74, 75], and rhythmic activities for a large number of oscillators [76]. It can also be used for a wide range of applications, including synchronization in complex networks [77], time-dependent delayed oscillations [78, 79], power systems analysis [80], and phase transitions under synchronization [81]. Thus, in applying the Kuramoto model to simulate the synchronization of preferences in a decision-making framework, we consider agents in the network as oscillators, with the position an indication of preference on which Parrondo's game to play.

5.1.3 Example

Here, we make use of the karate club network [82] to demonstrate community partition and the effect of synchronization on the network. The parameters used are specified in TABLE 5.1, with results in FIGURE 5.1.

TABLE 5.1: Table of parameters for Example 5.1.3.

Description	Parameter	Values
Natural frequency	ω_i	$U(1,3)$
Global coupling	K	$\{0,2\}$
Pair-wise coupling	a_{ij}	$\{0,1\}$
Population	N	34

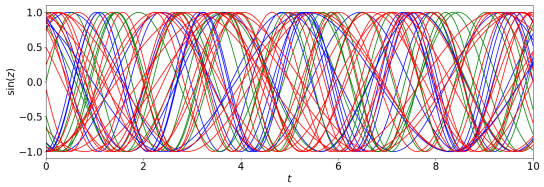

(A) Position $\sin(z_i(t))$ at discrete time t of the karate club, without synchronization.

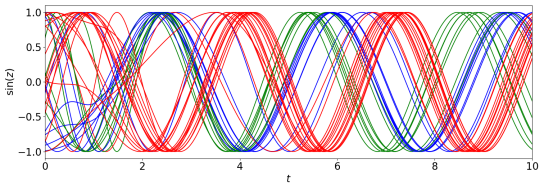

(B) Position $\sin(z_i(t))$ at discrete time t of the karate club, with synchronization, $K = 2$.

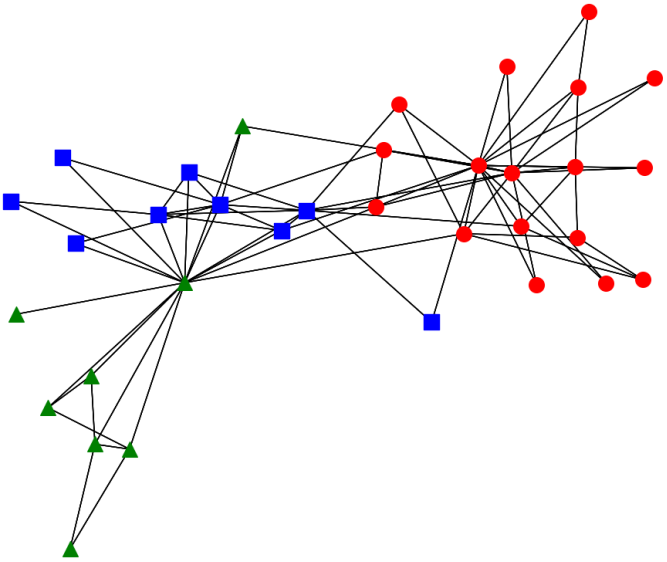

(C) Community structure of the karate club [82].

FIGURE 5.1: Empirical example of how synchronization affects the position of individual nodes in the karate network, and its respective communities.

It is clear that with synchronization, individuals (the oscillators) oscillate in near unison, but how will this affect the outcome of Parrondo's paradox? In the next section, we evaluate how network topology will have effect on Parrondo's games in a synchronization decision-making setting.

5.2 Parrondo's decision-making heuristic framework

We have seen on multiple occasions that the capital-dependent Parrondo's games are individually losing. However, upon random switching, they emerge as a winning outcome. Consider a scenario where the switching is based on the evolution of preference

based on network synchronization. Each individual is randomly assigned a threshold parameter $\beta_i \in [0, 1]$, such that, if $\sin(z_i) > \beta_i$, individual i decides to play game A of the capital-dependent Parrondo's game. We call this "follow own instincts", or strategy Φ (see FIGURE 5.2). It is yet unclear if this is a losing outcome, but strategy Φ will form one of our two strategies. We will come back to this.

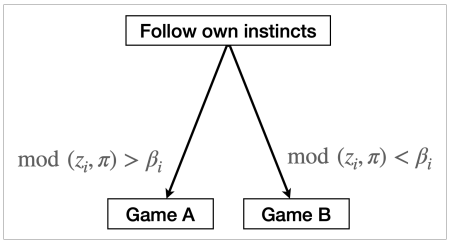

FIGURE 5.2: Strategy Φ: Follow own instincts.

As mentioned, the network can be further partitioned into communities $\mathcal{Q} = \{1, 2, \ldots, Q\}$, where the leader of i's community $C^{(i)}$ is $L^{(i)}$. The definition of a "leader" varies according to various social scenarios, but we define "leader" as the node with the highest degree of the community in our current context. If there are multiple candidate nodes for leadership, this role is randomly chosen among these candidate nodes. Consider the case where instead of following one's instinct, an individual instead chooses to "look to leader", or strategy Λ.

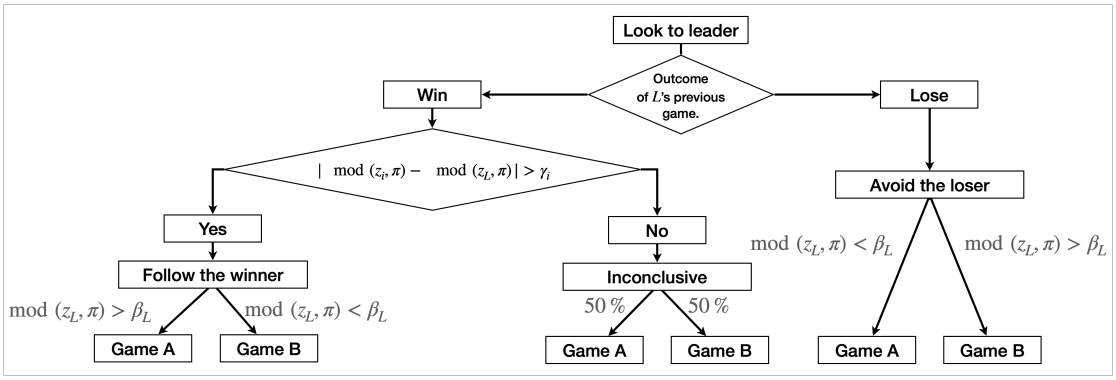

FIGURE 5.3: Strategy Λ: Look to leader.

By executing strategy Λ, the individual i considers the outcome of the last game that one's community leader, $L^(i)$ has played. If the community leader loses the last game played, then i "avoids the loser" by choosing to play the game opposite to what the leader would have chosen. If the leader has won the previous game played, then individual i "follow the winner" by playing the game that leader $L^{(i)}$ would have played, on the condition that their positions are considerably different. Here we define "considerably different" as $|\sin z_i - \sin z_j| > \gamma_i$, where γ_i is called the tolerance factor. Otherwise, "look to leader" is inconclusive and i randomly plays one of two games with random probability. This form of decision-making is consultative and encourages decisive action emerging from differing positions. A summary of strategy Λ is illustrated in FIGURE 5.3.

Finally, we call the switching between strategies Φ and Λ, strategy Σ. Under this strategy, individual i chooses to "follow own instinct" (strategy Φ) in the case where i wins the previous game played. If individual i lost the previous game, then "look to leader" (strategy Λ) is adopted. This is summarized in FIGURE 5.4.

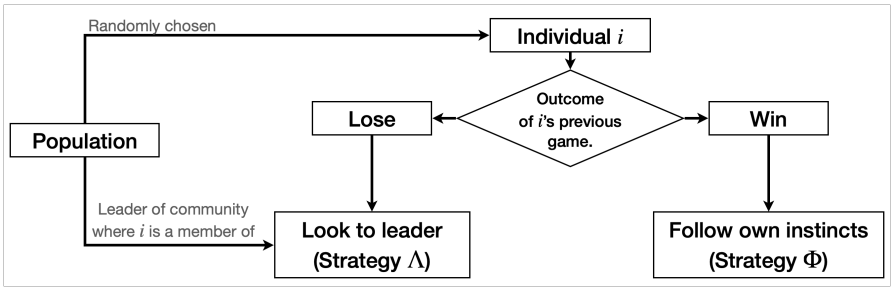

FIGURE 5.4: Strategy Σ: Outcome based decision-making switch.

Isolated individuals will continue to adopt strategies Φ, Λ, and Σ accordingly, albeit individual i and leader L are the same node. In general, under the Parrondo's paradox framework, there is no requirement for games A and B to be losing games. Instead, we require strategies Φ and Λ to be individually losing, but strategy Σ be a winning outcome.

5.3 Network topology and synchronization on decision-making

In this section, we explore various examples to ascertain how network topology and synchronization has an effect on the decision-making heuristic developed in the previous section.

5.3.1 Example (continued)

We start by continuing with Example 5.1.3, by considering the following simple betting games:

Game A - by selecting this game, the individual simply lose \$1.

Game B - by selecting this game, the individual gains \$3 if the capital is even, and loses \$5 if the capital is odd.

The games A and B in FIGURES 5.2 - 5.4 are those described above. The parameters of the example are specified in TABLE 5.2 for a karate club under synchronization, where node parameters are randomly chosen. The average fitness $\bar{d}(t)$ of each strategy, including strategy Σ, with and without synchronization, are plotted in FIGURE 5.5. The results are obtained by performing simulations averaged over 10^5 iterations.

It is clear that strategies Φ and Λ are both losing strategies. In a network structure without synchronization, strategy $\Sigma(K = 0)$, where each individual's position fluctuates at one's own natural frequency, the outcome is improved, however the outcome is still losing. This is not the case with synchronization, strategy $\Sigma(K = 5)$, a winning outcome is obtained. This example with simple betting games suggest that network

TABLE 5.2: Table of parameters for Example 5.3.1.

Description	Parameter	Values
Natural frequency	ω_i	$U(1,3)$
Global coupling	K	$\{0,5\}$
Pair-wise coupling	a_{ij}	$\{0,1\}$
Population	N	34
Threshold factor	β_i	$N(0,1)$
Tolerance factor	γ_i	$U(0,0.5)$

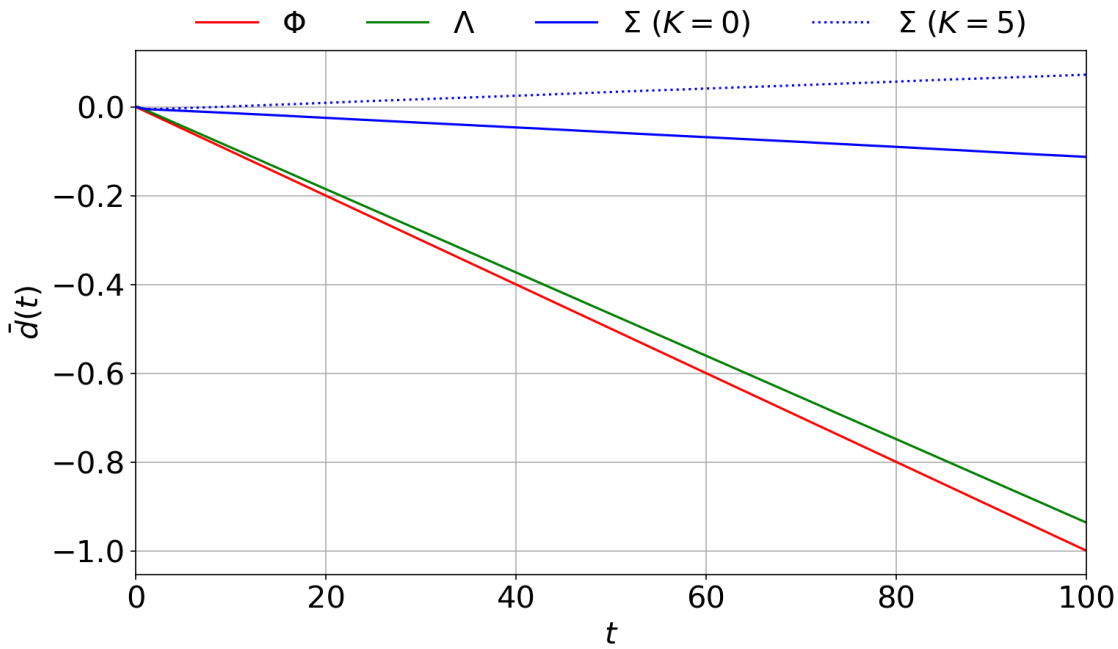

FIGURE 5.5: Karate club network under network synchronization for various decision-making strategies. It is clear that synchronization of the network has an effect on the outcome, i.e. average fitness $\bar{d}(t)$. Under synchronization, the network performs better, resulting in a winning outcome.

synchronization has an effect on the strength of the outcome of our decision-making heuristic. How is this a factor in the standard capital-dependent Parrondo's games?

In the following sections, we return to our typical games A and B from the capital-dependent Parrondo's games.

5.3.2 Synchronization strength on average fitness

Firstly, we investigate the effect of synchronization on the theoretical Barabási-Albert (BA) scale-free network and the Watts-Strogatz small-world network.

The BA network is derived from an algorithm for generating random scale-free networks using a mechanicsm called preferential attachment. These are networks where

a few nodes with high degree as compared to the other nodes of the network, which scales together with the population of the network.

The BA network is generated by attaching each new node with m edges that are preferentially attached to an existing nodes with higher degrees. While the BA network is a theoretical random network, it is commonly found in complex systems, including the World Wide Web, citation networks, and some social networks. The computational means of achieving a BA network is the function `barabasi_albert_graph(N, m)`. The WS network is grown where each node is joined with its k nearest neighbors in a ring topology, with a probability p of rewiring each edge, when a new node is introduced. This is achieved by using the function `watts_strogatz_graph(N, k, p)`. Similarly, the WS network is a random scale-free network that is small-world, as it generates local clustering, seen in many social networks, hence termed small-world.

We plot the average fitness of the population $\bar{d}(t)$ against time t, conducted over 10^5 randomised trials for biased parameter $\epsilon = 0.02$. The outcome, by varying the global coupling constant K for various values is summarized in FIGURE 5.6. We have seen in CHAPTER 1 that randomly switching between games A and B for $\epsilon = 0.02$ results in a losing outcome. Choosing this value of ϵ potentially results in a losing outcome for strategies Φ and Λ, which is what we would like to achieve. Moreover, the results reveal that under strategic switching Σ, the network of synchronized players manages to achieve a higher average fitness, with a stronger global coupling, K, resulting in stronger Parrondo's effect.

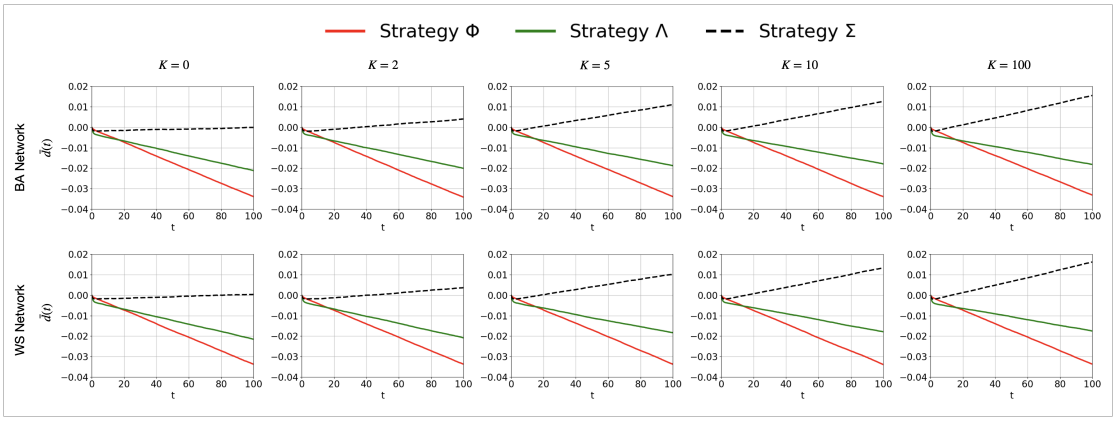

FIGURE 5.6: The average fitness of the population, $\bar{d}(t)$, for the Barabási-Albert network ($N = 100,\ m = 8$) and Watts-Strogatz network ($N = 100,\ k = 8,\ p = 0.5$) for strategies Φ, Λ, and Σ for various values of coupling $K = \{0, 2, 5, 10, 100\}$.

The key result here is that coupling does result in increased average fitness of the population. While the average fitness of the population is monotonically increasing with increasing K, this increase is sublinear.

5.3.3 Bias parameter and population size on Parrondo's paradox

We have seen that the coupling K affects the emergence of Parrondo's paradox. However, that is not the only independent variable that has an effect on the average fitness

of the population $\bar{d}(t)$. Thus, we identify and vary two other parameters: the bias parameter ϵ and network population N. While fixing the the synchronization coupling $K = 5$, we investigate the effect of ϵ and N on the Erdös–Rényi (ER) network. The ER network is useful for "proving" that a property holds for almost all networks. The ER network with population N, is generated by attaching new nodes to existing nodes each with probability p with an edge. This can be achieved by using the function `erdos_renyi_graph(N, p)`.

In order to definitely show the emergence of Parrondo's paradox, we have to identify the domain for ϵ and N where $\bar{d}$ at some t is negative for strategies Φ and Λ but positive for strategy Σ. After determining the domain of ϵ, $\forall N$, that results in a negative average fitness for strategies Φ and Λ, we then perform the same simulations for strategy Σ to determine the domain where Parrondo's paradox emerges. We examine the parameters in the following domains: $\epsilon \in [0.0, 0.03]$ and $N \in [25, 500]$. The average fitness of the population at $t = 100$ for strategy Σ is plotted in FIGURE 5.7a. The heat plot is obtained by conducted 10^4 randomised trials for each pairwise values of ϵ and N. FIGURE 5.7a also shows the domain for which Parrondo's paradox is observed, which requires $\bar{d} < 0$ for both strategies Φ and Λ, and $\bar{d} > 0$ for strategy Σ.

FIGURE 5.7a reveals that regardless of the value of ϵ, the average fitness of the population is shown to increase rapidly with small populations, and reach its peak in the domain $N \in [30, 45]$, and then decreases nonlinearly where the average fitness converge to the same value for all three strategies. This non-monotonic dependence of the average fitness on network size is a signature of complexity. This can be used to argue that the collective social behavior at criticality supports optimal information transmission within the network [83, 84]. An example of this non-linearity is shown in FIGURE 5.7b. Here, the value of epsilon is fixed at $\epsilon = 0.02$, while varying population size N for the same network setup, the average capital is shown for $t = 100$, conducted over 10^5 randomised trials. We see that the strength of Parrondo's paradox, determined by the average fitness, peaks at $N \approx 45$.

It is worth noting that in 1992, anthropologist Robin Dunbar extrapolated the correlation observed for non-human primates to predict a social group size for humans [85]. Using a regression equation on data for 38 primate genera, Dunbar predicted that the groups fell into three categories - small, medium and large. This is equivalent to social structures commonly denoted as bands, cultural lineage groups and tribes - with size ranges of 30-50, 100–200 and 500–2500 members, respectively. Effective decision-making groups often do not grow beyond the "small" category [86]. Here, the strength of Parrondo's paradox is maximised at a population size of about 45. Consequently, we have used the decision-making framework to provide a numerical basis for Dunbar's predictions.

Lastly, on how the average clustering coefficient of a network affects the outcome of Parrondo's paradox, we simulate this on the ER network, with $\epsilon = 0.02$ and population $N = 45$. The ER network is chosen here in order to have a range of clustering coefficients.

We note from FIGURE 5.8 that for clustering coefficient < 0.125, Parrondo effect for the ER network is not observed. This is due to the low clustering, and multiple isolated

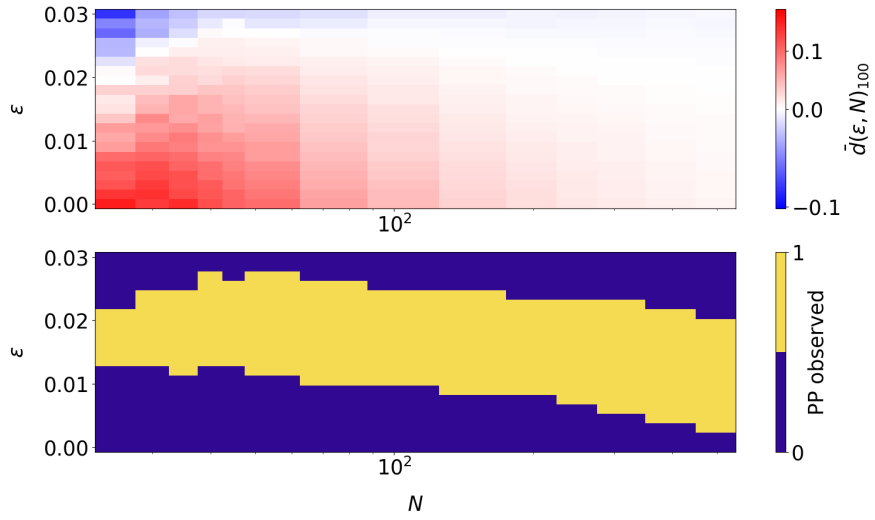

(A) Relationship between the average fitness of the population $\bar{d}$ at $t = 100$, and independent variables ϵ and N, and the domain for which Parrondo's paradox is observed.

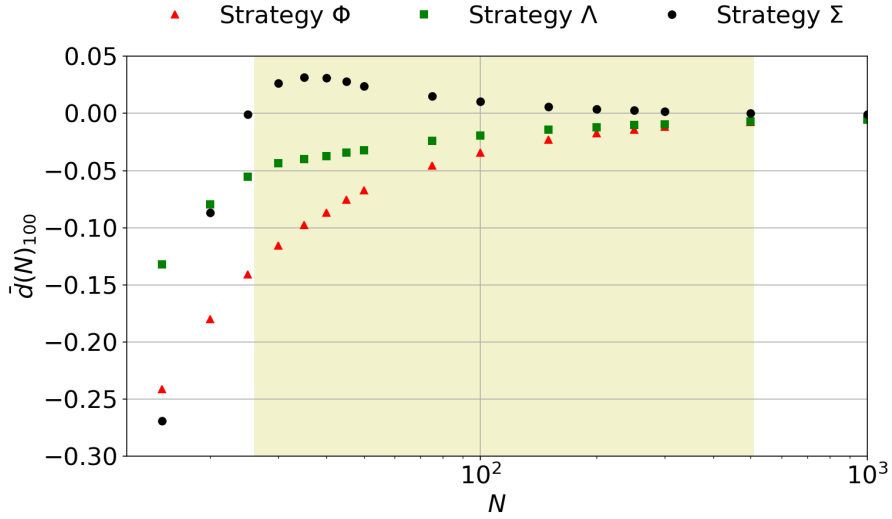

(B) Example of the nonlinear relationship between the average fitness of the population $\bar{d}(t)$ at $t = 100$ and population size N, for a fixed bias parameter $\epsilon = 0.02$. The shaded region denotes the domain of N for which the emergence of Parrondo effect is observed.

FIGURE 5.7: Relationship between of the average fitness of the population $\bar{d}$ at $t = 100$ for varying bias parameter ϵ and population size N for the ER network ($p = 0.2$).

nodes in the network, leading to strategy Φ being played most of the time, which we have shown to be a losing strategy. However, there is a phase transition for the clustering coefficient of approximately 0.125, at which point Parrondo's paradox is observed. This phase transition is likened to phenomena observed in statistical mechanics, which may suggest that interacting agents in a network exhibit phenomena observed in the canonical and microcanonical ensembles of spin-lattice glass and Ising model. Therein lies the connection between studying social systems and their inherent behaviours and statistical mechanics in Physics.

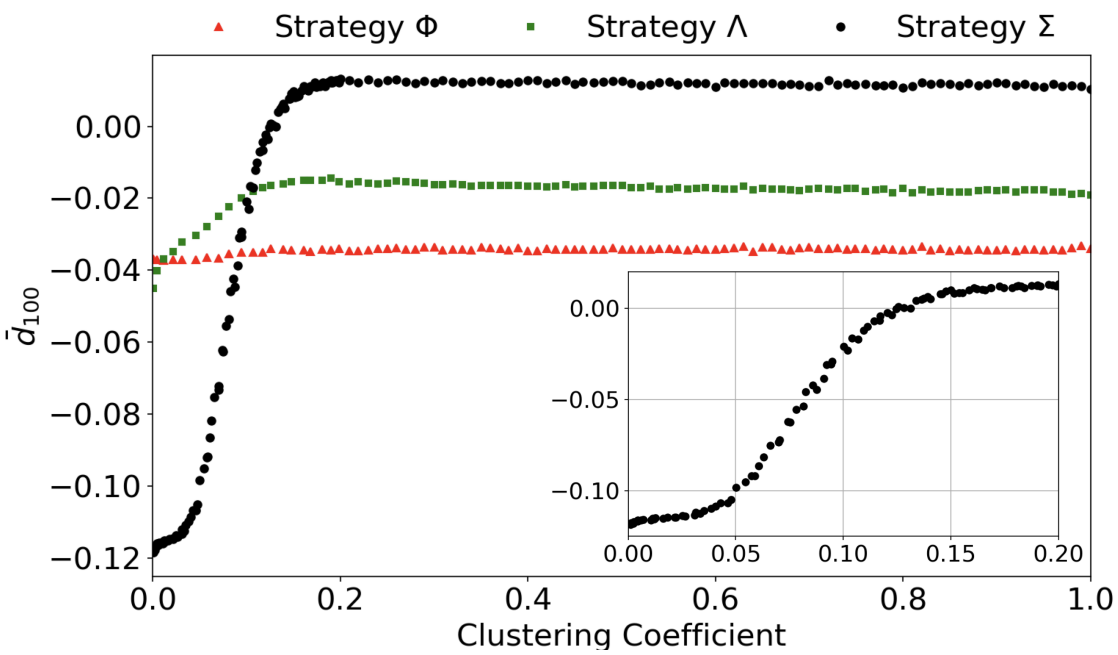

FIGURE 5.8: The average fitness of the population, $\bar{d}$ at $t = 100$, for the Erdös–Rényi network ($N = 45$) for strategies Φ, Λ, and Σ observed by varying the average clustering coefficient. A phase transition is observed between the absence and emergence of Parrondo's paradox.

5.4 Summary

Synchronization is an important theory that is commonly used for the understanding of self-organization phenomena in complex systems. This chapter has demonstrated that under synchronization, a network of interacting agents in its community structure can yield a better outcome when choosing between two losing strategies. Critically, we have a numerical basis for Dunbar's predictions for band sizes. In effect, it will be ideal for playing synchronized decision-making Parrondo's games of this nature for a population size of $N \approx 45$ and be in a group with a low clustering coefficient, but not resulting in isolated nodes. These findings would be beneficial to further studies exploring Parrondo's paradox in other multi-agent decision-making settings.

Chapter 6

Single-prioritization Voting for Controlled-collective Games

In this chapter, we explore another aspect of social decision-making—voting. We want to explore the dynamics of voting in a social setting. However, instead of a single agent making a decision and acting at each time step, we now have a group that collectively arrives at a decision, and all members act together. Previously, it was shown that agents should vote randomly than vote according to their own benefit in one turn. The former yields a winning tendency while the latter results in steady losses with increasing population size [31, 32, 33].

Here, we explore three different single-prioritization voting schemes and the emergence of real-life voting phenomena. Single-prioritization voting aims to choose one, and only one (hence single), the outcome from multiple choices. The choices available are three different losing controlled-collective games. Controlled-collective games are established rules placed on the game that all individuals playing the game must conform to. Collective games are those where every individual universally agrees to adopt the outcome as a result of the voting system, and controlled games are games where every individual behaves in a deterministic way, in our case, every individual aims to maximise individual outcomes.

6.1 Controlled-collective 3-option Parrondo's games

Since we have at least three existing losing games from our earlier discussions, the biased game A, the capital-dependent game B, and the history-dependent game B′, we shall use them in this chapter for our discussion. For clarity in this chapter, we shall call game B′, game C. The dynamics of all three games are the same as those mentioned in Chapter 1.

Instead of having three states in the case of the capital-dependent game, and four states in the case of the history-dependent game, a direct consequence of having three choices means we now have twelve possible states. For each capital-dependent state, we have $C \in \{0, 1, 2\}$ denoting the capital modulo 3, and four history-dependent states in the form $H = \{(h_{t-1}, h_{t-2})\}$, where we have permutations of $h_t \in \{L, W\}$. A product of considering three losing games is to construct a tuple to represent each state, thus, the

set of all states is $S = \{(C, H) \mid C \in \{0, 1, 2\}, H \in \{(L, L), (L, W), (W, L), (W, W)\}\}$. We now analyze the preference ranking of each game as a result of having three choices.

6.1.1 Preference ranking

Consider an individual with capital divisible by 3 (i.e. capital state 0, and the past two outcomes of playing Parrondo's games are (L, L). In this case, if we were to examine the winning probabilities, the winning probability of game A is $p_A = 0.495$ (note we are still using $\epsilon = 0.005$), the winning probability of game B is $p_{B1} = 0.095$, and the winning probability of game C is $p_1 = 0.895$. Thus, the preference ranking is: game C $\succ$ game A $\succ$ game B. Here, we denote "game A $\succ$ game B" if game A is preferred over game B. FIGURE 6.1 shows the preference ranking of all twelve states.

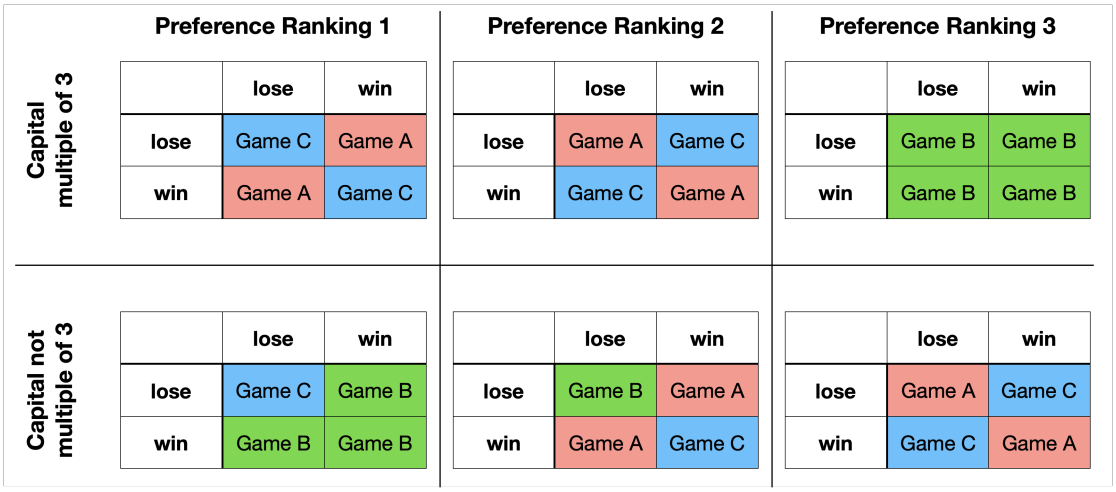

FIGURE 6.1: Compilation of the preference ranking when faced with three potential choices. The games are ranked in order of which game gives the best outcome for each of the twelve possible states.

FIGURE 6.2 further depicts the Markov chain, and the possible transitions in such a setup. The transition probabilities are intentionally left blank as they will be decided during each round of voting. While the probabilities change with discrete time t, the state transitions do not. Note that each state has two incoming arrows from two states and two outgoing arrows towards two states. They represent the two possible outcomes from a coin toss.

The Markov chain in FIGURE 6.2 can be described as an equation of detailed balance:

$$\pi(t + 1) = \Pi^{(k)}\pi(t), \tag{6.1}$$

where $\pi(t)$ is a column vector with 12 elements corresponding to the fraction of individuals in each of the states in S, and $\Pi(k)$ is a 12×12 dynamic transition matrix, dependent on the game chosen, $k \in \{A, B, C\}$. The entries of $\Pi^{(k)}$ can be derived from FIGURE 6.2 as follows:

$$\Pi_{ij}^{(k)} = \begin{cases} q_{j,i} & \text{if } \exists\ j \to i \\ 0 & \text{otherwise} \end{cases}, \tag{6.2}$$

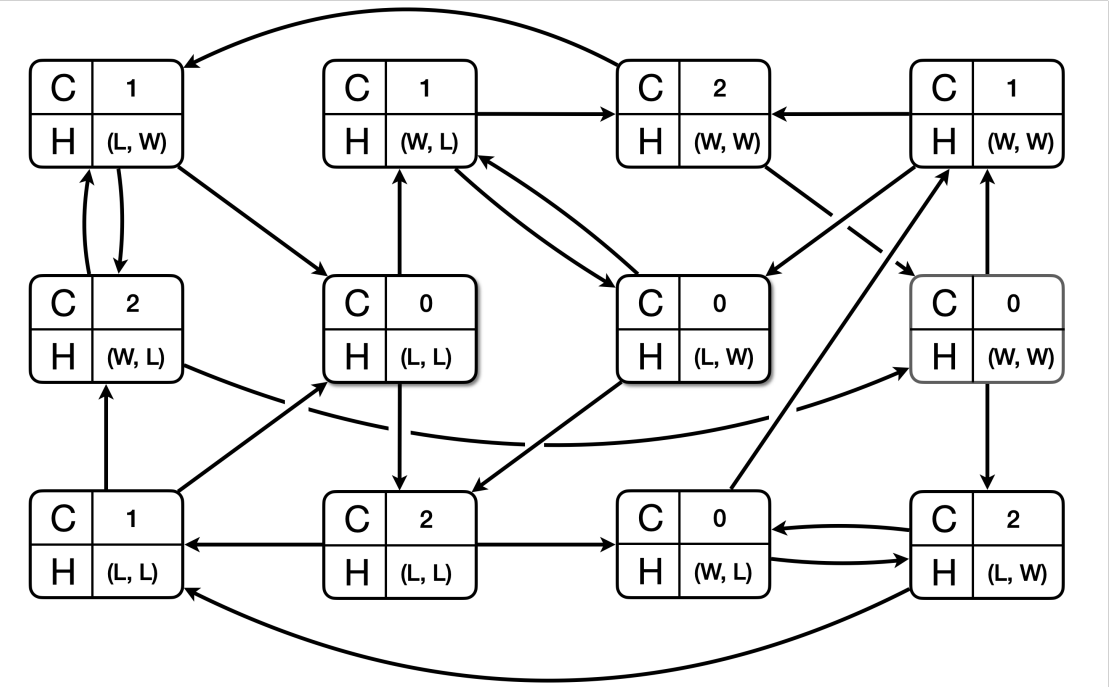

FIGURE 6.2: The possible Markov chain state transitions. The transition probabilities are intentionally omitted as it changes with discrete time.

where $q_{j,i}$ represents the transition probability from state j to state i, and $j \to i$ denotes a directed edge (or possible transition) from j to i. As discussed earlier, it follows that

$$\sum_i \Pi_{ij}^{(k)} = 1, \quad \forall\, j. \tag{6.3}$$

Since $\Pi^{(k)}$ is a sparse matrix, efficient computations can be performed numerically to verify results. For example, if the ensemble collectively plays game A, then $\Pi^{(A)}$ takes the form of a 12×12 transition matrix satisfying EQUATIONS (6.2) and (6.3). The q values for each column are assigned as follows: the state transiting $C \leftarrow C + 1 \pmod 3$ is $\frac{1}{2} - \epsilon$ and $C \leftarrow C - 1 \pmod 3$ is $\frac{1}{2} + \epsilon$.

6.2 Single prioritization Voting Schemes and Results

In a controlled-collective game of N individuals, with randomly assigned initial capital and historic states, the preferred first choice of each individual differs according to FIGURE 6.1. In the case where every individual is randomly assigned an initial state, that is, initial capital and history are assigned independently of each other, this results in $1/6$ of the individuals preferring to play game A as their first choice, $1/2$ preferring game B as their first choice, and $1/3$ preferring game C as their first choice. In this section, we want to examine how various single-prioritization voting systems affect the outcome of playing Parrondo's games. We will also discuss how some game rules adjustments can result in emerging well-known phenomena in single-prioritization voting.

6.2.1 Plurality voting

Plurality voting follows the idea that the option that receives the most votes, not necessarily achieving majority votes, is adopted by the entire ensemble, and all agents will play that option. Plurality voting may not satisfy the majority of the group's preference, thus potentially leading to a majority of the group being disenfranchised from this voting scheme.

We know that if the group population consist of only a single agent, the capital outcome of the game can always be maximized, thus achieving maximized fitness. That single agent, needs only to find consensus with oneself, and will always vote for the game of top preference ranking. However, what would happen with an increasing number of agents in the group?

In the first simulation, we empirically examine the outcome of choosing between three losing games for an ensemble of N agents. The single-prioritization voting scheme is plurality voting, where the entire group will play the option that receives the most votes. All agents of the group are controlled, and will always vote for one's top preference. The result of this simulation is shown in FIGURE 6.3, where the average fitness of the population $\bar{d}(t)$ is plotted against time t. Here, the average fitness is derived from conducting 10^6 experiments.

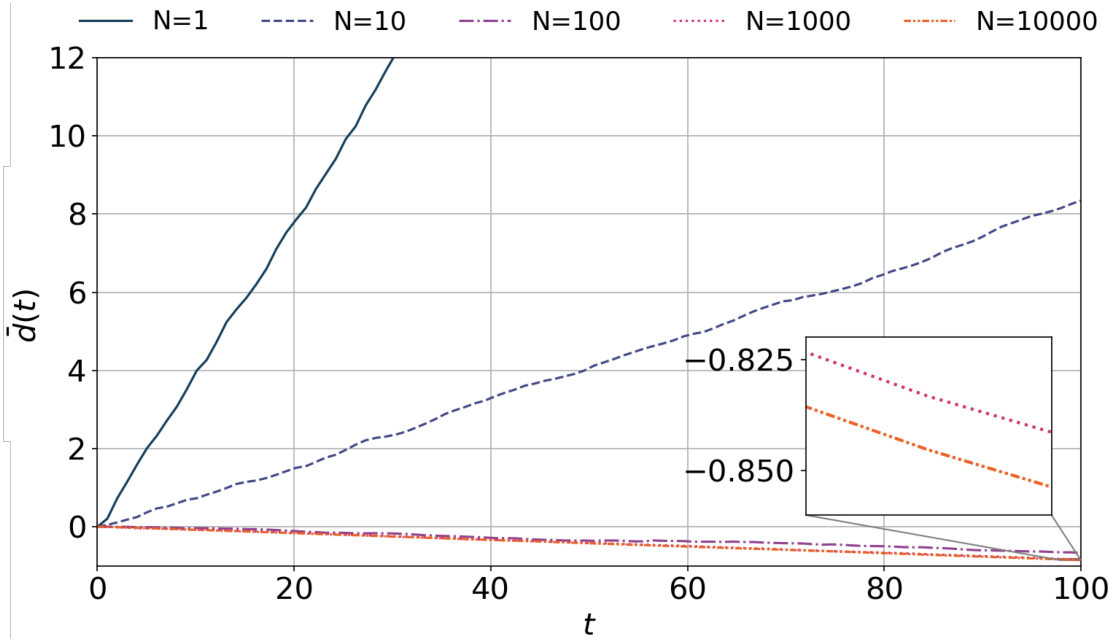

FIGURE 6.3: A comparison of the average fitness of the population after $t = 100$ time steps for an ensemble with $N = \{1,\ 10,\ 100,\ 1000,\ 10000\}$ individuals playing 3-choice controlled-collective game using plurality voting.

Clearly, the simulation results show that under a plurality voting regime, an increasing number of individuals does lead to a losing outcome. Parrondo effect weakens with an increasing number of individuals in the ensemble and eventually disappears. The spoiler effect is most prominent when an option results in vote splitting. Plurality voting is very susceptible to the spoiler effect when each individual can cast only a vote

for a single option. In the case of the 3-option controlled-collective game, game A is deemed to be the "conservative" game, where the probability of winning is close to the probability of losing, 0.495 and 0.505, respectively. We call game A the spoiler option.

An agent, in the case of our setup, with state $(0, (L, W))$ or $(0, (W, L))$, would ordinarily vote for game A as its top-ranking choice. However, if we entertain the idea that an agent voting for game A does not risk much, we can factor such decision-making into the setup[1]. Suppose such an agent switches strategy and chooses game C, one's second-ranked choice, for its top choice, this changes the initial controlled-collective game in two ways:

1. We now have a 2-option collective game, as no individual will vote for game A. The votes are split between games B and C.
2. Agents in the state (0, (L, W)) or (0,(W, L)), reduce their chance of winning by about half, i.e. from 0.495 to 0.245.

The result of this change is simulated for $N = 5000$ and is presented in FIGURE 6.4. Paradoxically, the combination of eliminating game A by considering it the "spoiler" option and forcing a subset of individuals to take bigger risks, results in a winning outcome for a 2-option collective game. Here, we showed that it is possible to turn a losing outcome of a 3-option controlled-collective game into a winning outcome by removing the "spoiler" option.

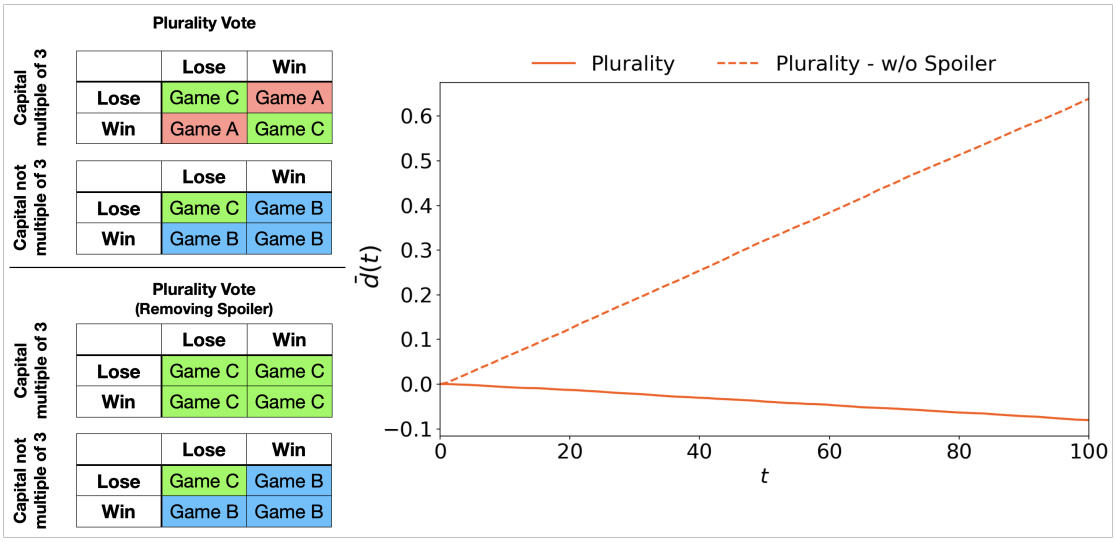

FIGURE 6.4: A comparison of the population's average fitness for an ensemble of $N = 5000$ voters. The solid line is the outcome of the 3-option controlled-collective game using plurality voting. The dashed line is the outcome when individuals with game A as the top choice choose instead to list game C as the top choice; this is a 2-option collective game.

[1]By factoring this in, we no longer are in the realm of controlled games as the agents are not rational, i.e. always maximizing one's probability to win. But this reveals an interesting dynamic worth discussing as an aside.

6.2.2 Ranked-choice voting

Another form of single-prioritization voting is ranked-choice voting. In such a voting scheme, the ensemble of agents in the group is required to rank all the options available in descending order of preference. For example, in a ballot with m options, each option is assigned a unique rank by individual i, such that the option with preference ranking '1' is the top choice. In the first round of vote counting, after every individual's top choice is counted, the option that receives the majority of the votes (50%+1 votes), will be chosen as the collective decision. If, however, no option receives the majority of the votes, then the option that receives the fewest votes is removed from the results pool, and the voters who voted for that option would have their vote counted for the next highest-ranked option that is not yet removed from the ballot. This process is repeated until an option exceeds the majority number of votes. The algorithm for ranked-choice voting is described in FIGURE 6.5. Under ranked-choice voting, we as the same question what would happen with an increasing number of agents in the group? We examine how this form of single-prioritization voting differs from plurality voting. FIGURE 6.6 shows the outcome of of ranked-choice voting with increasing population size.

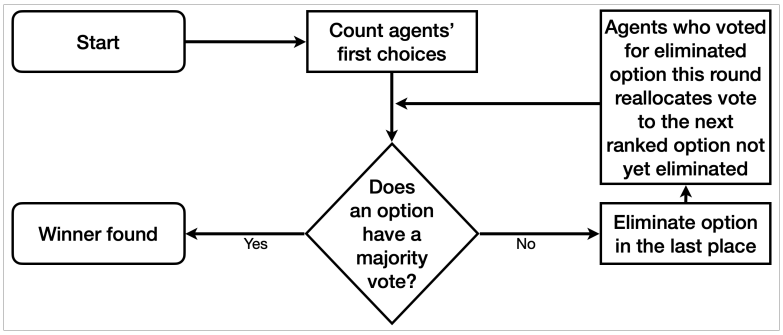

FIGURE 6.5: The ranked-choice voting algorithm.

Similar to the results from the simulations of plurality voting, we observe that increasing the number of agents in the group, from $N = 1$ to $N = 10,000$, frustrates the population's average fitness. However, unlike its plurality voting counterpart, ranked-choice voting does not lead to a negative average fitness of the population.

One should note, however, that ranked-choice voting also has its disadvantages, especially in the case of a 3-option ballot, as in our case; that is the effect of the centre squeeze. Centre squeeze is the phenomenon where "centrist" options, like game A, are predominantly "squeezed" out of the ranked-choice voting algorithm in the first round of voting. In the real world, this may lead to strategic voting where agents whose first choice was originally game A, see no prospect in game A being chosen but refuses to allow the outcome of the vote to force them to play game B. Thus, such agents "squeeze" game A out of the ballot, instead settling for game C as their first choice. This effectively results in a rank choice vote becoming a majority vote between games B and C.

We conduct an experiment comparing the outcome of 3-option ranked-choice voting and 2-option majority voting (comprising of only games B and C) controlled-collective game for $N = 5000$ agents. The average fitness of the population, at $t = 100$ are 6.3969

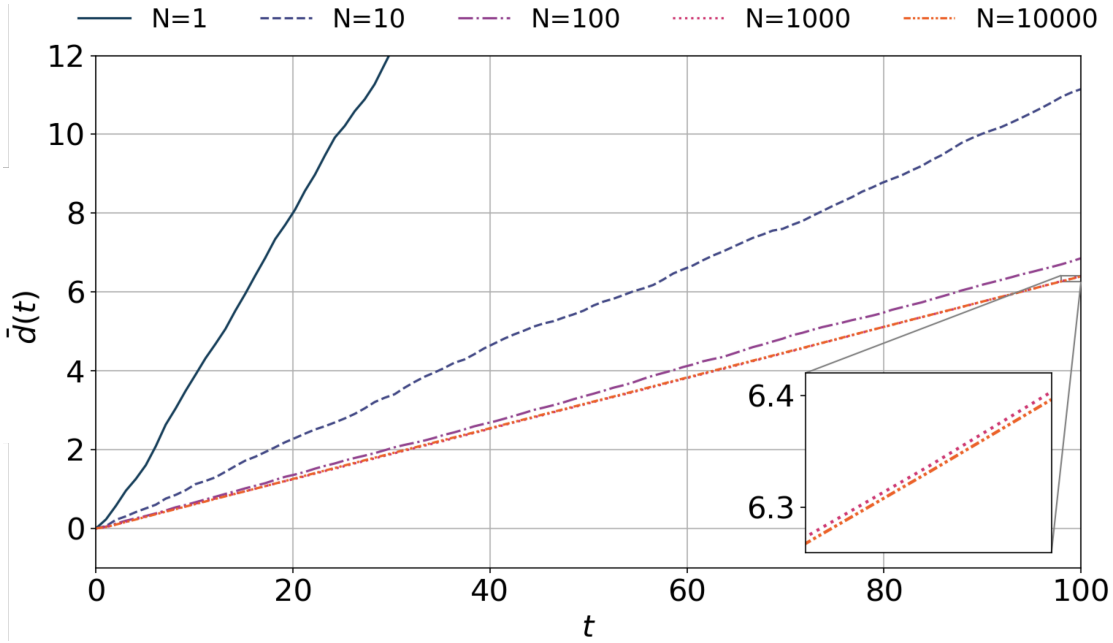

FIGURE 6.6: A comparison of average capital per agent after $t = 100$ time steps for an ensemble with $N = \{1,\ 10,\ 100,\ 1000,\ 10000\}$ agents playing 3-option controlled-collective game using ranked-choice voting.

and 6.3755, respectively. Consequently, we note that there are no significant differences in outcome, the presence (or absence) of game A as an option does not significantly alter the outcome of the voting process. This is the centre-squeeze effect of ranked-choice voting, where the presence or absence of a "centrist" option usually has little effect on the outcome of the vote. It is worth noting that games B and C often pose the most risk to a larger population of voters, as such game A is a safe option. The "irrelevance" of game A is further compounded by the fact that the risk involved in choosing game A is small, as there is a slight difference in the win-lose probability, thus "squeezing" it out of the initial set of options does not alter the eventual outcome.

6.2.3 Approval voting

The final type of single-prioritization voting considered in this chapter is approval voting. In approval voting, each agent votes for all the favourable options on the ballot. If an option is favourable to the voter, regardless of rank, the voter can vote for it. Unlike plurality voting, each voter can submit more than one preference. Unlike rank choice voting, the voting can be concluded in a single round, where each vote of approval counts toward the total number of votes for the option. The option with the most votes, by approval, will be the collective decision made by the group. Approval voting allows for flexibility as it does not require voters to rank all the options, while at the same time, "centrist" options are not squeezed out of the vote. This section presents a framework for modelling approval voting according to the preference ranking listed in FIGURE 6.1. In our simulation, an agent is

1. always approving of one's top choice, hence will vote for it,

2. approving of one's second choice with a probability $p2$, and
3. also approving of one's third choice, given that one also approves of the second choice with probability $p_{3|2}$.

Notice here that an agent in such a controlled game is rational as an individual will never vote for an option of lower preference ranking if one has not voted for one of higher ranking. The simulation results, using this framework, can be found in FIGURE 6.7, for a population size of $N = 5000$.

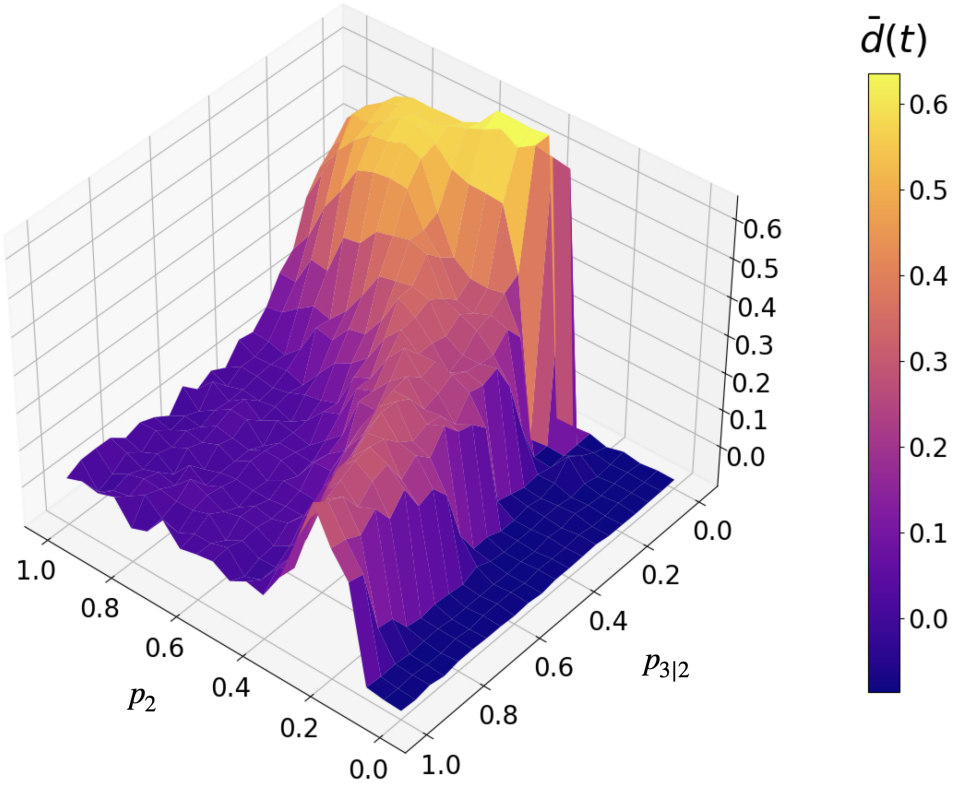

FIGURE 6.7: The average fitness of the population at $t = 100$ time steps for an ensemble with $N = 5000$ agents playing 3-option controlled-collective game using approval voting.

Approval voting can be beneficial in 3-option controlled-collective Parrondo's games. Let us consider a few interesting cases.

Firstly, consider the case where most agents are selfish, by approving of their first choice only, with a few exceptions voting for their second and third choices. This corresponds to the region of FIGURE 6.7 where $p_2 \approx 0,\ \forall p_{3|2}$. The collective gain is significantly lower, leading to a negative average fitness of the population. Selfish agents result in a similar outcome to plurality voting. Secondly, consider the case where the majority of agents approve of all the options. It is indicative from FIGURE 6.7 that in such a case ($p_2 \approx 1,\ p_{3|2} \approx 1$) is not as beneficial. It results in a positive average fitness of the population, but strong cooperation detriments the entire group.

The simulation also suggests that the best outcome can be achieved when 50% of the players approve of their second choice, while at the same time, not approving of their third choice. This gives rise to a variant of the phenomenon called the *Volunteer's dilemma*, where total cooperation might lead to lesser gains, and not cooperating is mutually destructive [87]. There is a balance where a ratio of voters (possibly multiple ratios) cooperating and not cooperating gives the best outcome. This is observed in FIGURE 6.7 as well. Deviation from the spur, either by total cooperation or antagonistic selfishness, we shift away from the beneficial outcome of adopting approval voting, resulting in a drastic decrease in average fitness.

6.3 Summary

In this chapter, we have discussed another aspect of social dynamics Parrondo's paradox, where an ensemble of agents is tasked to vote on one's preferred losing game. The dynamics of agents playing the collective Parrondo's games in a controlled manner through first-prioritization voting reveals the conditions for which a winning outcome can be achieved by switching between three losing games. This is an extension of the typical Parrondo's games, where, in general, only switching between two losing games is considered. The usefulness of various voting systems as a framework to vote for single prioritization is revealed when more losing games are considered. There are further advances in this field of work by changing the constraints imposed on the dynamics of the agents. For example, we have seen how, if individuals are not controlled, and behave differently, in the case of eliminating the spoiler option and ignoring the "centrist" option, the outcome may be different. These are uncontrolled games.

Furthermore, we can also consider a different form of collective decision-making, where instead of the entire group collectively agreeing to play the game that wins the single-prioritization vote, only a subgroup chooses to do so, while the rest rebel. In such cases, further analysis involving opinion dynamics may be required, which motivates future work. Lastly, single-prioritization voting systems can be replaced with other game-theoretic multi-voting systems. The variations and options available for research remain wide, which keeps this topic of discussion relevant.

Chapter 7

Conclusions and Future Work

Parrondo's paradox is a phenomenon in which two losing strategies can be combined to form a winning strategy. This may seem counterintuitive, but it is based on the idea that the combined strategies can create a situation in which some form of switching is exploited to achieve a ratcheting effect. In other words, by combining two seemingly disadvantageous strategies, the overall probability of success can be increased. As we have seen, despite its counterintuitive nature, Parrondo's paradox is a phenomenon with many practical applications, that continues to be studied by researchers today. This thesis has covered the emergence of Parrondo's paradox in two wider fields that are of significance. In this final chapter, we will conclude the study by summarising the key research findings in relation to the research aims. We will then discuss this thesis's value and contribution to the wider field of Parrondo's paradox, quantum algorithms, and social physics. Next, a review of the limitations of the study, and finally I will provide perspective on proposed opportunities for future research.

7.1 Contribution to the field

7.1.1 Quantum Parrondo's paradox

This thesis sets out to expand the contribution to the field of quantum Parrondo's paradox by considering quantum systems that have no analogous classical system and to provide a working example of how it can be useful in technology.

In particular, CHAPTERS 2 and 3 describe a quantum Parrondo's protocol that makes use of two quantum coins on a quantum random walker. When applying two individual quantum coins with a specified boost, it results in a quantum walker with a negative average position. However, under the same protocol, with switching between quantum coins, we have shown that it is possible to achieve strong Parrondo's paradox under the following conditions:

1. Shift operator $\hat{S}$ with biased boost for tossing two 2-sided fair quantum coins, and
2. Tossing two 4-sided fair quantum coins for switching mentioned in TABLE 2.3.

While there are multiple possible ways of achieving Parrondo's paradox under the conditions described, the means to generate a complete list is arduous. In these chapters, we suggested two main ways of switching between the two quantum coins to achieve

Parrondo's paradox: random stochastic and periodic sequence switching [88, 89]. The quantum coin-toss Parrondo's paradox is a new abstraction of Parrondo's paradox with no known classical analogue. In formulating the quantum Parrondo's game according to quantum coin tosses, we know that this has since been shown to be achievable by quantum technologies [90]. In the context of theoretical quantum Parrondo's paradox research, this work brings us closer to finding the best possible mean position in a 2-sided quantum coin-toss random walk Parrondo's game.

Furthermore, we introduced a third form of switching - deterministic aperiodic switching, or chaotic sequence switching [91]. The advantages of chaotic switching, namely its deterministic yet aperiodic nature, mean that we can utilise it for advances in quantum technologies. In particular, we outlined a method for semiclassical encryption that makes use of chaotic maps and two 2-sided quantum coin toss for encryption.

While chaos in quantum systems is not defined in the same way as it is in classical chaotic and dynamical systems, there are quantum systems whose fundamental physical properties exhibit properties of chaos [56]. Although there is no concept of entanglement within classical systems, research has shown that chaos and entanglement are very clearly and strongly related [51, 57]. Furthermore, the introduction of chaotic switching, when combined with Parrondo's paradox, extends the application of Parrondo's paradox to one that has real-world engineering applications. The benefits of quantum cryptography include secure communication, detection of eavesdropping, and increased security. Quantum cryptography is based on the laws of quantum physics, which is a more sophisticated and proven secure method of encryption. Furthermore, if a third party attempts to intercept the ciphertext, then the quantum state changes, modifying the expected outcome for the receiver. The semiclassical method introduced in this thesis is derived from semiclassical quantum Parrondo's paradox, which suggests its viability as a tool for further advances in quantum information technology.

Following the publication of these works, there have been further advances in aperiodic switching, resulting in Parrondo's paradox [44]. Additionally, experimental verification of the quantum coin-toss Parrondo's paradox confirms the theory presented in this thesis [90]. The proliferation of research in this area will only continue if there is known application and potential advances in technology through the implementation of quantum coin toss Parrondo's paradox. Thus, this work has led to the addition and scaffolding of knowledge in the field of quantum Parrondo's paradox. The furtherance of this will be discussed in SECTION 7.3.

7.1.2 Sociodynamical Parrondo's paradox

Existing literature focuses almost entirely on group performance by altering social rules. However, these social rules are often static, and agents in the network do not change their behaviour according to the outcome. Thus, the second aim is to develop a comprehensive framework that is applicable to researchers to extend the field of Parrondo's paradox applied to sociodynamical systems and show its diverse use in real-world situations.

In CHAPTERS 4 to 6, we outline three ways to examine the use of Parrondo's paradox in social settings to reveal real-world phenomena. We first established a preference aggregation framework for which agents in the network can affect and influence each other and play Parrondo's games through preference aggregation, decision-making, and a feedback loop. We demonstrated the robustness of the preference aggregation framework by showcasing various examples of social preference interactions and decision-making. For example, we showed, in the example "ill-informed advising the ill-informed", the dangers of closet-mindedness, where the openness to put weight on another's preference in decision-making does not improve on the choice between two losing options. In the same simulation, we showed that even a slight openness to consider the collective preference of one's connections ahead of one's own preference could lead to a positive outcome from playing two losing games [64].

We further demonstrated the robustness of the preference aggregation framework by explaining results through social phenomena, playing Parrondo's games with a dynamic feedback loop on a bi-directional network, and demonstrating the emergence of Simpson's paradox when partitioning a social network [67]. It was also in the simulations for preference aggregation Parrondo's paradox that we first observe hints of possible phase transitions. These phase transitions are indicators that there are critical changes at the micro-level (agent level) that result in a change at the macro-level (network). This was, again, observed in our description for network synchronization.

Lastly, we discussed another aspect of social dynamics Parrondo's paradox, where an ensemble of agents is tasked to vote on one's preferred losing game. The dynamics of agents playing the collective Parrondo's games in a controlled manner through first-prioritization voting reveals the conditions for which a winning outcome can be achieved by switching between three losing games [92]. To the best of our knowledge, this is the first work that explores three losing games in a social setting. We explained known cons of single-prioritization voting, such as the spoiler, centre squeeze, and volunteer's dilemma, in the context of voting between three losing Parrondo's games. Thus potentially opening up the exploration of Parrondo's paradox from a game theoretic analysis perspective.

The area of social dynamics Parrondo's paradox is largely unexplored. With its potential to incorporate various concepts from complexity theory, stochastic theory, and Markov theory, social dynamics Parrondo's paradox is an emerging field that will have its roots in social physics. We will discuss more in SECTION 7.3.

7.2 Suggestions for Improvements

7.2.1 Computational resource constraints that limit methodology

The bulk of this thesis involves simulations of complex systems. A complex system is composed of many interacting components, with outcomes often dependent on the dynamics of its interacting parts. With a large number of degrees of freedom, determining, in a meaningful manner, how each interacting component affects global properties, such as the expected position of in quantum coin-toss Parrondo's paradox or average fitness of the population in the case of social dynamics Parrondo's paradox, requires

both computational resource and time. During the course of this study, simulations were conducted for variables identified to potentially result in the emergence of Parrondo's paradox. For example, in the case of social dynamics Parrondo's paradox, we simulated mainly on theoretic network topologies, with a focus on parameters such as average degree and clustering coefficient instead of centrality or number of cliques. Additionally, we controlled a few variables which might limit the scope of results presented. For example, in the case of the quantum coin toss Parrondo's paradox, we only considered the case of fair quantum coins. Hypothetically, Parrondo's effect could also be observed for biased quantum coins in the form of EQUATION (2.6). These constraints were specifically chosen to limit the scope of the study in order to prioritise given the available computational resource.

7.2.2 Early research studies on the topic

Quantum Parrondo's paradox was first published in 2002 [28] with sporadic publications in the early 2000s [29, 26]. These publications seek to quantise the dynamics of the classical capital-dependent and history-dependent Parrondo's games. Research in quantum Parrondo's paradox took a lull until the late 2010s [93, 94] due to the resurgence in quantum information research and technology. Due to this resurgence of interest in quantum Parrondo's paradox, prior research studies that are relevant to this thesis were limited. This motivated an in-depth review on this topic to identify the literature gap [95], which in turn motivated the development of innovative quantum systems exhibiting Parrondo's paradox that have no known classical equivalence.

Social dynamics Parrondo's paradox, on the other hand, had a different early research. The earliest form of social Parrondo's paradox was in the form of cooperative Parrondo's paradox [13]. Following this, there was multiple isolated research focused on various forms of social rules governing the interactions between agents playing Parrondo's games. However, there is no unified framework that is robust enough to encompass or classify this research, thus it was difficult to observe how the research in this area evolved. This motivated the preference aggregation Parrondo's paradox, which essentially is a framework to summarise and classify social dynamics Parrondo's paradox. In essence, the outcome of this thesis was to find an underlying framework that is applicable to existing literature.

For these reasons, when there is very little or isolated research on a specific topic, this led to the need to define and develop new research directions for these two fields of study. Thus, while readers may not entirely agree with the direction taken, the work from this thesis is unique as they have not been explored by experts in the field.

7.3 Perspective for future research

7.3.1 Quantum coin-toss Parrondo's paradox

In this thesis, we have explored two main scenarios for the quantum coin-toss protocol: for a pair of 2-sided fair quantum coins and a pair of 4-sided fair quantum coins. While we have shown that the average position of the latter improves on the average position of the former, this outcome may not hold for any generalised pair of fair 2^N-sided

coins. It is clear that the shift operator $\hat{S}$ for an equivalent 2^N-sided protocol has an increasing number of degrees of freedom, each corresponding to the state of each face of the coin. As such, with increasing permutations, the question remains, will it be possible to achieve quantum Parrondo's paradox with two 2^N-sided quantum coins? This remains an open problem worth tackling with the use of available computational resources to tackle the complexity of the problem.

For a problem with a smaller number of degrees of freedom, one can consider whether quantum Parrondo's paradox can be achieved in the case of tossing two biased quantum coins, with a fair boost. In this thesis, we showed that the random tossing of two 2-sided fair quantum coins leads to weak Parrondo's paradox. Exploring the possibility of achieving strong Parrondo's paradox by tossing two 2-sided biased quantum coins motivates future work. In Chapter 2, we noted that a general quantum coin takes the form

$$\hat{C}(\rho, \alpha, \beta) = \begin{pmatrix} \sqrt{\rho} & \sqrt{1-\rho}e^{i\alpha} \\ \sqrt{1-\rho}e^{i\beta} & -\sqrt{\rho}e^{i\alpha\beta} \end{pmatrix}, \tag{7.1}$$

where $0 \leq \rho \leq 1$, $0 \leq \alpha, \beta \leq \pi$. Future research can investigate the effect of biased quantum coins, by varying parameters ρ, α, and β, and whether strong Parrondo's paradox can be realised with a fair boost $\hat{S}$.

Lastly, the secret key exchange quantum coin-toss encryption algorithm is a result of exploring classical chaos as a means for switching between tossing two fair quantum coins. This encryption algorithm is a practical outcome of research in quantum Parrondo's paradox. However, it is rooted in the Diffie-Hellman key exchange protocol, which is verifiably weakened with quantum computation. Thus, the natural course of evolution for such an algorithm, with the advent of quantum computation, is to develop a fully quantum chaotic implementation of the quantum coin-toss algorithm that can further enhance the security of the secret key exchange quantum coin-toss encryption algorithm. While this deviates from quantum Parrondo's paradox research, we believe that a breakthrough in exploring quantum chaotic switching for quantum coin-toss Parrondo's paradox will be a significant step in the right direction for a fully quantum chaotic encryption algorithm.

7.3.2 Sociodynamical Parrondo's paradox

In this thesis, we have developed a framework called the preference aggregation Parrondo's paradox. With limits to the scope that we can research for this thesis, there are many areas that are still unexplored but remain key cornerstones in scaffolding this research area.

Firstly, research in social dynamics Parrondo's paradox needs to be in tandem with advances in social network research. For example, in the past decade, there have been considerable advances in network sciences research such as multilayer networks, multiplex networks, and evolutionary dynamical networks [96, 97]. With increasing computational resources, simulating the outcome of playing Parrondo's games in such networks can facilitate advances in social dynamics Parrondo's paradox.

Secondly, a considerable gap in the present research in sociodynamical Parrondo's paradox is the definition of "losing games" in social settings. There are a significant

number of losing options in day-to-day sociodynamical situations (e.g. negotiating and compromising between people, ranking and ordering in decision-making etc.) that continue to be described as coin-toss games in social dynamics Parrondo's paradox research. Research should go into defining these "losing games" not as coin-toss games, but in the form of social rules and interactions between agents in a network. One possible direction is constructing Parrondo's games analogous to the pay-off table as seen in game theory. This will be significant for social dynamics Parrondo's paradox research as it will narrow the gap between the outcomes observed in Parrondo's paradox and real-world social settings.

The possibility of social science experiments pertaining to choosing between two losing outcomes will further allow the verification of empirical results of simulating social dynamics Parrondo's paradox. There are multiple instances where choosing between two losing options is necessary, especially in social settings. A key push for social dynamics Parrondo's paradox is to have real-world social experiments that can verify empirical results.

Lastly, a phase transition is observed in our simulation results, which is likened to phenomena observed in statistical mechanics. This may suggest that interacting agents in a network exhibit phenomena observed in the canonical and microcanonical ensembles of spin-lattice glass and Ising model. Therein lies the connection between studying social systems and their inherent behaviours and statistical mechanics in Physics. Further studies have to be done to investigate this relationship and the underlying reasons for the phase transitions.

7.4 Summary

In this thesis, we explored two applications of Parrondo's paradox. First in quantum physics, and then in social physics. This thesis sought to explore a relatively secluded topic and has contributed to the extension of knowledge in both these applications. The extension in the field of quantum Parrondo's paradox has led to the discovery of a new secret key exchange quantum coin-toss encryption algorithm that has the potential to be developed into a semiclassical quantum cryptography tool. The contributions to sociodynamical Parrondo's paradox have revealed several interesting outcomes in social dynamics that are also observed in real-world social phenomena such as preference aggregation, decision-making, and voting.

Parrondo's paradox is the convergent of various concepts from convex linear combination, complexity theory, stochastic theory, Markov theory, discrete theory, nonlinear theory, dynamical systems, and fractals, all in a compact model. While much is still unexplored in Parrondo's paradox, this thesis provides a springboard for pathways into two such fields: quantum and social physics.

Bibliography

[1] Armand Ajdari and Jacques Prost. "Drift induced by a spatially periodic potential of low symmetry: Pulsed dielectrophoresis." In: *Comptes Rendus de l'Academie des Sciences. Serie 2. Fascicule b. Mecanique* 315.13 (Dec. 1992), pp. 1635–1639. ISSN: 1620-7742.

[2] Juliette Rousselet et al. "Directional motion of brownian particles induced by a periodic asymmetric potential". In: *Nature* 370.6489 (Aug. 1994), pp. 446–447. DOI: 10.1038/370446a0.

[3] Gregory P. Harmer et al. "Brownian ratchets and Parrondo's games". In: *Chaos: An Interdisciplinary Journal of Nonlinear Science* 11.3 (Sept. 2001), pp. 705–714. DOI: 10.1063/1.1395623.

[4] The Institute of Mathematical Sciences. *The flashing Brownian ratchet*. URL: https://www.imsc.res.in/~sitabhra/research/persistence/page2.html (visited on 14/6/2022).

[5] Paul C. Bressloff. "Molecular motors". In: *Stochastic Processes in Cell Biology: Volume I*. Cham: Springer International Publishing, 2021, pp. 173–232. ISBN: 978-3-030-72515-0. DOI: 10.1007/978-3-030-72515-0_4.

[6] Kang Hao Cheong, Jin Ming Koh, and Michael C. Jones. "Paradoxical Survival: Examining the Parrondo Effect across Biology". In: *BioEssays* 41.6 (May 2019), p. 1900027. DOI: 10.1002/bies.201900027.

[7] Tao Wen et al. "Extending the Lifespan of Multicellular Organisms via Periodic and Stochastic Intercellular Competition". In: *Physical Review Letter* 128 (21 May 2022), p. 218101. DOI: 10.1103/PhysRevLett.128.218101.

[8] Gregory P. Harmer and Derek Abbott. "Losing strategies can win by Parrondo's paradox". In: *Nature* 402.6764 (Dec. 1999), pp. 864–864. DOI: 10.1038/47220.

[9] D. Abbott and G. P. Harmer. "Parrondo's paradox". In: *Statistical Science* 14.2 (May 1999). DOI: 10.1214/ss/1009212247.

[10] Gregory P. Harmer, Derek Abbott, and Juan M. R. Parrondo. "Parrondo's Capital and History-Dependent Games". In: *Advances in Dynamic Games: Applications to Economics, Finance, Optimization, and Stochastic Control*. Ed. by Andrzej S. Nowak and Krzysztof Szajowski. Boston, MA: Birkhäuser Boston, 2005, pp. 635–648. ISBN: 978-0-8176-4429-1. DOI: 10.1007/0-8176-4429-6_33.

[11] Jin Ming Koh and Kang Hao Cheong. "Generalized Solutions of Parrondo's Games". In: *Advanced Science* 7.24 (Nov. 2020), p. 2001126. DOI: 10.1002/advs.202001126.

[12] Juan M. R. Parrondo, Gregory P. Harmer, and Derek Abbott. "New Paradoxical Games Based on Brownian Ratchets". In: *Physical Review Letter* 85 (24 Dec. 2000), pp. 5226–5229. DOI: 10.1103/PhysRevLett.85.5226.

[13] Raúl Toral. "Cooperative Parrondo's games". In: *Fluctuation and Noise Letters* 01.01 (2001), pp. L7–L12. DOI: 10.1142/S021947750100007X.

[14] Ljupco Kocarev and Zarko Tasev. "Lyapunov exponents, noise-induced synchronization, and Parrondo's paradox". In: *Physical Review E* 65 (4 Apr. 2002), p. 046215. DOI: 10.1103/PhysRevE.65.046215.

[15] Maurizio Porfiri, Russell Jeter, and Igor Belykh. "Antiresonance in switched systems with only unstable modes". In: *Physical Review Research* 3 (2 Apr. 2021), p. L022001. DOI: 10.1103/PhysRevResearch.3.L022001.

[16] Jin Ming Koh and Kang Hao Cheong. "Automated electron-optical system optimization through switching Levenberg–Marquardt algorithms". In: *Journal of Electron Spectroscopy and Related Phenomena* 227 (Aug. 2018), pp. 31–39. DOI: 10.1016/j.elspec.2018.05.009.

[17] Kang Hao Cheong and Jin Ming Koh. "A hybrid genetic-Levenberg Marquardt algorithm for automated spectrometer design optimization". In: *Ultramicroscopy* 202 (July 2019), pp. 100–106. DOI: 10.1016/j.ultramic.2019.03.004.

[18] Kang Hao Cheong et al. "Alternating lysis and lysogeny is a winning strategy in bacteriophages due to Parrondo's paradox". In: *Proceedings of the National Academy of Sciences* 119.13 (Mar. 2022). DOI: 10.1073/pnas.2115145119.

[19] Jean-Pascal Capp et al. "Does Cancer Biology Rely on Parrondo's Principles?" In: *Cancers* 13.9 (May 2021), p. 2197. DOI: 10.3390/cancers13092197.

[20] S. G. Babajanyan, Eugene V. Koonin, and Kang Hao Cheong. "Can Environmental Manipulation Help Suppress Cancer? Non-Linear Competition Among Tumor Cells in Periodically Changing Conditions". In: *Advanced Science* 7.16 (July 2020), p. 2000340. DOI: 10.1002/advs.202000340.

[21] Kang Hao Cheong et al. "A Paradoxical Evolutionary Mechanism in Stochastically Switching Environments". In: *Scientific Reports* 6.1 (Oct. 2016). DOI: 10.1038/srep34889.

[22] Zhi Xuan Tan and Kang Hao Cheong. "Nomadic-colonial life strategies enable paradoxical survival and growth despite habitat destruction". In: *eLife* 6 (Jan. 2017). DOI: 10.7554/elife.21673.

[23] Kang Hao Cheong, Zong Xuan Tan, and Yan Hao Ling. "A time-based switching scheme for nomadic-colonial alternation under noisy conditions". In: *Communications in Nonlinear Science and Numerical Simulation* 60 (July 2018), pp. 107–114. DOI: 10.1016/j.cnsns.2017.12.012.

[24] Zhi-Xuan Tan et al. "Predator Dormancy is a Stable Adaptive Strategy due to Parrondo's Paradox". In: *Advanced Science* 7.3 (Dec. 2019), p. 1901559. DOI: 10.1002/advs.201901559.

[25] Tao Wen, Eugene V. Koonin, and Kang Hao Cheong. "An alternating active-dormitive strategy enables disadvantaged prey to outcompete the perennially active prey through Parrondo's paradox". In: *BMC Biology* 19.1 (Aug. 2021). DOI: 10.1186/s12915-021-01097-y.

[26] Piotr Gawron and Jarosław A. Miszczak. "Quantum implementation of Parrondo's paradox". In: *Fluctuation and Noise Letters* 05.04 (Dec. 2005), pp. L471–L478. DOI: 10.1142/s0219477505002902.

[27] J. Košík, J. A. Miszczak, and V. Bužek. "Quantum Parrondo's game with random strategies". In: *Journal of Modern Optics* 54.13-15 (Sept. 2007), pp. 2275–2287. DOI: 10.1080/09500340701408722.

[28] A.P. Flitney, J. Ng, and D. Abbott. "Quantum Parrondo's games". In: *Physica A: Statistical Mechanics and its Applications* 314.1-4 (Nov. 2002), pp. 35–42. DOI: 10.1016/s0378-4371(02)01084-1.

[29] A P Flitney, D Abbott, and N F Johnson. "Quantum walks with history dependence". In: *Journal of Physics A: Mathematical and General* 37.30 (July 2004), pp. 7581–7591. DOI: 10.1088/0305-4470/37/30/013.

[30] David Bulger, James Freckleton, and Jason Twamley. "Position-dependent and cooperative quantum Parrondo walks". In: *New Journal of Physics* 10.9 (Sept. 2008), p. 093014. DOI: 10.1088/1367-2630/10/9/093014.

[31] L Dinís and J. M. R Parrondo. "Optimal strategies in collective Parrondo games". In: *Europhysics Letters* 63.3 (Aug. 2003), pp. 319–325. DOI: 10.1209/epl/i2003-00461-5.

[32] Luis Dinís and Juan M.R. Parrondo. "Inefficiency of voting in Parrondo games". In: *Physica A* 343 (Nov. 2004), pp. 701–711. DOI: 10.1016/j.physa.2004.06.076.

[33] J. M.R. Parrondo et al. "Collective decision making and paradoxical games". In: *The European Physical Journal Special Topics* 143.1 (Apr. 2007), pp. 39–46. DOI: 10.1140/epjst/e2007-00068-0.

[34] Ho Fai Ma et al. "Effect of Information Exchange in a Social Network on Investment". In: *Computational Economics* 54.4 (Aug. 2017), pp. 1491–1503. DOI: 10.1007/s10614-017-9723-3.

[35] C. M. Arizmendi. "Paradoxical Way for Losers in a Dating Game". In: *AIP Conference Proceedings* 913.1 (2007), pp. 20–25. DOI: 10.1063/1.2746718.

[36] Raúl Toral. "Capital Redistribution Brings Wealth By Parrondo's Paradox". In: *Fluctuation Noise Letters* 02.04 (Dec. 2002), pp. L305–L311. DOI: 10.1142/s0219477502000907.

[37] Tobias Osborne. *Advanced quantum theory, Lecture 1*. URL: https://www.youtube.com/watch?v=Og13-bSF9kA (visited on 27/6/2022).

[38] David A. Meyer and Heather Blumer. "Parrondo Games as Lattice Gas Automata". In: *Journal of Statistical Physics* 107.1/2 (2002), pp. 225–239. DOI: 10.1023/a:1014566822448.

[39] David A. Meyer. "Noisy quantum Parrondo games". In: *SPIE Proceedings*. Ed. by Derek Abbott, Jeffrey H. Shapiro, and Yoshihisa Yamamoto. SPIE, May 2003. DOI: 10.1117/12.497095.

[40] Yu-Guang Yang et al. "Two Quantum Coins Sharing a Walker". In: *International Journal of Theoretical Physics* 58.3 (Nov. 2018), pp. 700–712. DOI: 10.1007/s10773-018-3968-z.

[41] Degang Wu and Kwok Yip Szeto. "Extended Parrondo's game and Brownian ratchets: Strong and weak Parrondo effect". In: *Phys. Rev. E* 89 (2 Feb. 2014), p. 022142. DOI: 10.1103/PhysRevE.89.022142.

[42] Marco Taboga. *Similar matrix*. URL: https://www.statlect.com/matrix-algebra/similar-matrix (visited on 19/7/2022).

[43] Marcelo A. Pires and Sílvio M. Duarte Queirós. "Parrondo's paradox in quantum walks with time-dependent coin operators". In: *Physical Review E* 102 (4 Oct. 2020), p. 042124. DOI: 10.1103/PhysRevE.102.042124.

[44] Zbigniew Walczak and Jarosław H. Bauer. "Parrondo's paradox in quantum walks with three coins". In: *Physical Review E* 105 (6 June 2022), p. 064211. DOI: 10.1103/PhysRevE.105.064211.

[45] Marius-F. Danca, Michal Fečkan, and Miguel Romera. "Generalized Form of Parrondo's Paradoxical Game with Applications to Chaos Control". In: *International Journal of Bifurcation and Chaos* 24.01 (2014), p. 1450008. DOI: 10.1142/S0218127414500084.

[46] M. Bucolo et al. "Does chaos work better than noise?" In: *IEEE Circuits and Systems Magazine* 2.3 (2002), pp. 4–19. DOI: 10.1109/MCAS.2002.1167624.

[47] P. Arena et al. "Game theory and non-linear dynamics: the Parrondo Paradox case study". In: *Chaos, Solitons & Fractals* 17.2 (2003), pp. 545–555. ISSN: 0960-0779. DOI: 10.1016/S0960-0779(02)00397-1.

[48] Tang Tze Wei, Andrew Allison, and Abbott Derek. "Investigation of chaotic switching strategies in Parrondo's games". In: *Fluctuation and Noise Letters* 04.04 (2004), pp. L585–L596. DOI: 10.1142/S021947750400221X.

[49] Govind Paneru et al. "Lossless Brownian Information Engine". In: *Physical Review Letter* 120 (2 Jan. 2018), p. 020601. DOI: 10.1103/PhysRevLett.120.020601.

[50] C. Neill et al. "Ergodic dynamics and thermalization in an isolated quantum system". In: *Nature Physics* 12.11 (July 2016), pp. 1037–1041. DOI: 10.1038/nphys3830.

[51] C. J. Turner et al. "Weak ergodicity breaking from quantum many-body scars". In: *Nature Physics* 14.7 (May 2018), pp. 745–749. DOI: 10.1038/s41567-018-0137-5.

[52] Roberto Venegeroles. *On the topological conjugacy problem for interval maps*. 2014. DOI: 10.48550/ARXIV.1411.3066.

[53] W. Diffie and M. Hellman. "New directions in cryptography". In: *IEEE Transactions on Information Theory* 22.6 (1976), pp. 644–654. DOI: 10.1109/TIT.1976.1055638.

[54] Ralph C. Merkle. "Secure Communications over Insecure Channels". In: *Communications of the ACM* 21.4 (Apr. 1978), pp. 294–299. ISSN: 0001-0782. DOI: 10.1145/359460.359473.

[55] David Adrian et al. "Imperfect Forward Secrecy: How Diffie-Hellman Fails in Practice". In: *Proceedings of the 22nd ACM SIGSAC Conference on Computer and Communications Security*. CCS '15. Denver, Colorado, USA: Association for Computing Machinery, 2015, pp. 5–17. ISBN: 9781450338325. DOI: 10.1145/2810103.2813707.

[56] Federico Carollo et al. "Nonequilibrium Quantum Many-Body Rydberg Atom Engine". In: *Physical Review Letter* 124 (17 Apr. 2020), p. 170602. DOI: 10.1103/PhysRevLett.124.170602.

[57] Sosuke Ito. "Stochastic Thermodynamic Interpretation of Information Geometry". In: *Physical Review Letter* 121 (3 July 2018), p. 030605. DOI: 10.1103/PhysRevLett.121.030605.

[58] Robert C Wilson and Anne GE Collins. "Ten simple rules for the computational modeling of behavioral data". In: *eLife* 8 (Nov. 2019). Ed. by Timothy E Behrens, e49547. ISSN: 2050-084X. DOI: 10.7554/eLife.49547.

[59] Lin-gang Wang et al. "Game-model research on coopetition behavior of Parrondo's paradox based on network". In: *Fluctuation and Noise Letters* 10.01 (2011), pp. 77–91. DOI: 10.1142/S0219477511000417.

[60] Ye Ye et al. "Cooperation and competition in history-dependent Parrondo's game on networks". In: *Fluctuation and Noise Letters* 10.03 (2011), pp. 323–336. DOI: 10.1142/S0219477511000594.

[61] Ye Ye et al. "Effects of behavioral patterns and network topology structures on Parrondo's paradox". In: *Scientific Reports* 6.1 (Nov. 2016). DOI: 10.1038/srep37028.

[62] Réka Albert and Albert-László Barabási. "Statistical mechanics of complex networks". In: *Rev. Mod. Phys.* 74 (1 Jan. 2002), pp. 47–97. DOI: 10.1103/RevModPhys.74.47.

[63] Dario A. Zappalà, Alessandro Pluchino, and Andrea Rapisarda. "Selective altruism in collective games". In: *Physica A: Statistical Mechanics and its Applications* 410 (2014), pp. 496–512. ISSN: 0378-4371. DOI: 10.1016/j.physa.2014.05.032.

[64] Joel Weijia Lai and Kang Hao Cheong. "A comprehensive framework for preference aggregation Parrondo's paradox". In: *Chaos: An Interdisciplinary Journal of Nonlinear Science* 32.10 (Oct. 2022), p. 103107. DOI: 10.1063/5.0101321.

[65] Teresa Amabile and Steven Kramer. *The power of small wins*. URL: https://hbr.org/2011/05/the-power-of-small-wins (visited on 13/10/2022).

[66] Teresa Amabile and Steven Kramer. *The Progress Principle: Using Small Wins to Ignite Joy, Engagement, and Creativity at Work*. Harvard Business Review Press, 2011. ISBN: 9781422142738.

[67] Joel Weijia Lai and Kang Hao Cheong. "Risk-taking in social Parrondo's games can lead to Simpson's paradox". In: *Chaos, Solitons & Fractals* 158 (May 2022), p. 111911. DOI: 10.1016/j.chaos.2022.111911.

[68] Ward Edwards. "The theory of decision making." In: *Psychological Bulletin* 51.4 (1954), pp. 380–417. DOI: 10.1037/h0053870.

[69] Nibedita Mukherjee et al. "Comparison of techniques for eliciting views and judgements in decision-making". In: *Methods in Ecology and Evolution* 9.1 (Jan. 2018). Ed. by Mark Everard, pp. 54–63. DOI: 10.1111/2041-210x.12940.

[70] Jure Leskovec and Andrej Krevl. *SNAP Datasets: Stanford Large Network Dataset Collection*. http://snap.stanford.edu/data. June 2014.

[71] Jure Leskovec and Julian Mcauley. "Learning to Discover Social Circles in Ego Networks". In: *Advances in Neural Information Processing Systems*. Ed. by F. Pereira et al. Vol. 25. Curran Associates, Inc., 2012.

[72] Aaron Clauset, M. E. J. Newman, and Cristopher Moore. "Finding community structure in very large networks". In: *Physical Review E* 70 (6 Dec. 2004), p. 066111. DOI: 10.1103/PhysRevE.70.066111.

[73] Yoshiki Kuramoto. "Self-entrainment of a population of coupled non-linear oscillators". In: *International Symposium on Mathematical Problems in Theoretical Physics*. Ed. by Huzihiro Araki. Berlin, Heidelberg: Springer Berlin Heidelberg, 1975, pp. 420–422. ISBN: 978-3-540-37509-8.

[74] A. Jadbabaie, N. Motee, and M. Barahona. "On the stability of the Kuramoto model of coupled nonlinear oscillators". In: *Proceedings of the 2004 American Control Conference*. Vol. 5. 2004, pp. 4296–4301. DOI: 10.23919/ACC.2004.1383983.

[75] Wei Zou and Jianwei Wang. "Dynamics of the generalized Kuramoto model with nonlinear coupling: Bifurcation and stability". In: *Physical Review E* 102 (1 July 2020), p. 012219. DOI: 10.1103/PhysRevE.102.012219.

[76] Ernest Montbrió and Diego Pazó. "Kuramoto Model for Excitation-Inhibition-Based Oscillations". In: *Physical Review Letters* 120 (24 June 2018), p. 244101. DOI: 10.1103/PhysRevLett.120.244101.

[77] Francisco A. Rodrigues et al. "The Kuramoto model in complex networks". In: *Physics Reports* 610 (Jan. 2016), pp. 1–98. DOI: 10.1016/j.physrep.2015.10.008.

[78] M. K. Stephen Yeung and Steven H. Strogatz. "Time Delay in the Kuramoto Model of Coupled Oscillators". In: *Physical Review Letters* 82 (3 Jan. 1999), pp. 648–651. DOI: 10.1103/PhysRevLett.82.648.

[79] Sara Ameli, Maryam Karimian, and Farhad Shahbazi. "Time-delayed Kuramoto model in the Watts–Strogatz small-world networks". In: *Chaos: An Interdisciplinary Journal of Nonlinear Science* 31.11 (Nov. 2021), p. 113125. DOI: 10.1063/5.0064022.

[80] Yufeng Guo et al. "Overviews on the applications of the Kuramoto model in modern power system analysis". In: *International Journal of Electrical Power & Energy Systems* 129 (July 2021), p. 106804. DOI: 10.1016/j.ijepes.2021.106804.

[81] Xuebin Wang, Can Xu, and Zhigang Zheng. "Phase transition and scaling in Kuramoto model with high-order coupling". In: *Nonlinear Dynamics* 103.3 (Feb. 2021), pp. 2721–2732. DOI: 10.1007/s11071-021-06268-8.

[82] M. Girvan and M. E. J. Newman. "Community structure in social and biological networks". In: *Proceedings of the National Academy of Sciences of the United States of America* 99.12 (June 2002), pp. 7821–7826. DOI: 10.1073/pnas.122653799.

[83] Bruce J. West, Elvis L. Geneston, and Paolo Grigolini. "Maximizing information exchange between complex networks". In: *Physics Reports* 468.1-3 (Oct. 2008), pp. 1–99. DOI: 10.1016/j.physrep.2008.06.003.

[84] B. J. West et al. "Relating size and functionality in human social networks through complexity". In: *Proceedings of the National Academy of Sciences* 117.31 (July 2020), pp. 18355–18358. DOI: 10.1073/pnas.2006875117.

[85] R.I.M. Dunbar. "Neocortex size as a constraint on group size in primates". In: *Journal of Human Evolution* 22.6 (June 1992), pp. 469–493. DOI: 10.1016/0047-2484(92)90081-j.

[86] A. Hernando et al. "Unravelling the size distribution of social groups with information theory in complex networks". In: *The European Physical Journal B* 76.1 (July 2010), pp. 87–97. DOI: 10.1140/epjb/e2010-00216-1.

[87] Andreas Diekmann. "Volunteer's Dilemma". In: *Journal of Conflict Resolution* 29.4 (1985), pp. 605–610. DOI: 10.1177/0022002785029004003.

[88] Joel Weijia Lai and Kang Hao Cheong. "Parrondo effect in quantum coin-toss simulations". In: *Physical Review E* 101.5 (May 2020), p. 052212. DOI: 10.1103/physreve.101.052212.

[89] Joel Weijia Lai et al. "Parrondo paradoxical walk using four-sided quantum coins". In: *Physical Review E* 102.1 (July 2020), p. 012213. DOI: 10.1103/physreve.102.012213.

[90] Munsif Jan et al. "Experimental Realization of Parrondo's Paradox in 1D Quantum Walks". In: *Advanced Quantum Technologies* 3.6 (May 2020), p. 1900127. DOI: 10.1002/qute.201900127.

[91] Joel Weijia Lai and Kang Hao Cheong. "Chaotic switching for quantum coin Parrondo's games with application to encryption". In: *Physical Review Research* 3 (2 June 2021), p. L022019. DOI: 10.1103/PhysRevResearch.3.L022019.

[92] Joel Weijia Lai and Kang Hao Cheong. "Evaluation of single-prioritization voting systems in controlled collective Parrondo's games". In: *Nonlinear Dynamics* 107.3 (Jan. 2022), pp. 2965–2974. DOI: 10.1007/s11071-021-07087-7.

[93] Jishnu Rajendran and Colin Benjamin. "Implementing Parrondo's paradox with two-coin quantum walks". In: *Royal Society Open Science* 5.2 (Feb. 2018), p. 171599. DOI: 10.1098/rsos.171599.

[94] Jishnu Rajendran and Colin Benjamin. "Playing a true Parrondo's game with a three-state coin on a quantum walk". In: *EPL (Europhysics Letters)* 122.4 (June 2018), p. 40004. DOI: 10.1209/0295-5075/122/40004.

[95] Joel Weijia Lai and Kang Hao Cheong. "Parrondo's paradox from classical to quantum: A review". In: *Nonlinear Dynamics* 100.1 (Feb. 2020), pp. 849–861. DOI: 10.1007/s11071-020-05496-8.

[96] John Scott. "Social network analysis: developments, advances, and prospects". In: *Social Network Analysis and Mining* 1.1 (Oct. 2010), pp. 21–26. DOI: 10.1007/s13278-010-0012-6.

[97] A. Abraham, A.E. Hassanien, and V. Snášel. *Computational Social Network Analysis: Trends, Tools and Research Advances*. Computer Communications and Networks. Springer London, 2009. ISBN: 9781848822290.